GEMS & GEMOLOGY

SUMMER 2021
VOLUME LVII

THE QUARTERLY JOURNAL OF THE GEMOLOGICAL INSTITUTE OF AMERICA

Effects of Blue Fluorescence on Diamond Appearance

Chinese Freshwater "Edison" Pearls

Chart of Pearl Value Factors

Namak Mandi: Pakistan's Gem Trading Hub

GEMS & GEMOLOGY®
Summer 2021
VOLUME 57, No. 2


p. 103


p. 126


p. 141


p. 154

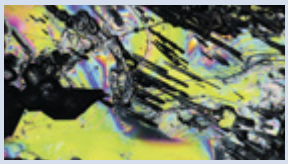
p. 165


p. 175

Editorial

Feature Articles

Charts

Field Reports

Regular Features

GEMS & GEMOLOGY

gia.edu/gems-gemology

Subscriptions
Copies of the current issue may be purchased for $29.95 plus shipping. Subscriptions are $79.99 for one year (4 issues) in the U.S. and $99.99 elsewhere. Canadian subscribers should add GST. Discounts are available for renewals, group subscriptions, GIA alumni, and current GIA students. To purchase print subscriptions, visit store.gia.edu or contact Customer Service. For institutional rates, contact Customer Service.

Database Coverage
Gems & Gemology's impact factor is 0.767, according to the 2019 Thomson Reuters Journal Citation Reports (issued July 2020). *G&G* is abstracted in Thomson Reuters products (Current Contents: Physical, Chemical & Earth Sciences and Science Citation Index—Expanded, including the Web of Knowledge) and other databases. For a complete list of sources abstracting *G&G*, go to gia.edu/gems-gemology, and click on "Publication Information."

Manuscript Submissions
Gems & Gemology, a peer-reviewed journal, welcomes the submission of articles on all aspects of the field. Please see the Author Guidelines at gia.edu/gems-gemology or contact the Managing Editor. Letters on articles published in *G&G* are also welcome. Please note that Field Reports, Lab Notes, Gem News International, Micro-World, Diamonds from the Deep, and Charts are not peer-reviewed sections but do undergo technical and editorial review.

Gems & Gemology is published quarterly by the Gemological Institute of America, a nonprofit educational organization for the gem and jewelry industry.

Postmaster: Return undeliverable copies of *Gems & Gemology* to GIA, The Robert Mouawad Campus, 5345 Armada Drive, Carlsbad, CA 92008.

Our Canadian goods and service registration number is 126142892RT.

Any opinions expressed in signed articles are understood to be opinions of the authors and not of the publisher.

About the Cover

John McDevitt King's mixed-media painting "Overblue" illustrates how gems and fine art are intertwined. The artist acknowledges the subtle effects of fluorescence on diamond appearance—usually none. But when fluorescence is strong, it may soften the light/dark contrast with a unique glow. The proportions of the sketched diamonds relate to the reported occurrence of fluorescence strength, starting with the most common (None to Faint) and receding to Medium to Strong, all the way to the scarcely encountered Very Strong. King, a longtime senior leader of GIA's laboratory, is an author of G&G*'s Winter 1997 fluorescence article and many others.*

Printing is by L+L Printers, Carlsbad, CA.

GIA World Headquarters The Robert Mouawad Campus 5345 Armada Drive Carlsbad, CA 92008 USA

ISSN 0016-626X

Effects of Blue Fluorescence on Diamond Appearance, Color Treatment and Brightening of "Edison" Pearls, and a Pioneering Gemstone Market in Pakistan

Welcome to the Summer installment of *Gems & Gemology*! This issue sizzles with new content, including the relationship between fluorescence and diamond appearance, a deep dive into the world of pearls with advances in color treatment detection and a comprehensive classification system, and the evolution of the Namak Mandi gemstone market in Peshawar, Pakistan.

Our lead article looks at the long-debated effects of blue fluorescence on the appearance of diamonds with D-to-Z color grades. Some argue that colorless to near-colorless diamonds possessing strong or very strong fluorescence will appear hazy or "oily." Others express concern that lower-color diamonds may appear one color grade better depending on fluorescence intensity. A GIA team led by Yun Luo quantitatively characterizes the effects of fluorescence intensity on perceived transparency and appearance to help reduce biases in the industry and promote consumer confidence.

"...quantitatively characterizes the effects of fluorescence intensity on perceived transparency and appearance..."

Advances in freshwater culturing techniques have dramatically improved the quality of freshwater cultured pearl output from China, making color treatment detection a key element of the identification process in gemological laboratories. In the second article of this issue, Chunhui Zhou and fellow researchers study 23 freshwater "Edison" pearls with a mix of natural and treated colors. A combination of various gemological tests and advanced analytical methods presented in this study prove effective in detecting color treatment and optical brightening.

Next, Joyce Wing Yan Ho and Sally Chan Shih present GIA's comprehensive pearl classification system based on seven value factors—size, shape, color, luster, surface, nacre, and matching. This article is accompanied by an illustrated wall chart intended as a valuable visual reference.

In the final article, Habib Ur Rehman and coauthors journey to the Namak Mandi market in Peshawar, the largest rough gemstone trading hub in Pakistan. They document its transformation over the last 50 years from a salt market to the bustling "intersection of anxiety" engaged in modern gem commerce. The authors also examine the gemstone supply chain, the continued use of traditional cutting tools, and the shift toward ethical pricing and trading practices.

As always, our regular columns provide an array of gemological insights from around the world. Highlights of the *Lab Notes* section include an impressive emerald imitation in the form of dyed beryl, a desirable Melo pearl discovered while preparing a Melo shell for consumption, and an exquisite opal strand displaying bright and vibrant play-of-color. The *Micro-World* section explores the inner landscapes of gemstones, offering a glimpse into Earth's natural forces, including two high-quality diamonds with noteworthy green chromium-colored diopside and purplish pink pyrope garnet inclusions, respectively, and heavily etched blue beryl from Pakistan. In *Gem News International*, you'll find a characterization of natural freshwater pearls from Russia, Scotland, and Germany, as well as an examination of 28 non-bead cultured freshwater pearls grown over 14 years in Lake Biwa, Japan (a precursor to a more detailed review), and much more.

We hope you enjoy the latest issue of *Gems & Gemology*!

Duncan Pay | Editor-in-Chief | dpay@gia.edu

Measurement and Characterization Of the Effects of Blue Fluorescence On Diamond Appearance

Yun Luo, David Nelson, Troy Ardon, and Christopher M. Breeding

In this study, the effects of blue fluorescence on the appearance of diamonds—including table-down color, face-up color, brightness, and transparency—are quantitatively characterized using customized measurement systems. The results show that UV intensity in the light source affects table-down color, face-up color, and brightness of diamonds. A standardized lighting environment containing a fixed UV component is essential for accurate and consistent color evaluation that fully incorporates the effects of blue fluorescence. The "hazy" appearance that often impacts apparent diamond transparency is mainly attributed to light scattering from structural defects, but our results also indicate that strong fluorescence causes minor contrast loss in the face-up patterns of some polished diamonds. The presence of both strong fluorescence and light-scattering structural defects increases the apparent haziness. The transparency changes induced by structural defects, fluorescence, or both can be characterized by a bulk contrast evaluation method using the diamond's face-up pattern. Fluorescence is an intrinsic property of diamond that can improve the color of some stones when they are exposed to a lighting environment with significant UV content, such as daylight, but fluorescence alone does not noticeably reduce transparency.

Fluorescence in diamond is a subject that has generated lively discussion in the trade for decades. It is believed that diamonds with D to F color grades (i.e., colorless), which do not possess enough color to offset the presence of fluorescence, are prone to appear hazy when combined with strong or very strong blue fluorescence. Lower-color diamonds with medium to very strong blue fluorescence may appear up to one color grade better due to the blue fluorescence "neutralizing" the yellow color. The trade has expressed concerns that the true color of diamonds is not represented under light containing UV (<400 nm) and considers diamonds color graded under such light as over-graded (Cowing, 2010). Conversely, some global markets believe that fluorescence may have a beneficial impact on color and thus lower-color diamonds with fluorescence will sell at a slight premium (table 1). These mixed perceptions on the effect of fluorescence on overall diamond appearance have impacted the value of diamonds with fluorescence since the late 1970s but have been amplified in recent years (table 1).

Based on visual observations under different lighting conditions, several studies have investigated the effect of blue fluorescence on the color and overall appearance of diamonds. Moses et al. (1997) concluded that strongly blue fluorescent diamonds were per-

In Brief

- Fluorescence is an important property of gem diamonds that impacts their value and pricing in the marketplace.
- Analysis indicates that a gem diamond's visible color is only occasionally impacted in those with strong to very strong fluorescence and depends on the amount of UV in the light source.
- Modulation transfer function (MTF) is a very useful tool for examining contrast loss as a measurement of haziness in gem diamonds.
- The hazy appearance sometimes observed in gem diamonds is primarily caused by atomic-scale light scattering defects or nano-inclusions. Strong fluorescence by itself does not cause haziness, but it may produce more contrast loss in some diamonds that already have a hazy appearance.

See end of article for About the Authors and Acknowledgments.
Gems & Gemology, Vol. 57, No. 2, pp. 102–123,
http://dx.doi.org/10.5741/GEMS.57.2.102

Figure 1. The 127.01 ct Portuguese diamond was graded by GIA as M color and VS_1 clarity (A,B) with very strong blue fluorescence (C); photos courtesy of the Smithsonian Institution. The Portuguese diamond has been cited as a classic example of a stone being "over blue" and exhibiting a noticeably oily or hazy appearance (D). It is also shown being worn by American actress Peggy Hopkins Joyce (E). Photos by NMNH Photo Services (A), Chip Clark (B), and Harold & Erica Van Pelt (D).

ceived to have a better color appearance when viewed face-up, with no discernible trend table-down, and that there was no observable relationship between fluorescence and transparency. Bouman et al. (2018) found that diamonds observed table-down in outdoor conditions showed improved color grades, whereas fluorescence did not directly correlate with the color grade in the face-up position. Despite no clear evidence of fluorescence negatively affecting diamond color and appearance in these studies, pricing adjustments based on fluorescence continue in the trade (tables 1 and 2).

Historically, three major challenges needed to be overcome in order to understand better the effect of fluorescence on diamond appearance: the lack of a standard methodology to quantify color and fluorescence, the fact that color and fluorescence correspond to a range of values, and the lack of an accepted illumination standard.

The absence of a standardized characterization system, together with the fact that both color grades and fluorescence evaluations correspond to a range of measurable values, makes consistent and accurate visual comparison difficult. For example, if we choose a high K color (closer to J) diamond with medium-low blue fluorescence to compare with a low K (closer to L) stone with medium-high blue fluorescence, the effect of medium fluorescence will be different because the two samples fall at opposite ends of continuous yet independent ranges for both color and fluorescence. Even with carefully aligned visual observations and spectroscopy-based measurement techniques for color and fluorescence, we still need image-based measurements that more accurately reflect how the stones appear in "real life" and can be directly linked to human visual perception. No previous study has utilized imaging systems to demonstrate and quantify the effects of fluorescence on diamond appearance. Even if we can visually identify the effect of fluorescence on face-up color by comparing very strongly fluorescent stones against inert stones under certain lighting conditions, these differences are not readily obvious in images taken under different lighting environments.

Figure 1 shows the famous 127.01 ct Portuguese diamond, housed at the Smithsonian Institution. It has been cited as a classic example of a very strong blue fluorescent diamond displaying a noticeably oily or hazy appearance. Photos of this legendary diamond taken under different lighting setups show various aspects of its appearance, including clarity, color, and haziness. It is not easy to find the right combination of illumination and camera resolution to accurately and precisely display these effects with sufficient reproducibility.

The last but perhaps most important challenge is the standardization of illumination for color measurement and visual observation. In King et al. (2008), the GIA team concluded that a standard light source for diamond color grading should possess key daylight elements—including a UV component to truly and accurately represent how a diamond appears to

TABLE 1. Approximate percentage pricing differential from nonfluorescent diamonds.

Color Grade	FL Intensity (blue)	Clarity Grade					
		IF to VVS		VS		SI	
		2017	2020	2017	2020	2017	2020
D-F	Very Strong	–10 to –15%	n/a	–6 to –10%	n/a	0 to –3%	n/a
	Strong	–7 to –10%	–18 to –25%	–3 to –5%	–12 to –22%	0 to –1%	–8 to –16%
	Medium	–3 to –7%	–14 to –21%	–1 to –2%	–9 to –17%	0	–6 to –13%
	Faint	–1%	–9 to –15%	0%	–6 to –12%	0	–4 to –8%
G-H	Very Strong	–7 to –10%	n/a	–3 to –5%	n/a	0	n/a
	Strong	–5 to –7%	–13 to –17%	–2 to –3%	–10 to –15%	0	–7 to –11%
	Medium	–1 to –3%	–10 to –14%	0 to –2%	–8 to –12%	0	–5 to –8%
	Faint	–1%	–7 to –11%	0	–5 to –9%	0	–3 to –5%
I-K	Very Strong	0 to +2%	n/a	0 to +2%	n/a	0 to +2%	n/a
	Strong	0 to +2%	–6 to –12%	0 to +2%	–5 to –11%	0 to +2%	–4 to –10%
	Medium	0 to +2%	–5 to –9%	0 to +2%	–4 to –8%	0 to +2%	–3 to –7%
	Faint	0	–4 to –6%	0	–3 to –5%	0	–2 to –4%
L-M	Very Strong	0 to +2%	n/a	0 to +2%	n/a	0 to +2%	n/a
	Strong	0 to +2%	n/a	0 to +2%	n/a	0 to +2%	n/a
	Medium	0 to +2%	n/a	0 to +2%	n/a	0 to +2%	n/a
	Faint	0	n/a	0	n/a	0	n/a

Data source: Rapaport price lists (https://www.diamonds.net/Prices/DetailedInfo.aspx)
n/a: data not available from Rapaport 2020 update

the human eye. For the results of this study to ultimately have significance for the diamond trade and its practices and regulations, we require an illumination standard that includes UV content and thus accounts for the effects of fluorescence on diamond appearance.

Taking advantage of recent technological advances, the focus of this study was to use customized, image-based measurement systems to quantitatively characterize the effect of fluorescence on the color, brightness (i.e., the internal and external white light return), and transparency of gem diamonds viewed in both table-down and face-up orientations under well-characterized lighting conditions. Our goal is to provide a better understanding of the effect of blue fluorescence on diamond appearance and quantify it instrumentally. We believe this will help to reduce the confusion and biases in the industry and serve as a solid scientific foundation to ensure public trust with respect to diamond fluorescence.

MATERIALS AND METHODS

Polished Diamond Samples. Four sets of round brilliant diamonds, color graded by GIA as D, F, G, and H, were used to measure table-down and face-up color. Each set was assembled with the same color grade and

TABLE 2. Average price for one-carat, VS_1-clarity, triple EX (a trade term for Excellent cut, polish, and symmetry), round brilliant cut diamonds with different fluorescence intensities.

Color Grade	NON	FNT	MED	STR	VST	FNT	MED	STR	VST
D	$8613	$7860	$7425	$7171	$6748	–9%	–14%	–17%	–22%
E	$8082	$7463	$6816	$6389	$6282	–8%	–16%	–21%	–22%
F	$7689	$7007	$6527	$6432		–9%	–15%	–16%	
G	$6877	$6536	$6047	$5941		–5%	–12%	–14%	
H	$6675	$6220	$5917	$5544	$5346	–7%	–11%	–17%	–20%
I	$5705	$5395	$5226	$4942	$4628	–5%	–8%	–13%	–19%
J	$4933	$4314	$4411	$4209		–13%	–11%	–15%	

Data source: Diamond prices posted on Blue Nile for October 26, 2019 (www.bluenile.com)

TABLE 3. Four sets of round brilliant diamonds examined in this study.

Sample ID	Shape	Color	Fluorescence Intensity	Weight (ct)	Cut	Symmetry	Polish	Table (%)	Depth (%)	Crown Angle (°)	Pavilion Angle (°)	Girdle Thickness (%)
x0237	Round	D	NON	0.53	EX	EX	EX	58	61.3	33.6	41.3	3.4
x4632	Round	D	FNT	0.61	EX	EX	EX	59	61.0	32.4	41.3	4.4
x0517	Round	D	MED	0.74	EX	EX	EX	58	61.3	34.0	41.2	3.6
x8912	Round	D	STR	0.61	EX	EX	EX	59	60.9	33.4	41.4	3.3
x8789	Round	D	VST	0.63	EX	EX	EX	58	60.9	33.4	41.2	3.5
x0059	Round	F	NON	0.56	EX	EX	EX	58	61.7	34.9	41.2	3.4
x7519	Round	F	FNT	0.50	EX	EX	EX	57	61.7	34.7	41.4	2.8
x8316	Round	F	MED	0.52	EX	EX	EX	58	61.9	34.5	41.3	3.5
x7510	Round	F	STR	0.51	EX	EX	EX	58	61.9	34.6	41.3	3.3
x8814	Round	F	VST	0.62	EX	EX	EX	58	61.6	34.2	41.3	3.5
x2150	Round	G	NON	0.51	EX	EX	EX	57	62.1	34.5	41.2	3.6
x2008	Round	G	FNT	0.52	EX	EX	EX	57	62.3	35.0	41.2	3.6
x1977	Round	G	MED	0.41	EX	EX	EX	57	62.5	34.9	41.1	4.0
x2109	Round	G	STR	0.51	EX	EX	EX	57	62.1	35.0	41.0	3.7
x2356	Round	G	VST	0.50	EX	EX	EX	57	62.3	35.1	40.8	4.0
x7596	Round	H	NON	0.53	EX	EX	EX	57	61.6	34.3	41.0	3.7
x0271	Round	H	FNT	0.50	EX	EX	EX	57	61.5	34.0	41.3	3.3
x7635	Round	H	MED	0.51	EX	EX	EX	57	61.3	33.7	41.0	3.4
x8812	Round	H	STR	0.61	EX	EX	EX	58	61.2	33.9	41.2	3.5
x8937	Round	H	VST	0.54	EX	EX	EX	57	61.4	34.4	41.0	3.4

similar sizes and proportions, but with fluorescence intensities varying from None to Very Strong (table 3). All faceted diamonds used in this study carried GIA reports and represented a range of diamond types.

TABLE 4. The 13 diamond plates used in this study, sorted by fluorescence intensity according to lightness values from fluorescence measurements.

Sample ID	Thickness (mm)	Lightness	Strain	Diamond Type
5358_A	1.709	3	Medium	IaB
CBP-0368	4.314	3	Strong	IaAB (low)
CBP-0069	2.205	6	Medium	IaAB
CBP-0632	3.057	7	Strong	IaAB
5359_A	0.876	12	Medium	IaB
CBP-0413	2.661	37	Weak	IaAB
CBP-0067	2.761	39	None	IaAB
CBP-0098	2.225	43	None	IaAB
CBP-0929	3.745	44	Strong	IaB>A
CBP-0151	2.437	46	None	IaAB
CBP-0033	2.768	47	None	IaAB
CBP-0361	2.864	49	Strong	IaB>A
CBP-0926	2.467	62	Strong	IaB>A

Higher lightness value corresponds to stronger fluorescence intensity.

Diamond Plates. Eleven rough and two faceted diamonds were cut into plates with parallel windows (table 4). All samples were analyzed by ultraviolet/visible/near-infrared (UV-Vis-NIR), Fourier-transform infrared (FTIR), and photoluminescence (PL) spectroscopy to provide additional information about the diamond type and atomic structural defects present. In addition, the birefringence of each sample was examined under crossed polarized light in the microscope to assess internal strain. Color and fluorescence intensity were characterized for correlation with the transparency and contrast studies.

Color Measurement Systems. Two customized imaging systems were set up to measure the table-down and face-up color of diamond samples in this study. The table-down color measurement system consists of a sample chamber with a rotational stage, a light integration hemisphere, a lens-camera assembly, and a light source with tunable UV content (figure 2A). The emission spectra from the light source show four steps of UV intensity (0, 25, 50, and 100% LED power with UV emission at 368 nm, corresponding to calculated UV content of <1, 2, 3, and 5%, respectively). For the purposes of this study, UV content refers to

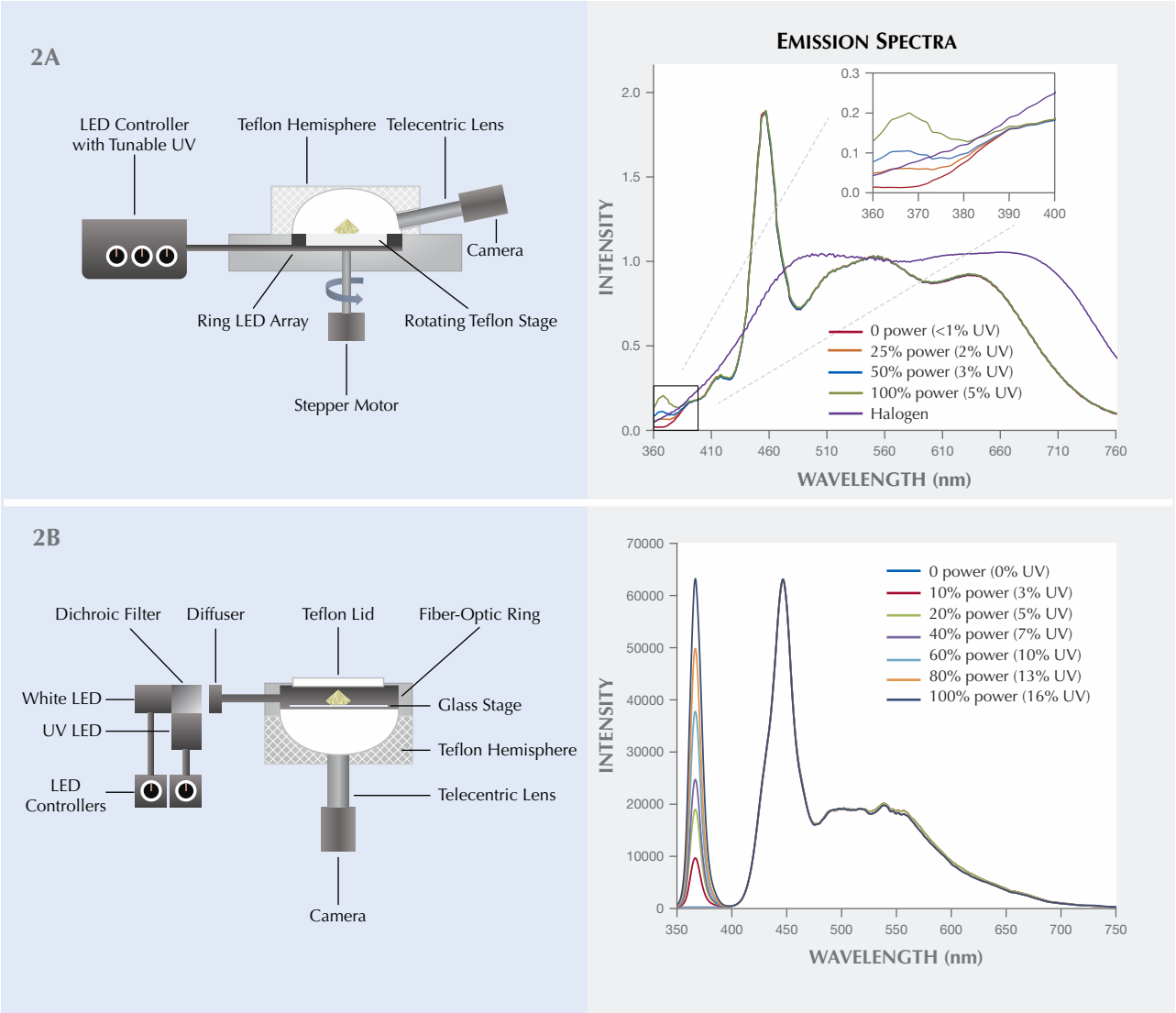

Figure 2. Color measurement experiment setups used for this study include both table-down and face-up systems. 2A is the table-down color measurement system (left), together with its LED light spectra at different UV intensities compared to a halogen light source with daylight filter (right). 2B shows the face-up color measurement system (left) and the spectra of the light source with different UV intensities (right).

the percentage of the total emission that occurs in the UV range (300–400 nm) and is defined as follows:

$$\%\,\mathrm{UV} = \frac{\text{area under UV part of emission curve at 300–400 nm}}{\text{area under complete emission curve at 300–850 nm}} \times 100$$

The face-up color measurement system was configured using a sample chamber, lens-camera assembly, and a light source with tunable UV intensity (366 nm emission) at increments of 0, 10, 20, 40, 60, 80, and 100% LED power, corresponding to calculated UV content of ~0, 3, 5, 7, 10, 13, and 16%, respectively (figure 2B). Both of these color measurement systems were based on image processing technology. In the table-down measurement system, the numerical values of lightness, chroma, and hue (LCH; described in box A) are used to characterize the effect of fluorescence on table-down diamond color in precise increments. Note that reported LCH values have been normalized to light background values. Due to camera software differences, values for hue, saturation, and lightness (see box A) were used in the face-up measurement system to correlate color grades and brightness with fluorescence.

Fluorescence Measurement System. A fluorescence measurement system consisting of a sample cham-

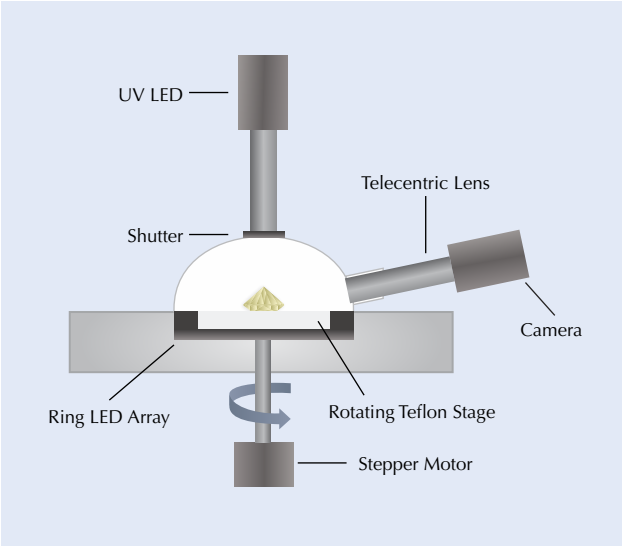

Figure 3. The fluorescence measurement experiment setup used in this study.

ber with a rotational stage, a lens-camera assembly, and a 365 nm UV-LED source was set up to measure the fluorescence intensity of diamond samples in this study (figure 3).

Microscope Imaging. A darkfield imaging system was designed to produce images that represent how diamonds would be viewed during grading. The system consists of a Nikon D800E, a Nikon SB-900 Speedlight, a Sigma 150 mm macro lens, a Stackshot macro rail package, and custom mounting fixtures. Software to control the camera and Stackshot hardware were used to automatically capture and stack a series of images for each diamond through a range of focal planes. The final processed images were used in this study to evaluate face-up appearance.

We set up two different microscopes to help understand the effect of blue fluorescence on diamond appearance under magnification. As shown in figure 4, the standard GIA microscope contains a UV component in the fluorescent overhead lamp and from the halogen bulb in the recessed light chamber used for darkfield illumination. The other testing microscope, an LED-based system, has no UV peak but does have some emissions in the wavelength range of 400 to 420 nm from the overhead lamp. The darkfield illumination of this testing microscope contains absolutely no UV or observable wavelengths below 420 nm (i.e., it is completely lacking a UV component). Photos of stones under the microscope were taken by camera through the ocular lens.

Figure 4. Light spectra collected from a standard GIA microscope overhead fluorescent lamp and darkfield illumination in the recessed light chamber (halogen) show that both contain a UV component (left). For comparison, spectra from an LED testing microscope with no UV component (either in the overhead lamp or in darkfield illumination) are shown on the right.

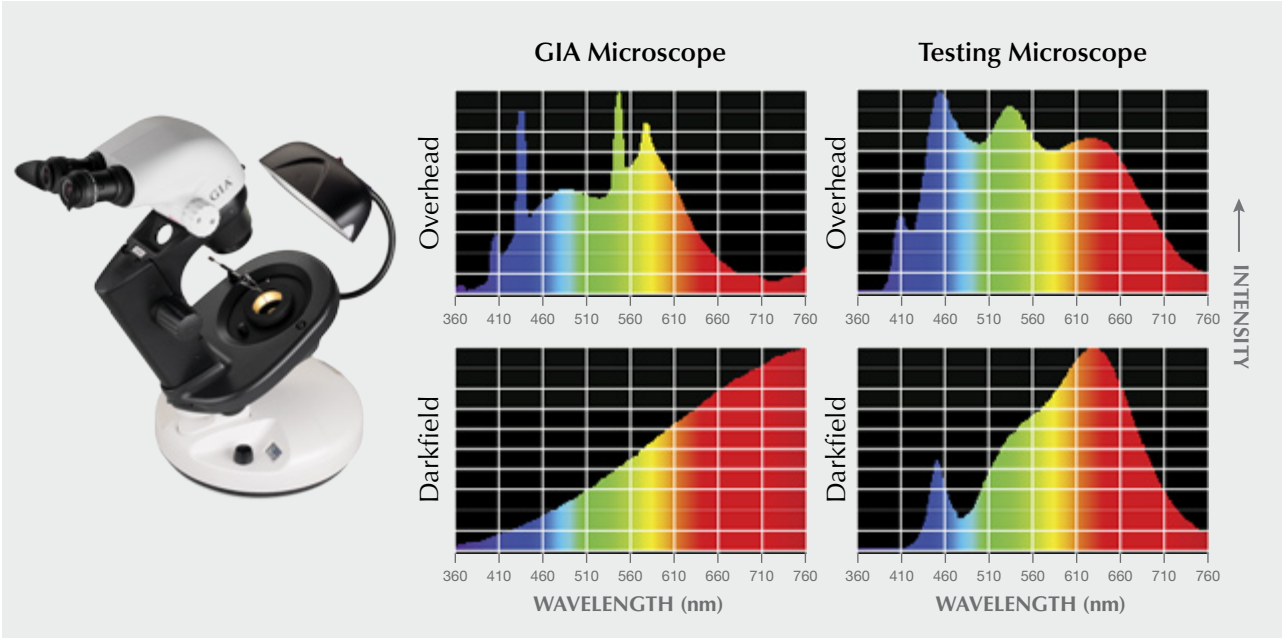

BOX A: MEASURE WHAT YOU SEE—COLOR AND FLUORESCENCE

Whenever an object is viewed, the color seen is a result of the interaction of the light source, the viewer, and the object. In attempting to achieve an accurate and consistent color and fluorescence intensity evaluation, it is important to use a standardized lighting environment that creates reproducible measurement results that characterize color and fluorescence intensity in a quantitative fashion.

Light Sources and Illuminants. A *light source* is a physical device that emits light with relative energy distribution in the ultraviolet to visible spectral range. It can be turned on and off and used in visual color evaluation.

The *color temperature* of a light source is the temperature of an ideal black-body radiator that radiates light of a color comparable to that of the light source, expressed in kelvins (K). There are three common color temperature ranges: warm light (2700 K to 3000 K), cool white (3000 K to 5000 K), and daylight (5000 K to 6500 K).

An *illuminant* is an emission spectrum defined mathematically by a relative spectral power distribution that may or may not be physically achievable as a source.

By CIE definitions, the commonly used "illuminant A" represents incandescent light from a tungsten filament and the "illuminant F" series represents a range of fluorescent lamps. Both can be readily reproduced. The D series illuminants represent natural daylight and include D65 (which refers to average zenith daylight at noon with a correlated color temperature of approximately 6500 K) and D50 (which typically refers to horizon daylight in the early morning or late afternoon with a correlated color temperature of approximately 5000 K). Unlike illuminant A and F series, the D series illuminants were defined as having specific correlated color temperature, chromaticity, and spectral power distribution, without corresponding standard light sources (visit https://cie.co.at/ for more information). Although natural daylight is commonly referred to as a standard light, the appearance and spectral characteristics of natural daylight are affected by various conditions such as the season, time of day, atmospheric conditions, and altitude. All of these factors affect how we can accurately and consistently evaluate color appearance under natural daylight. Thus, the use of simulated daylight has become the standard and accepted method for accurate color quality evaluations in many industries such as paints, plastics, textiles, graphic arts, and computer technology. It is important to note that various common sources available in the market to simulate daylight may be quite different in spectral power distribution from each other and even from any real natural daylight. Sunlight at the earth's surface typically has a UV component between 3% and 5% (calculated from "Reference Solar Spectral Irradiance: Air Mass 1.5," National Renewable Energy Laboratory, www.nrel.gov/grid/solar-resource/spectra-am1.5.html). Therefore, a standardized daylight spectrum containing a UV component is essential to providing realistic, accurate, and consistent color and fluorescence intensity evaluations for diamond.

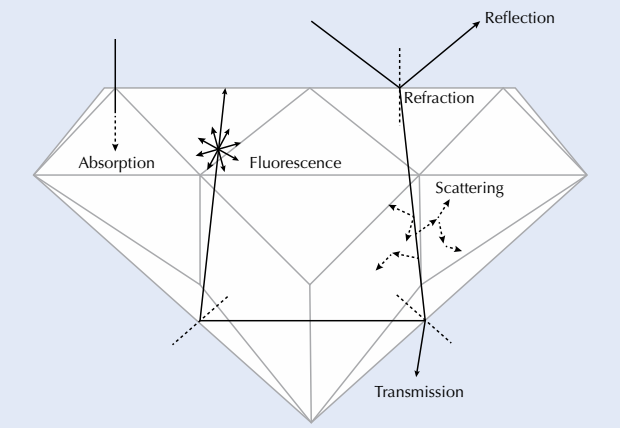

Figure A-1. Light can interact with a faceted diamond in several different ways, as shown here.

Light Interaction with Diamonds. When light strikes a diamond, a small fraction of the light is reflected while the rest is transmitted through the stone. As the light passes through, it may be refracted, absorbed, or scattered by atomic-scale defects in the diamond structure or inclusions, and it can be internally reflected by specially arranged facets in a well-cut diamond. Ultimately, the resultant wavelengths of light that exit the stone and return to the observer create the color of the diamond (figure A-1). Scattering occurs when the transmitted and internally reflected light interacts with microscopic foreign particles or atomic-scale structural imperfections, causing the light to change directions. In most cases, scattering is thought to be responsible for an apparent reduction in contrast and a hazy appearance. When the particulate matter that is often responsible for light scattering is the same size or smaller than the wavelength of light in the visible range (400–700 nm), the scattering will cause a milky opalescence phenomenon known as the Tyndall effect. While scattering does affect appearance, absorption of the light by atomic-scale defects tends to have the greatest impact on diamond color by preventing particular wavelengths from being transmitted to our eyes. Additionally, when the UV component of light is absorbed by certain diamond defects, additional light of a different wavelength in the visible range is often emitted, and this is known as fluorescence. In this paper, we specifically examined the impact of blue fluorescence (by far the most common fluorescence color in natural diamond) on the appearance of faceted diamonds.

Color Space. There are different color spaces defined by the color science community to communicate and express the color of objects. GIA describes color in terms of hue, tone, and saturation (King et al., 1994). Hue refers to the diamond's characteristic color, tone to the color's relative lightness or darkness, and saturation to the color's depth or strength. In this study, we use CIE L*C*H color space (figure

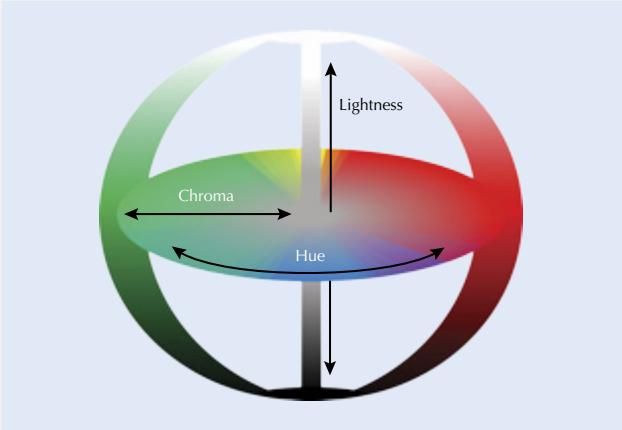

Figure A-2. Conventional color space includes three attributes: lightness, chroma, and hue.

A-2) according to GIA convention to evaluate color attributes and accurately express color and fluorescence intensity measurements in numerical terms. In this color space, L indicates lightness (also referred to as tone), C represents chroma (also known as saturation), and H is the hue.

Lightness (tone): The attribute by which a perceived color is judged to be equivalent to one of a series of grays ranging from black to white (ASTM, 1996).

Chroma (saturation): The attribute used to indicate the color's degree of departure from a gray of the same lightness (ASTM, 1996). It typically refers to a color's purity, intensity, or saturation.

Hue: The attribute of color perception by means of which a color is judged to be red, orange, yellow, green, blue, purple, or intermediate between adjacent pairs of these, considered in a closed ring (ASTM, 1996).

Due to system limitations, HSL color space was used for color evaluation in the face-up measurement system. While broadly comparable to LCH, the HSL color space consists of H indicating hue angle, S representing saturation, and L indicating lightness (H and L are defined above, while S correlates with chroma).

Color and Fluorescence Measurements. To help readers better understand the correlation of color terminology with the visual appearance of diamonds, figure A-3 shows images of four GIA research stones with numerical values for lightness, chroma, and hue using the color measurement experiment setup with a halogen light source with daylight filter. All of the research stones are in the D-to-Z yellow hue range, and chroma measurements are indicative of the GIA color grades D, H, J, and L.

Figure A-4 shows a different set of four research stones under UV light (365 nm). Their blue fluorescence intensities are indicated by the lightness measurement under UV, which corresponded to Faint and Strong fluorescence descriptions as reported by GIA. These are useful examples to show that each fluorescence description covers a range of actual fluorescence intensities. Samples A and B are both described as having Faint fluorescence, while samples C and D are reported as Strong, despite the obvious differences in lightness and apparent fluorescence intensities.

Figure A-3. Examples of color measurements on a set of GIA research stones show the variance in color space attributes with color grades.

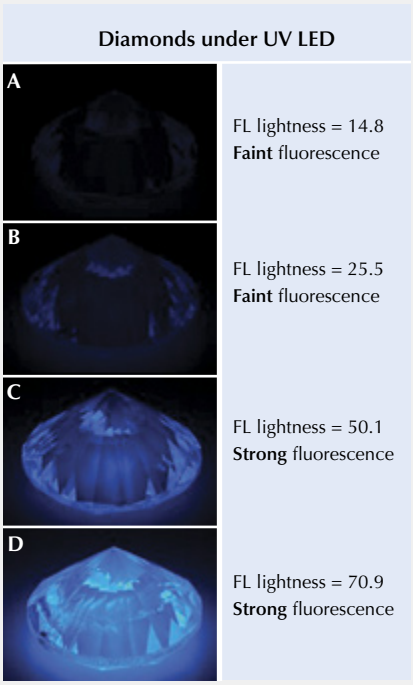

Figure A-4. Fluorescence measurements on a set of GIA research stones show the correlation between fluorescence intensity and lightness.

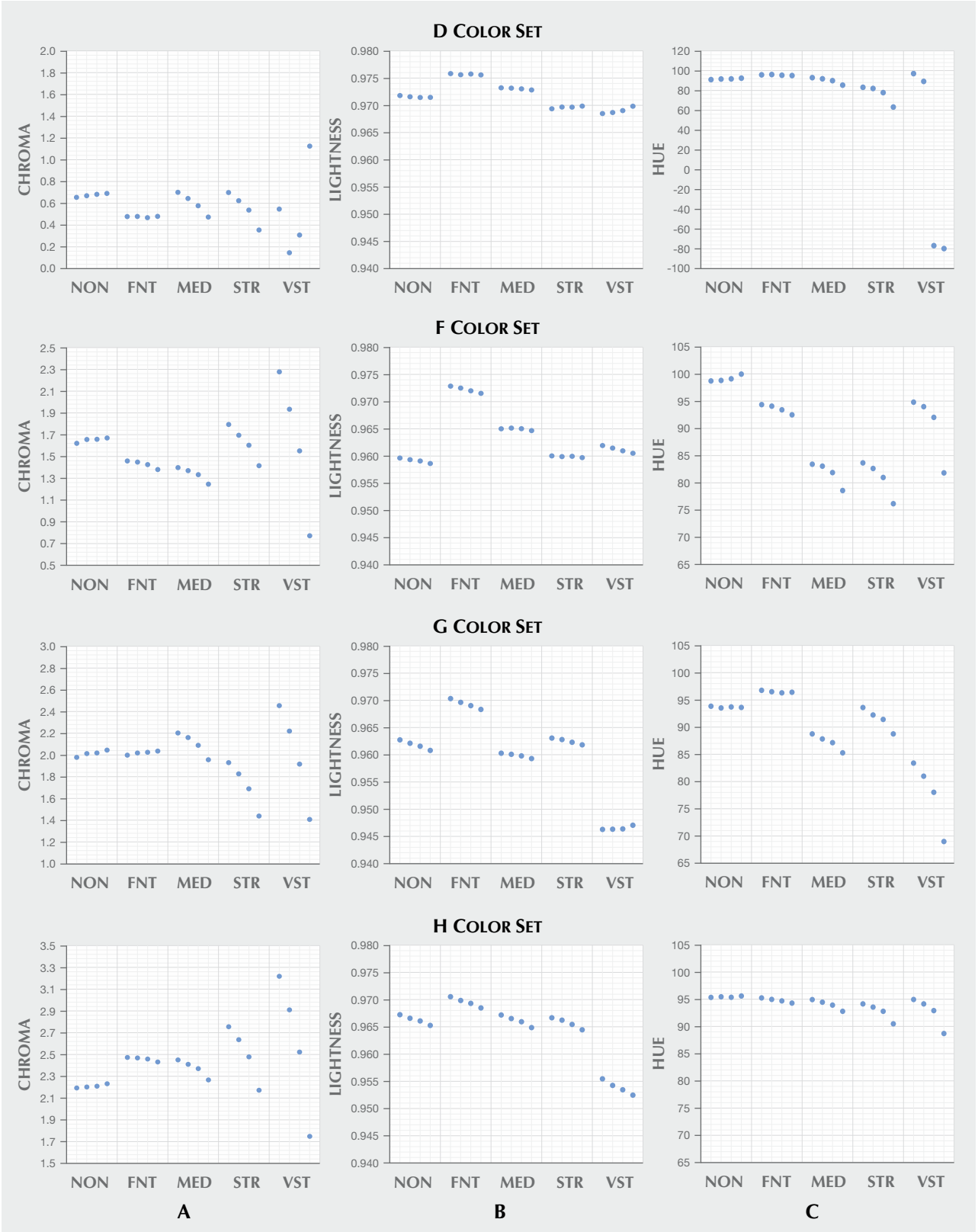

Figure 5. Trends of chroma, lightness, and hue can be seen under different UV intensities using the table-down color measurement system on D, F, G, and H color sample sets. The four consecutive data points in each color and fluorescence value (from left to right in each grouping) represent data collected at UV increments of <1%, 2%, 3%, and 5%.

	Without UV	With UV	Lightness		Chroma		Hue	
			No UV	UV	No UV	UV	No UV	UV
F color, NON FL			0.96	0.96	1.6	1.7	99	100
F color, VST FL			0.96	0.96	2.3	0.8	95	82

Figure 6. Stones in the F color set with fluorescence descriptions of None and Very Strong are seen without UV and with high UV intensities from the table-down color measurement system, along with corresponding attributes.

Modulation Transfer Function Measurement System. A modulation transfer function (MTF) measurement system was configured using a sample chamber, a lens-camera assembly, a light source with tunable UV content, and a micro slide with a sinusoidal array. The MTF measurement system uses image processing technology to produce percentage contrast values from the sinusoidal array target. Box B explains how MTF can be used to assess diamond transparency.

RESULTS

Table-Down Color. Similarly sized diamonds representing a cross section of color grades and fluorescence descriptions were measured on the table-down color measurement system (table 3). Each sample was measured under the same lighting environment with UV content of <1%, 2%, 3%, and 5% at 368 nm. Figure 5A shows how chroma values change with different UV intensities for D-, F-, G-, and H-color diamonds with fluorescence descriptions of None, Faint, Medium, Strong, and Very Strong. Diamonds with fluorescence descriptions of None or Faint show a negligible difference in chroma values as the UV content increases. Those with Medium fluorescence start to show a slight decrease in chroma values as UV content increases. Diamonds with Strong or Very Strong fluorescence descriptions show obvious reductions in chroma values with increasing UV content. The color can change as much as two color grades for diamonds with Very Strong fluorescence as UV content increases from <1% to 5%. The D-color diamond with Very Strong fluorescence shows a sharp reduction in chroma between <1% and 2% UV content, followed by a sharp increase in chroma as UV content increases to 3% and 5%. The reduction in chroma corresponds to a desaturation of the subtle yellow color component as it becomes "neutralized" by blue fluorescence; the increase in chroma is caused by the fluorescence emission, which begins to dominate the color and shifts the hue from yellow toward blue.

Figures 5B and 5C show how lightness and hue values for these diamonds change under different UV intensities. For lightness, D- and F-color diamonds do not show an obvious change as UV content increases, whereas nearly all G- and H-color diamonds show a consistent decrease in lightness values across fluorescence descriptions. Diamonds with fluorescence descriptions of None or Faint show negligible changes in hue value as UV content increases. Diamonds with Medium fluorescence start to show some change in hue value with higher UV content, and those with Strong or Very Strong fluorescence show sharp changes in hue value as UV content increases. The D-color diamond with Very Strong fluorescence shows a significant change in hue value, from 100 to –80, as UV content increases to 3%. This dramatic change in hue value represents a hue change from yellow to blue.

The diamonds in the F color set with fluorescence descriptions of None and Very Strong are shown in figure 6 in lighting environments with no UV con-

	Without UV	With UV	Lightness		Chroma		Hue	
			No UV	UV	No UV	UV	No UV	UV
F color, NON FL			0.97	0.97	0.3	0.3	58	59
F color, VST FL			0.92	0.93	0.3	0.4	139	163

Figure 7. The same stones in the F color set from figure 6 are seen here without UV and with maximum UV intensities from the face-up imaging system, along with corresponding attributes.

tent (<1%) and with relatively high UV content (5%) when table-down color measurements were made. When we add UV to the lighting environment, there is no obvious color change in the diamond with a fluorescence description of None. The diamond with Very Strong fluorescence, however, shows a desaturated color as UV is added to the lighting environment. This demonstrates how blue fluorescence can neutralize a yellow color in some diamonds by the complementary color principle. The hue angle moved from normal yellow (95) to blue (82), and the chroma value decreased from 2.3 to 0.8.

Face-Up Color. Faceted diamonds (table 3) with a range of fluorescence descriptions were imaged using light with incrementally higher UV content. For each face-up image, a square region confined to the table of the diamond was selected for measurement. The average hue, saturation, and lightness for the array of pixels in the selected area were calculated for each image. A diamond's face-up color is affected by the pattern and reflections from light return, which depend mainly on cutting parameters. Thus, the quantified hue, saturation, and lightness values in this process are not comparable to the color derived from the table-down color measurement system. Using the stone with a fluorescence description of None in each color grade as the baseline, the resulting values are compared to the level of UV content for the related images to examine the effect of UV on the face-up color and appearance of diamonds with different fluorescence descriptions.

The color of diamonds with weak or no fluorescence is shown to be unaffected by UV, while the color of diamonds with stronger fluorescence is systematically altered. The stones in the F color set with fluorescence descriptions of None and Very Strong from the face-up imaging system show that for diamonds with little to no fluorescence, the color and appearance do not change with the addition of UV, but for diamonds with fluorescence, the addition of UV causes the hue and lightness values to increase and saturation to decrease. This makes sense if we consider that the mechanism of fluorescence converts invisible UV light into visible light, thereby increasing the observed light return. Saturation values for diamonds with fluorescence are reduced with exposure to UV as the blue fluorescence neutralizes their normally yellow hue. However, if the measured hue changed from the yellow to blue range, we may see a slight increase in saturation with increasing UV (figure 7, bottom). Our results are consistent with the face-up trends visually observed by Moses et al. (1997), which suggested that the strongly fluorescent diamonds were perceived to have a better color appearance when viewed face-up.

Transparency. *Microscope Imaging*. Figure 8 shows a D-color diamond with Very Strong fluorescence (left) next to a nonfluorescent D-color diamond (right)

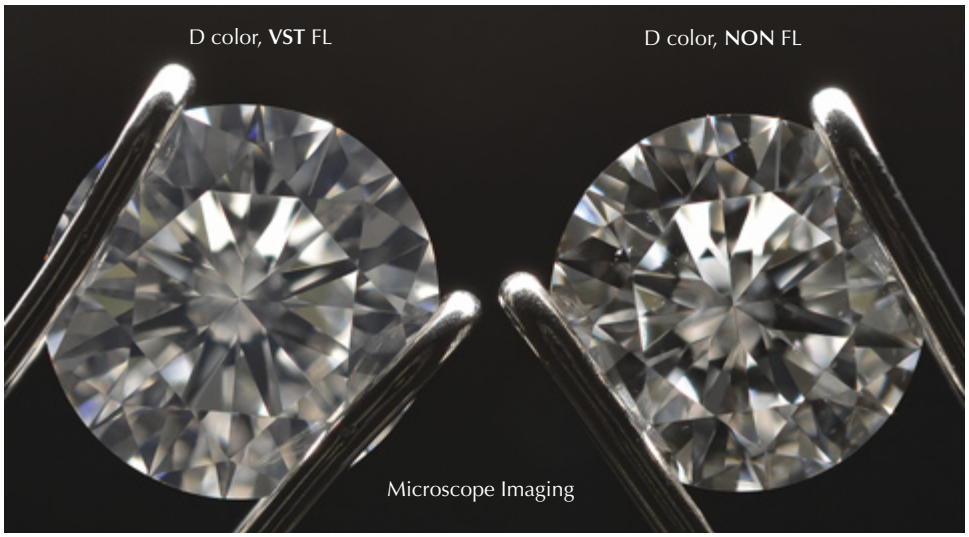

Figure 8. The stones with Very Strong fluorescence and None in the D color set are shown under the same microscope setup for transparency evaluation.

under the same lighting condition (samples from the D color set in table 3). With the same color grade and similar proportions, the diamond with Very Strong fluorescence appears slightly more "milky white" than the diamond with no fluorescence; the pattern of the diamond with Very Strong fluorescence also looks softer than the pattern in the diamond with no fluorescence, which is very crisp and sharp. We have examined many diamonds with the same color grade, similar proportions, and fluorescence descriptions ranging from None to Very Strong that do not have a hazy appearance (figure 9A). We also observed two diamonds, one with a fluorescence description of None and the other with Strong fluorescence, that showed

Figure 9. Diamond images with different degrees of haziness/transparency are plotted by fluorescence intensity.

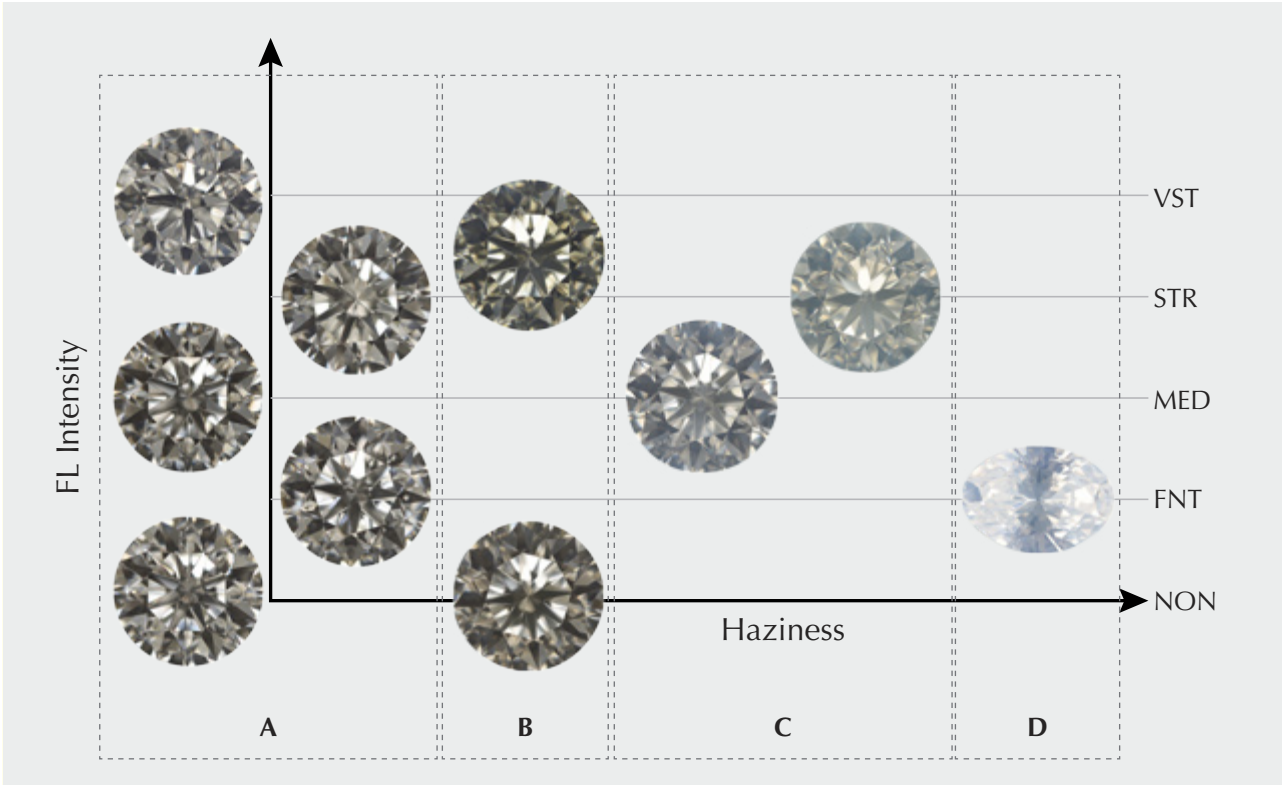

Figure 10. Sets of diamonds with different UV intensities were examined and imaged under microscope darkfield illumination, with and without UV content.

the same degree of slight haziness (figure 9B). We have seen diamonds with Medium and Strong fluorescence that have very obvious haziness (figure 9C), and a diamond with Faint fluorescence that was so milky it received a Fancy White color grade (figure 9D). Given that there is no significant correlation between the occurrence of haziness and fluorescence intensity from our observations, we believe there is no inherent link between the two.

In order to distinguish between haziness created by light scattering and contrast loss due to fluorescence, pairs of diamonds with pertinent differences were compared microscopically in two different darkfield lighting environments (figure 4): one containing UV and one without UV. With UV, the diamond with a fluorescence description of None appears quite clear, while the diamond with Strong fluorescence looks very hazy (figure 10A, left). Without UV, the diamond

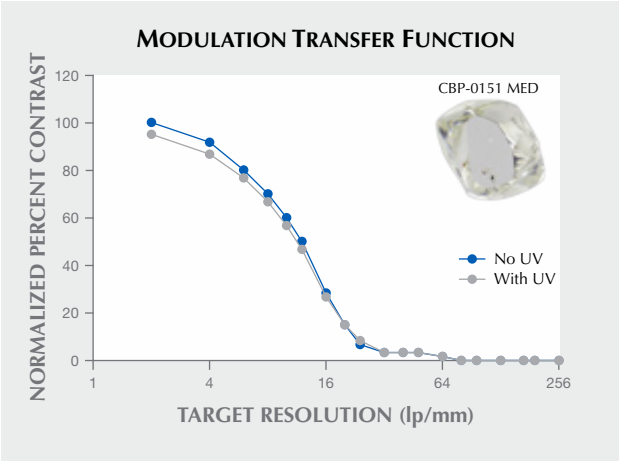

Figure 11. MTF measurement is shown for a diamond with Medium fluorescence. The reduction in percentage contrast values under UV excitation indicates contrast loss due to fluorescence.

with Strong fluorescence is still hazy, though possibly to a somewhat lesser degree (figure 10A, right). Thus, it appears that fluorescence is not the main contributor to the haziness of this diamond. Figure 10B shows two G-color diamonds with no apparent haziness. Viewed under the microscope lighting with UV content (left), it is easy to see blue luminescence from the diamond with Very Strong fluorescence. However, this diamond does not show obvious haziness under lighting environments with or without UV content. The last pair shown (figure 10C) have Strong fluorescence. Without UV, one appears clear while the other is hazy. With UV content, we observe the same thing. However, it appears that the haziness of the diamond, together with the fluorescence, makes the stone look brighter and whiter.

Modulation Transfer Function. Contrast reproduction and optical resolution of diamond samples with a range of fluorescence intensities were measured using modulation transfer function analysis as described in box B. Measurements were made while the samples were exposed to UV and while they were not exposed to UV. By comparing measurements of samples with different fluorescence intensities, the effect of fluorescence on contrast reproduction and optical resolution can be observed. For this study, contrast measurements collected with and without UV are normalized to a single maximum measured contrast.

Figure 11 shows differential percentage contrast measurements for one diamond plate with Medium fluorescence. In this figure, the x-axis units are line-pairs per millimeter and the y-axis units are normalized percentage contrast. Because the contrast values for the series collected with UV exposure are less than the contrast values for the series collected without UV exposure, a reduction in contrast due to UV exposure is measured in this fluorescent diamond plate.

The differences in contrast between measurements made with and without UV exposure for the 13 diamond plates included in this study are shown in figure 12. Fluorescent samples are shown to have reduced contrast when exposed to UV, while inert samples are unaffected. The summed contrast difference for each sample is plotted against fluores-

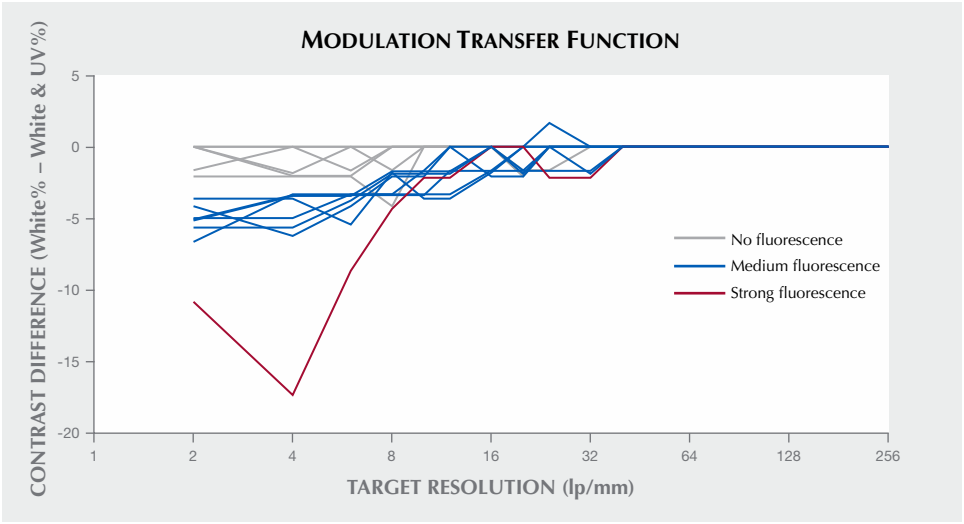

Figure 12. Contrast loss under UV excitation was determined on 13 diamond plates.

BOX B: MEASURE WHAT YOU SEE—TRANSPARENCY

When looking at a gem diamond, an observer usually focuses on color, clarity, and cut. Rarely does transparency come to mind, as most people assume that all gem diamonds are completely transparent. This is not always the case, however, and reduced transparency can have a significant effect on a diamond's appearance. While transparency can be assessed visually, that approach tends to be subjective and difficult to quantify. Evaluating the contrast in a stone is a more objective approach to this problem.

Transparency: The degree of regular transmission, and thus the property of a material by which objects may be seen through a sheet of that material (ASTM, 1996).

Haziness: An appearance produced by the scattering of light in a specimen, responsible for the apparent reduction in contrast of objects viewed through it (ASTM, 1996).

In optical science, a modulation transfer function (MTF) is routinely used to measure the ability of an optical component to transfer contrast at a given resolution—i.e., its optical transparency. Optical components (a lens, for example) can cause resolution and contrast to be reduced (figure B-1, top) when used in an optical system. This effect can be characterized by measuring lightness across a series of equally spaced, alternating black and white lines imaged through the lens (figure B-1, bottom) and calculating contrast as the difference in lightness between the black and white lines. Then, by comparing this contrast measurement to a maximum measurable contrast, using the formula in figure B-2, the percentage contrast can be determined. Percentage contrast measurements using a range of line-pair frequencies describe the transparency of the lens. We adapted this concept to evaluate the transparency of diamond plates with different fluorescence intensities under lighting environments with and without a UV component. An optical target from Edmund Optics with line-pair frequencies ranging from 2 to 256 lp/mm (line-pairs per millimeter) was used for this study.

Diamond Plates. MTF was used to measure the transparency of the diamond plates, which are placed between a lens-camera assembly and an optical target (figure B-3, A). An image is captured and cropped to include only the area of interest. A custom application calculates the average lightness value for each column of pixels in the image and uses those values to identify the locations of a series of local maxima and minima that correspond to the location of line-pairs in the optical target (figure B-3, B). Lightness values at these locations are paired together across each row of pixels, and their differences in value are assembled into a density plot to observe their distribution. The average value in the data set is used to calculate the normalized percentage contrast for that target (figure B-3, C). The percentage contrast values are calculated using an image of a plate taken with no UV stimulation against an image taken with UV stimulation; therefore, the plate is being measured against itself. Doing this removes concerns about path length differ-

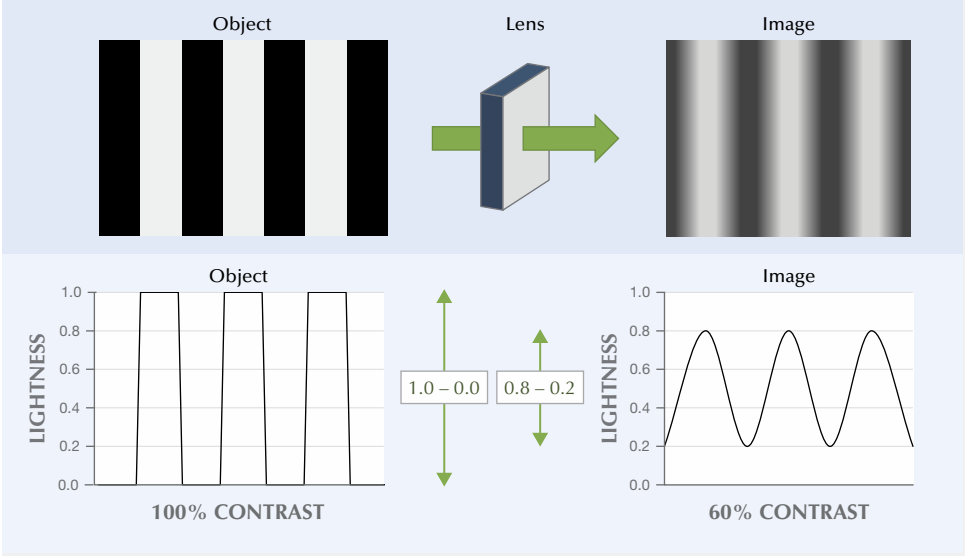

Figure B-1. An object imaged through a lens is shown to have reduced contrast and resolution.

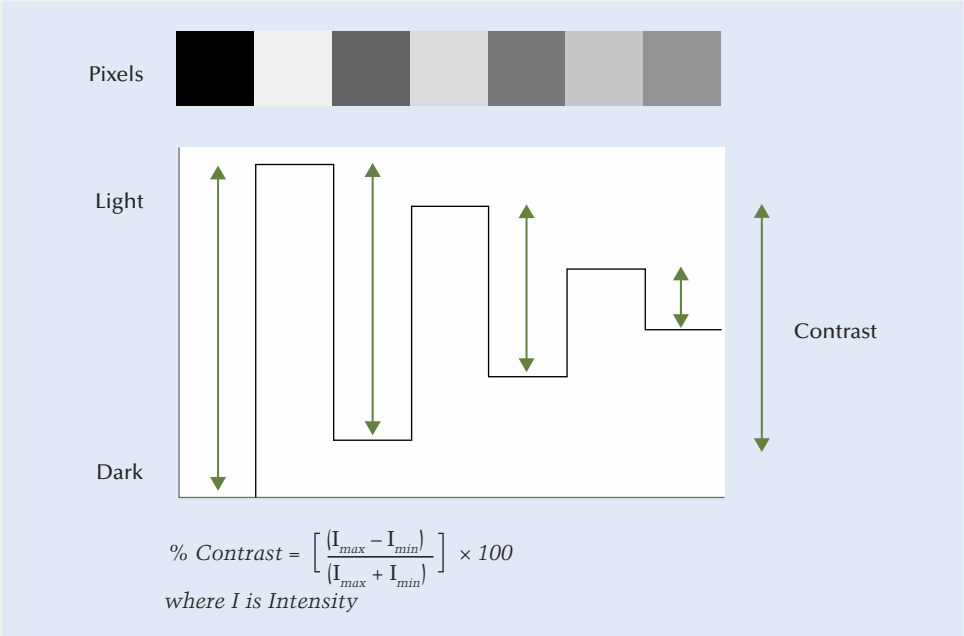

Figure B-2. Contrast was calculated as shown here for the modulation transfer function (MTF) study.

ences, which allows us to compare bulk fluorescence values.

Polished Diamonds. Patterns of bright and dark areas produced by light interacting with the facets of a well-polished diamond create a mechanism by which an observer can gauge the transparency of that diamond. When a diamond is very transparent, these patterns are perceived to be high in contrast, while for less transparent stones the perceived contrast is reduced—dark areas are less dark, bright areas less bright. The effects of poor polishing were not investigated in this study.

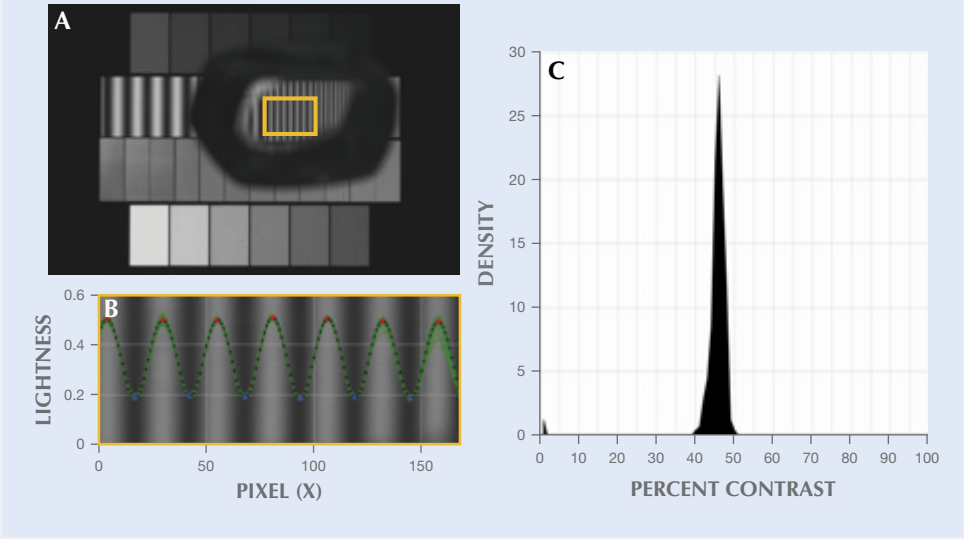

Figure B-3. An optical target is imaged through a diamond plate to conduct MTF measurements. Custom software analyzes a select area of the image and produces the percentage contrast value.

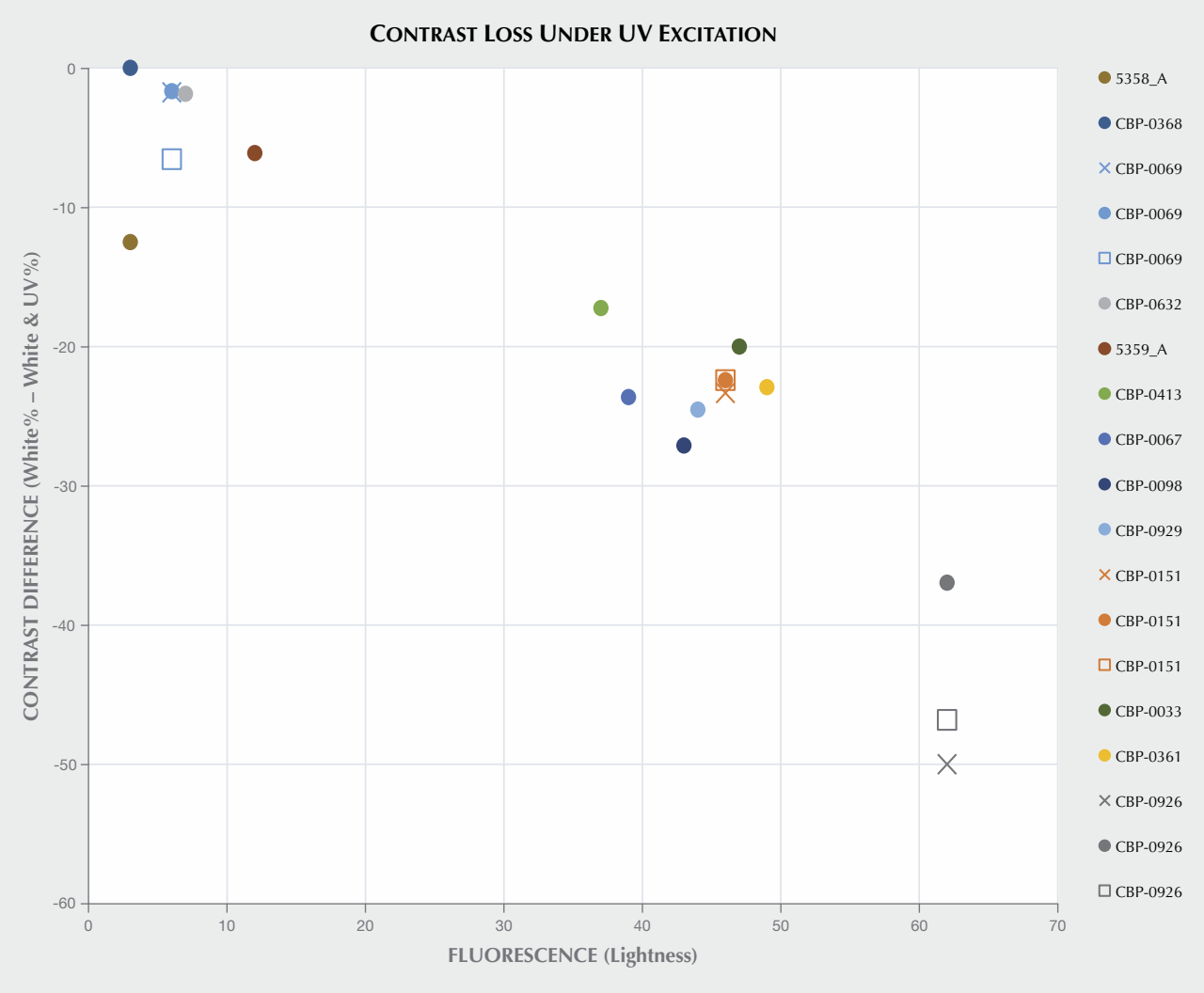

Figure 13. Correlation was observed between fluorescence intensity and contrast difference from measurements made with and without UV.

cence intensity in figure 13 and shows a correlation between these two factors. Replicated measurements for three samples are included in this figure to demonstrate measurement repeatability. The observed changes in contrast difference do not correlate with strain intensity or diamond type, strongly suggesting that the contrast loss is primarily due to fluorescence.

DISCUSSION

Illumination Standardization. Fluorescence is an intrinsic property of more than 30% of the diamonds seen by GIA's laboratory (Moses et al., 1997). Some in the diamond trade argue that because typical office lighting lacks 365 nm and 385 nm UV content, it reveals the "true color" of diamonds. Based on figure 14, we can see that office lighting does in fact contain some amount of UV light. We also need to keep in mind that blue fluorescence caused by the N3 defect can be activated by wavelengths up to 420 nm (Luo and Breeding, 2013). If a lighting environment includes light in the 390–420 nm range, a diamond's color will be viewed with some amount of blue fluorescence from the N3 defect. While most commercial light sources do contain light in the 400–420 nm range (blue light) but little in the UV range (<400 nm), our work investigates the effects of varying the amount of UV light (and thus the fluorescence produced) on a diamond's appearance. Consider, for example, a fluorescent lamp with no emission below 390 nm (figure 15). A diamond with strong fluorescence (left) glows blue

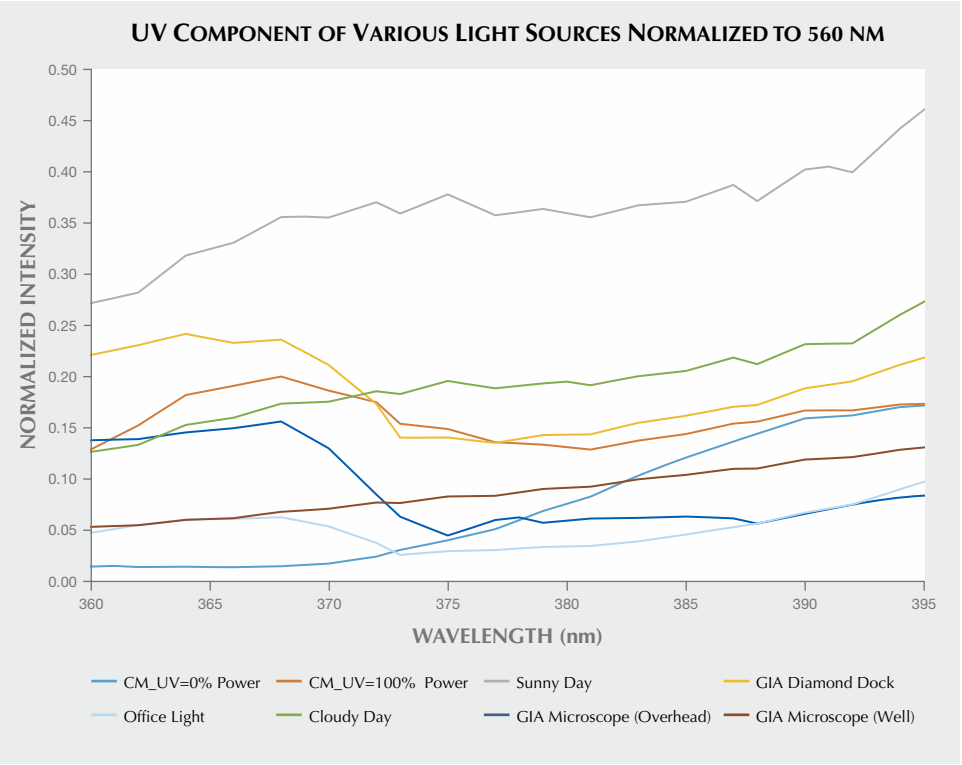

Figure 14. A comparison of the UV content of common light sources, including the color measurement system (CM) used for this study, the GIA DiamondDock, the GIA microscope overhead and well light, office light, and daylight. All spectra have been normalized at the 560 nm value by convention (King et al., 2008).

in this light, while a nonfluorescent diamond (right) does not. This illustrates the importance of using standardized illumination with fixed UV content to define the color grade of a diamond.

UV content is typically reported as a peak intensity output percentage normalized to a certain wavelength. However, depending on the shape and position of the UV peak, the fluorescence reaction will differ and consequently the visual appearance of the fluorescence and its effect on diamond color will also be different (Luo and Breeding, 2013). In order to consistently evaluate fluorescence and its effects on overall appearance, we again emphasize that an agreed-upon standard of illumination for color meas-

Figure 15. Two G-color stones with similar size were imaged for comparison under the overhead lamp from the testing microscope with no UV peak at 365 nm but with wavelength in the 390–420 nm range.

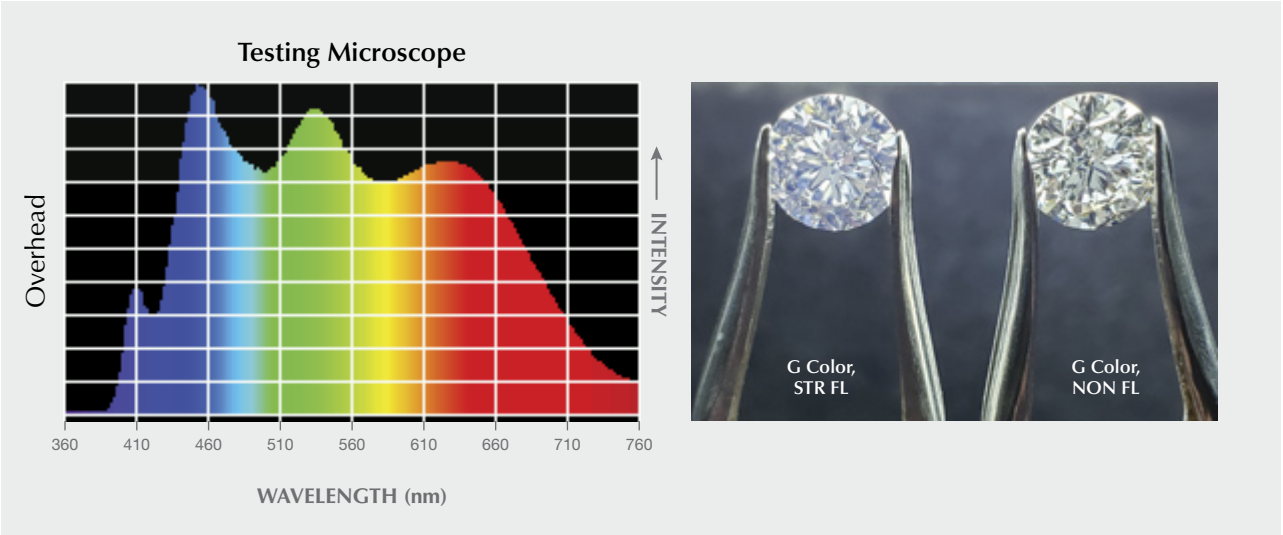

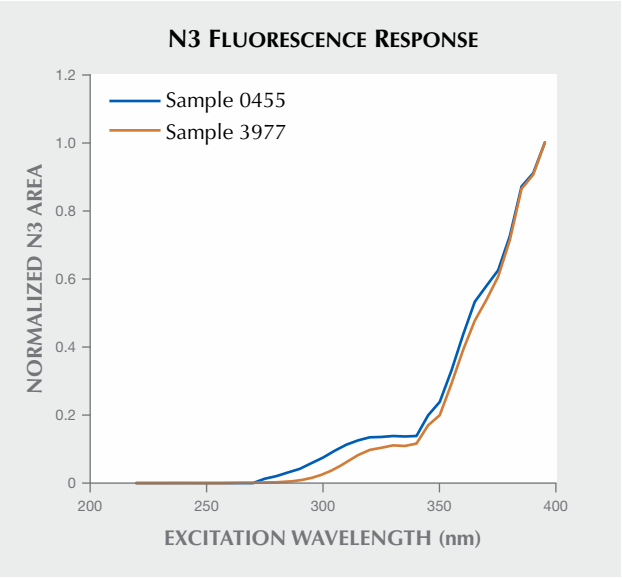

Figure 16. Two samples containing N3 were excited with narrow bands of light and the emission spectra were recorded. The area under the N3 zero-phonon line was calculated for each spectrum and plotted against its excitation wavelength, with both plots being normalized to one. Data obtained from Luo and Breeding (2013).

urement and visual observation with a fixed UV content of specific known wavelength is essential.

Fluorescence N3 Center Excitation Curve. An important metric when considering a light source is how much UV light it contains. However, quantifying the amount of UV contained in a light source is not a straightforward thing to do in a way that is useful in understanding the effect of fluorescence intensity. Different wavelengths of UV light will excite the N3 defect at different efficiencies, meaning different excitation wavelengths of a given intensity will produce different intensities of emission.

To get an idea of how the different wavelengths affect the N3, we used data from a previous study where two samples were run on a luminescence spectrometer that excited the sample with a narrow band of light and recorded the emission spectrum (Luo and Breeding, 2013). Figure 16 shows the normalized area under the N3 zero-phonon line against the excitation wavelength. We can see that from 225 to 275 nm, there is essentially no emission for the excitation used. From 275 to about 340 nm, there is a slow increase, and then from 340 to 395 nm there is a rapid increase. Above 395 nm, the excitation band overlapped too much with the N3, so accurate area measurements were not possible. The shape of these plots tracks with the previously reported photoluminescence excitation (PLE) spectrum of the 440 nm side band of the N3 (Luo and Breeding, 2013).

A light source used to inspect or grade diamonds may contain a distribution of UV light intensities as a function of wavelength. Each of these wavelengths will interact with the N3 defect and, based on the efficiency of absorption and fluorescence reaction, contribute varying amounts to the total visual fluorescence. If we use the area under the N3 zero-phonon-line (ZPL) as a proxy for visual fluorescence intensity, we can see that the wavelength of the UV source will affect the intensity of the fluorescence. In theory, based on the chart in figure 16, we would expect a stone containing only N3 excited with a given intensity of pure 350 nm light to be approximately one-third as bright as the same stone excited with an equal intensity of pure 375 nm light.

Figure 14 shows the UV component of a number of common light sources, all normalized to the full spectrum's value at 560 nm. If we take these spectra and multiply them by the normalized N3 area curves and integrate that total area, we can compare the relative fluorescence brightness we would expect from each light source. To compare different light sources, we calculated the integrated area under the normalized N3 area excitation curves (N3) multiplied by the UV component of the listed light source (normalized to 560 nm) from 360 to 395 nm. In table 5, we see some surprising results. The expected fluorescence brightness for the table-down color measurement system with 0% UV LED power is not 0, but is over half the value of the system at 100% UV LED power, due to a slight UV component of the LEDs used to generate the "white light" portion of the spectrum. This is important to note because even a system labeled as a "white light" source may contribute to fluorescence.

Blue Fluorescence Effect on Color and Brightness. GIA has consistently used approximately 2% UV content in the GIA DiamondDock. Using the GIA DiamondDock as a standard for UV content (table 5), if diamonds with similar color but different fluorescence intensities are brought into an environment with higher UV content—such as outdoors under sunlight—we would not expect any observable change in color or brightness among diamonds with fluorescence descriptions of None, Faint, or

Medium. In contrast, we should see changes in color and brightness in diamonds with Strong or Very Strong fluorescence that make them appear more colorless in sunlight. If we view these same examples in an environment with reduced UV content (such as most office lighting), the diamonds with fluorescence descriptions of None, Faint, or Medium will appear unchanged while those with Strong or Very Strong fluorescence will appear more yellow and less bright.

Blue Fluorescence Effect on Transparency. When we view a nonfluorescent diamond, we typically see a very distinct pattern with sharp boundaries between dark and light areas (figure 8, right) created by the facet arrangement. If we look at this pattern in a diamond with Very Strong fluorescence, in a lighting environment with some UV content (figure 8, left), we see that the fluorescence makes the stone brighter; however, because the dark areas are less dark and the light areas gain a blue hue from the fluorescence, contrast is reduced. For this study, we focused on the round brilliant cut; other shapes or cutting styles were not evaluated and may be affected differently. From our MTF studies, contrast loss was measureable at line-pair frequencies less than 20 lp/mm for plates with Medium, Strong, or Very Strong fluorescence. Five senior diamond graders at GIA were given the same micro slide used in the MTF measurements and asked to note the highest frequency of line-pairs they could resolve in a standard grading environment with a 10× loupe. The graders reported anywhere between 32 lp/mm and 48 lp/mm as the limit of their visual resolution. Therefore, any contrast difference measured at frequencies less than 40 lp/mm could potentially be noticeable to a diamond grader under controlled conditions.

TABLE 5. Comparison of N3 excitation curves by various UV light sources.

Light Source	Total Area Under Curve
GIA microscope overhead light	11.09
Office light	16.41
Color measurement system with no UV	18.18
GIA microscope well light	18.71
Color measurement system with UV	30.95
GIA DiamondDock	36.62
Daylight – cloudy day	40.22
Daylight – sunny day	73.96

Total integrated area = $\int_{360}^{395} N3 \times UV \, d\lambda$

Several studies (Gu et al., 2019; Eaton-Magaña et al., 2019) have suggested that a milky or hazy appearance observed in Fancy white, type IaB diamonds is due to nano-inclusions or complex structural defects known as dislocation loops. Light scattering (see the Tyndall effect in box A) caused by these imperfections creates the milky or hazy appearance in these diamonds and affects their transparency. When observed with a diamond in the face-up orientation, scattering will cause a contrast loss in the facet pattern similar to that caused by fluorescence. When a diamond is strongly fluorescent and also contains light-scattering structural defects, these producers of contrast loss seemingly combine to cause a noticeably milky or hazy appearance.

Characterization of Contrast Loss Caused by Fluorescence and Haziness. Both fluorescence and light scattering cause contrast loss when looking at a diamond face-up, and it can be difficult to distinguish between their effects. We designed a bulk contrast evaluation system and explored its ability to measure contrast loss. In this evaluation, no considerations were made regarding the cause of haziness in the sample, which could be fluorescence, nano-inclusions, or dislocation loops—we only measured the contrast in the face-up pattern. The x-axis units in figure 17 are lightness, where 0 is darkest and 100 is lightest. The y-axis units describe the quantity of pixels in the image that have the corresponding lightness value. For a relatively clear diamond (top), we see the largest distance between the majority of dark pixels and the majority of the lightest pixels. As the sample gets hazier (middle and bottom), we see contrast loss (and a shrinking of this distance between the majority of the lightest and darkest pixels)—pixels that make up the dark areas in the facet pattern are lighter, and the lightest areas in the facet pattern are darker. The authors consider this bulk contrast evaluation method a relatively easy and consistent way to evaluate haziness and its impact on clarity grading of diamonds.

CONCLUDING REMARKS

Among the D-to-Z color gem diamonds that fluoresce, our results strongly suggest that the color will be noticeably impacted only in those few that show Strong to Very Strong blue fluorescence. Of course, the degree of impact depends largely on the amount

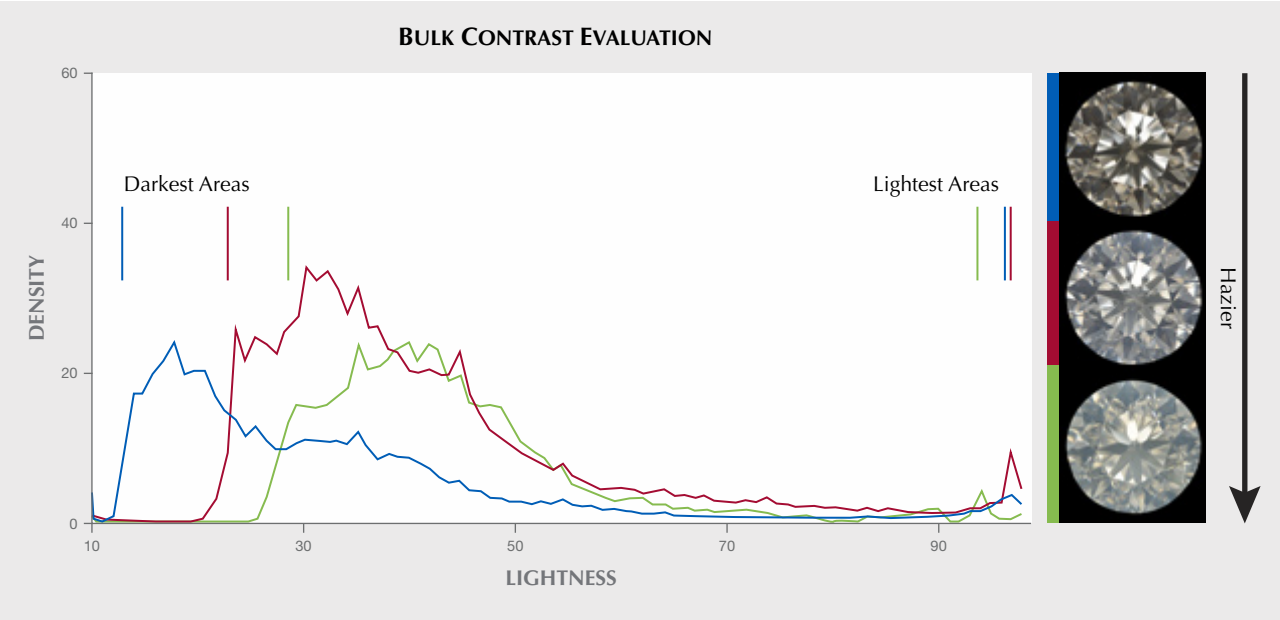

Figure 17. The bulk contrast measurement used in our study provides a relatively easy way to evaluate the face-up appearance of diamonds.

of UV component in the lighting source, meaning that a standardized lighting environment with a fixed amount of UV is critical for consistency in the color grading of diamonds. The GIA DiamondDock's UV content of ~2% provides an appropriate compromise between the UV content in sunlight (3% to 5%) and that in most fluorescent and LED illumination sources used indoors (less than 1%).

We observed that stronger fluorescence produces some contrast loss in gem diamonds. However, our results show that this contrast loss from strong fluorescence does not by itself cause the milky or hazy appearance observed in some diamonds by the trade. Atomic-scale defects in the diamond structure or nano-inclusions appear to be the main causes of the milky or hazy appearance. The occurrence of strong fluorescence in combination with these features may cause a diamond to appear even milkier or hazier, but we saw no evidence that strong fluorescence alone produces noticeable haziness in diamonds that did not already contain light-scattering structural defects or nano-inclusions. The bulk contrast method presented here may also serve as a reliable way to quantitatively evaluate the effect of contrast loss on apparent transparency in future diamond grading processes. We are reviewing these quantitative and semi-quantitative results to see how they might be included in GIA grading reports. We believe this new information will help to create more accurate information in the trade and ultimately allow consumers to select diamonds based on unbiased scientific and aesthetic factors.

ABOUT THE AUTHORS

Dr. Luo is a director of metrology and quality control, Mr. Nelson is a senior metrologist, Mr. Ardon is a research associate, and Dr. Breeding is a senior manager of analytics, at GIA in Carlsbad, California.

ACKNOWLEDGMENTS

The authors thank GIA's Tom Moses, Wuyi Wang, Tsung-Han Tsai, and Jennifer Hwang for many helpful discussions. Assistance from Mitchell Lyn and Curtis Berry in collecting image data at GIA is also greatly appreciated. The authors are grateful for the constructive comments from the three peer reviewers of this article.

REFERENCES

ASTM (1996) *ASTM Standards on Color and Appearance Measurement*, 5th ed. West Conshohocken, Pennsylvania.

Bouman M., Anthonis A., Smans S., Corte K., Chapman J. (2018) The effect of blue fluorescence on the colour appearance of round-brilliant-cut diamonds. *Journal of Gemmology*, Vol. 36, pp. 298–315.

Cowing M. (2010) The over-grading of blue-fluorescent diamonds: The problem, the proof and the solutions. *Journal of Gemmology*, Vol. 32, pp. 38–51.

Eaton-Magaña S., Ardon T., Breeding C.M., Shigley J.E. (2019) Natural-color fancy white and fancy black diamonds: Where color and clarity converge. *G&G*, Vol. 55, No. 3, pp. 320–337, http://dx.doi.org/10.5741/GEMS.55.3.320

Gu T., Ohfuji H., Wang W. (2019) Origin of milky optical features in type IaB diamonds: Dislocations, nano-inclusions, and polycrystalline diamond. *American Mineralogist*, Vol. 104, pp. 652–658, http://dx.doi.org/10.2138/am-2019-6699

King J.M., Moses T.M., Shigley J.E., Liu Y. (1994) Color grading of colored diamonds in the GIA Gem Trade Laboratory. *G&G*, Vol. 30, No. 4, pp. 220–242, http://dx.doi.org/10.5741/GEMS.30.4.220

King J.M., Geurts R.H., Gilbertson A.M., Shigley J.E. (2008) Color grading "D-to-Z" diamonds at the GIA Laboratory. *G&G*, Vol. 44, No. 4, pp. 296–321, http://dx.doi.org/10.5741/GEMS.44.4.296

Luo Y., Breeding C.M. (2013) Fluorescence produced by optical defects in diamond: Measurement, characterization, and challenges. *G&G*, Vol. 49, No. 2, pp. 82–97, http://dx.doi.org/10.5741/GEMS.49.2.82

Moses T., Reinitz I., Johnson M., King J., Shigley J. (1997) A contribution to understanding the effect of blue fluorescence on the appearance of diamonds. *G&G*, Vol. 33, No. 4, pp. 244–259, http://dx.doi.org/10.5741/GEMS.33.4.244

Detection of Color Treatment and Optical Brightening in Chinese Freshwater "Edison" Pearls

Chunhui Zhou, Joyce Wing Yan Ho, Sally Chan Shih, Tsung-Han Tsai, Ziyin Sun, Stephanie Persaud, and Li-Jian Qi

Color origin is an important part of pearl identification for gemological laboratories. Freshwater cultured pearls can exhibit a wide range of colors, which can be either naturally formed or artificially modified by post-harvest treatments. The most common color treatments are dyeing and irradiation. In this project, a group of 23 freshwater "Edison" pearls (a trade name referring to near-round to round freshwater bead cultured pearls invented and produced by Zhejiang Grace Pearl Jewellery Co Ltd in China), reportedly with a mix of natural and treated colors, were analyzed using various gemological and advanced instrumental techniques in order to distinguish their color origin. A number of techniques, including microscopic observation, long-wave UV fluorescence observation, long-wave and short-wave fluorescence spectroscopy, Raman spectroscopy, and trace element analyses, were used in this study. Of the 23 freshwater samples, 19 have been confirmed as bead cultured pearls and 4 have been identified as non-bead cultured pearls. In addition, seven samples have been identified as color-treated, while five of the remaining 16 samples were also identified as being optically brightened (a process commonly used on freshwater cultured pearls to improve appearance factors such as luster). Our results proved that color treatment in these freshwater pearls could be confidently identified using this combination of techniques, as could optical brightening processes that are routinely applied to untreated, naturally colored freshwater cultured pearls post-harvest.

Currently, China is the world's largest producer of cultured pearls, and the majority are cultured in freshwater environments such as rivers, lakes, and ponds (Cartier and Ali, 2013; Zhu et al., 2019). Over the last several decades, advances in freshwater culturing techniques have also significantly improved the quality of Chinese freshwater cultured pearls on the market, such as Ming pearls and "Edison" pearls, to the point where these round bead cultured products can rival saltwater cultured pearls such as akoya, South Sea, and Tahitian pearls (Scarratt et al., 2000; Akamatsu et al., 2001; Fiske and Shepherd, 2007; Hänni, 2011; Karampelas, 2012; Zhou and Zhou, 2015; Otter et al., 2017; Li et al., 2018; Bui et al., 2019). The term "Edison pearl" specifically refers to the bead cultured pearls produced by Grace Pearls of China, while "Ming pearl" is a more generic term that describes high-quality bead cultured freshwater pearls produced by other producers. Recently, stricter enforcement of the Chinese government's environmental policies has impacted the output of freshwater cultured pearls, as many farms were closed down due to pollution problems (Zhou and Lu, 2018). Increasing demand for high-quality freshwater cultured pearls in China and around the world will likely shift the production toward larger, rounder, and more attractive colored pearls in the future.

Detection of color treatment is an important part of pearl identification in gemological laboratories, both for saltwater and freshwater pearls (Elen, 2001; Wang et al., 2006; Karampelas et al., 2007, 2011; Zhou et al., 2012, 2016; Tsai and Zhou, 2020). Freshwater cultured pearls, in particular, can exhibit a

See end of article for About the Authors and Acknowledgments.
Gems & Gemology, Vol. 57, No. 2, pp. 124–134,
http://dx.doi.org/10.5741/GEMS.57.2.124

Figure 1. Five loose "Edison" Chinese freshwater cultured pearls (11–14 mm) surrounded by a 17-inch necklace featuring variously colored round Edison pearls (10.5–13.5 mm). Photo by Robert Weldon/GIA, courtesy of Betty Sue King, King's Ransom.

Figure 2. Twenty-three freshwater Edison pearls ranging in size from 7.63 × 7.46 mm to 13.60 × 13.46 mm were examined in this study; these pearls show various bodycolors that are either natural or modified. Photos by Sood Oil (Judy) Chia.

wide variety of coloration, including white, cream, yellow, orange, brown, pink, and purple. In addition to various artificial color modification treatments, freshwater cultured pearls are also routinely processed after harvest by bleaching and optical whitening and brightening using optical brightening agents (OBA) (Zhou et al., 2020). These two processes have very different mechanisms: Bleaching removes, or reduces the concentrations of, the color-causing pigmentations within pearls, while optical brighteners add an artificial optical effect to pearls, making them look less yellow by increasing the overall amount of blue light emitted due to these chemicals' blue fluorescence properties. It is important to be able to differentiate naturally colored pearls from their treated counterparts from a gemological laboratory point of view, which is the underlying reason for this study.

The global pandemic that started at the beginning of 2020 caused little disruption to the production of freshwater cultured pearls in China, as the harvest usually takes place at the end of the year and the Chinese government's fast control of the virus minimized the impact. However, the export of freshwater cultured pearls has been significantly affected, and dealers are trying to boost domestic sales by emphasizing a strong online presence (Zhou and Chen, 2020). The parent company of Grace Pearl, Zhejiang Dongfang Shenzhou Pearl Group, continues to develop new freshwater pearl products such as the "China Red" (orange and red variety of Edison pearls) and "mini-Akoya" (small white-colored bead cultured pearls), which have gained popularity in the market (Wong, 2020). The capability to accurately detect color treatment can further increase consumer confidence when purchasing these high-quality freshwater pearl products, such as the loose pearls and necklace shown in figure 1.

MATERIALS AND METHODS

The present study focuses on the identification of treated freshwater cultured pearls from a group of 23 variously colored samples (figure 2). These pearls were supplied by Zhejiang Grace Pearl Jewellery Co Ltd in China, the original producer of so-called "Edison" pearls. The 23 undrilled samples range in size from 7.63 × 7.46 mm to 13.60 × 13.46 mm. These were reportedly grown in the cultured pearl farms owned by the company. Such pearls are usually bead

nucleated using *Hyriopsis cumingii* or hybrids of the Chinese *Hyriopsis cumingii* and the Japanese *Hyriopsis schlegelii* mussels. Some of these samples were further treated post-harvest by the producer to enhance their appearance attributes such as bodycolor, overtone, or luster. These samples contained initial labels stating "treated" and "natural," however, no information of optical brightening was mentioned. We regarded these pearls as "unknown" samples and performed the same testing procedures regardless of the labels.

All samples were examined using various standard gemological techniques, including visual observation under a gemological microscope, microscopic imaging using a Nikon SMZ 1500 stereomicroscope, observation of the fluorescence reactions under a conventional 5-watt long-wave UV (LWUV) (365 nm) lamp, and real-time microradiography (RTX) analysis using a Pacific X-ray Imaging (PXI) GenX-90P system with a 4-micron microfocus, 90 kV voltage, and 0.18 mA current X-ray source, fitted with a PerkinElmer 4"/2" dual-view flat panel detector.

A number of advanced instrumental techniques were also applied in this study. These include Raman spectroscopy using a Renishaw inVia Reflex micro-Raman spectrometer system with a 50× magnification Leica objective lens and a 514 nm argon-ion laser (scanning range from 100 to 1600 cm^{-1}), ultraviolet (UV) fluorescence spectroscopy under both long-wave UV excitation with a 385 nm LED light source (M385L2, Thorlabs) and an Avantes AvaSpec-Mini spectrometer (scanning range from 400 to 950 nm), and short-wave UV excitation with a 275 nm LED light source (M275L4, Thorlabs) and an Avantes AvaSpec-Mini spectrometer (scanning range from 300 to 1100 nm). Trace element analyses were conducted using a Thermo Scientific ARL Quant'x energy-dispersive X-ray fluorescence (EDXRF) spectrometer (calibrated with MACS-1 and MACS-3 carbonate standards) and a Thermo Fisher Scientific iCAP Qc inductively coupled plasma–mass spectrometry, coupled with an Elemental Scientific NWR213 laser ablation system (LA-ICP-MS) (three spots on each sample's surface, 55 µm spot size). More details on these gemological and instrumental methods for the application of pearl identification can be found in previously published papers (Zhou et al., 2017, 2019; Nilpetploy et al., 2018; Homkrajae et al., 2019; Sturman et al., 2019; Tsai and Zhou, 2020).

In Brief

- Cultured freshwater "Edison" pearls can exhibit a wide range of colors, which can be either naturally formed or artificially modified by post-harvest treatments.
- The color origin of these pearls can be confidently determined with a combination of conventional gemological tests and advanced analytical methods.
- Some naturally colored "Edison" pearls have also been subjected to an optical brightening process.

RESULTS

Gemological Observations. All 23 samples were either round or near-round, ranging from 7.63 × 7.46 mm to 13.60 × 13.46 mm and from 3.04 ct to 17.47 ct. Their bodycolors exhibited various hues such as pink, gray, purple, orange, yellow, or brown in different degrees of tones and saturations. Standard real-time microradiography analysis revealed that the majority contained a drilled bead nucleus, as expected for Edison pearls. However, four of the 23 samples showed irregular linear internal growth features found in many freshwater non-bead cultured pearls (Scarratt et al., 2000; Krzemnicki et al., 2010), although their external appearances were indistinguishable from the rest of the samples in this group. The four non-bead cultured pearls were FW02, FW03, FW05, and FW07, which were all relatively small (8–9 mm). Technically these pearls were not considered Edison pearls, and they were probably formed by accident when the bead nuclei were rejected by the mussels during growth.

Under a conventional gemological microscope, all of the pearls appeared to have even color distribution. Minor color concentration spots were found on the surface of five samples (FW02, FW07, FW08, FW17, and FW23), yet they were rather sporadic and difficult to see because they were small and faint. Nevertheless, FW08 and FW17 appeared to be color treated based on their bodycolors, possessing "golden" colors that looked very unnatural to the unaided eye and under the microscope. In the authors' experience, such color appearances are almost nonexistent in freshwater cultured pearls. Furthermore, while freshwater pearls may exhibit varying degrees of fluorescence under LWUV excitation based on their bodycolor intensities (usually weaker fluorescence with darker or more saturated colors), the strong, spotty, and more bluish fluorescence found in five of the samples (FW01, FW04, FW06, FW11, and

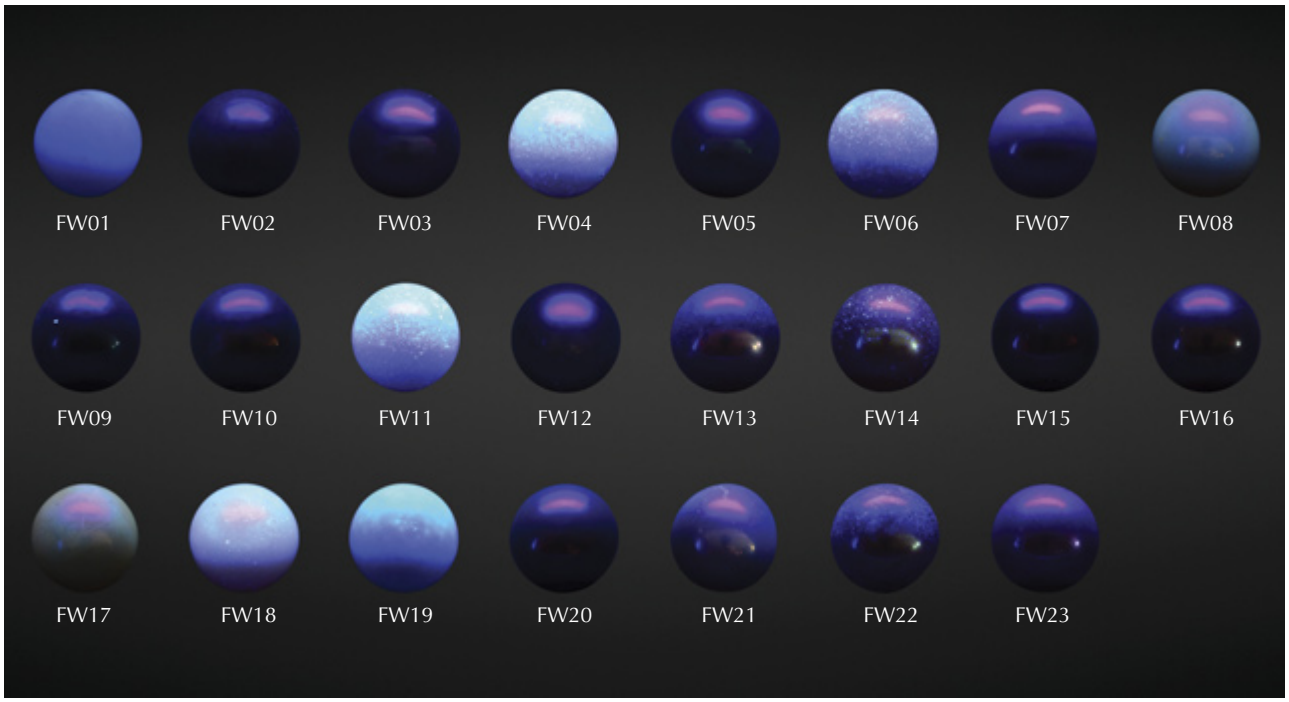

Figure 3. The 23 pearls displayed different fluorescence reactions under LWUV excitation, indicating that FW01, FW04, FW06, FW11, and FW19 might have been optically brightened. While exhibiting similar fluorescence intensity, FW18's fluorescence hue looked less bluish and was consistent with its light bodycolor. FW08 and FW17 displayed unusual orangy yellow fluorescence potentially due to the dye on their surfaces. The rest of the group was inert under LWUV excitation. Photos by Sood Oil (Judy) Chia.

FW19) suggested that they had been optically brightened. The remaining pearls were either inert under LWUV excitation or exhibited an even yellowish or whitish reaction (figure 3). In order to confidently identify color treatments and optical brightening processes, additional advanced testing techniques were employed.

Advanced Testing Results. Raman spectroscopy has long been one of the most important spectroscopic techniques used in identifying natural pigments in some mollusk shells and pearls, in addition to confirming their major mineral constituents (mainly aragonite but also rarely calcite and vaterite) (Karampelas et al., 2007; Soldati et al., 2008a,b; Karampelas et al., 2009; Bersani and Lottici, 2010; Wehrmeister et al., 2011; Karampelas et al., 2019a,b). It is particularly useful in detecting natural polyenic molecules in freshwater pearls, thus enabling the separation of naturally colored and treated-color pearls. Raman spectroscopic analysis with a 514 nm argon-ion laser revealed aragonite peaks at 703/705 cm^{-1} (doublet) and a main peak at 1086 cm^{-1} due to the ν_4 in-plane bending mode and the ν_1 symmetric mode, respectively, for all samples. However, six of the 23 pearls (FW07, FW08, FW09, FW17, FW20, and FW23) showed significantly reduced aragonite peaks and higher fluorescence background. Besides aragonite Raman peaks, strong polyene peaks in the approximate ranges of 1125–1134 and 1508–1527 cm^{-1} due to ν_2 vibration from stretching of C–C single bonds and ν_1 vibration from stretching of C=C double bonds were observed for 14 of the 23 samples in this study (figure 4). In addition, minor bands at around 1017 and 1298 cm^{-1} that are also associated with polyene pigments were found on these pearls. Upon closer examination, the main polyenic peaks can be divided into two groups with subtle Raman shift differences: one group exhibiting peaks between 1125–1128 cm^{-1} and 1508–1511 cm^{-1} (FW03, FW05, FW10, FW11, FW12, FW13, FW15, FW16, and FW22), while the other group exhibits peaks between 1133–1134 cm^{-1} and 1526–1527 cm^{-1} (FW04, FW06, FW14, FW18, and FW21). The rest of the pearls showed high background fluorescence or lacked any pigment peaks (figure 5), indicating their artificial color origin, ex-

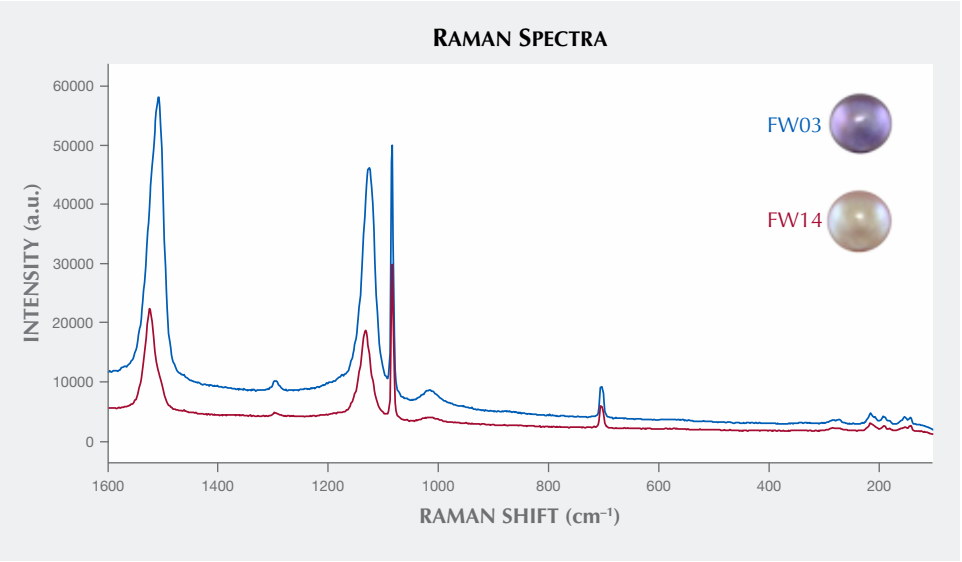

Figure 4. Representative Raman spectra of naturally colored freshwater pearls (FW03 in blue and FW14 in red), both exhibiting main aragonite Raman peaks at 703/705 and 1086 cm^{-1}. In addition, FW03 showed natural pigment peaks at 1128 and 1511 cm^{-1}, which were slightly shifted to 1134 and 1527 cm^{-1} for FW14. Spectra are not baseline corrected.

cept FW01 and FW19, which had very light bodycolors to start with. Based on Raman results, seven colored pearls in this group have been identified as treated (FW02, FW07, FW08, FW09, FW17, FW20, and FW23). This also matched with the microscopic observations discussed in the previous section, where the five pearls showing minor surface color concentrations were all confirmed by Raman spectroscopy as color treated.

While Raman spectroscopy was effective in detecting the organic pigments in naturally colored freshwater pearls, further trace element analyses using EDXRF and LA-ICP-MS techniques provided additional information on the nature of the dye materials as they were particularly useful in detecting the artificial inorganic pigments. Five of the seven treated pearls (FW02, FW07, FW09, FW20, and FW23) were found to contain an abnormally high amount of silver (Ag) on their surfaces with both analytical techniques, indicating the dark colors were modified using silver nitrate. The concentrations of Ag found on the surfaces of these pearls ranged from 306 to 2850 ppm, while no detectable amount of Ag was found on the rest of the samples. The other two treated-color "golden" pearls (FW08 and FW17) may have been modified by organic dyes, as neither EDXRF nor LA-ICP-MS detected any anomalies in their trace element concentrations. However, certain

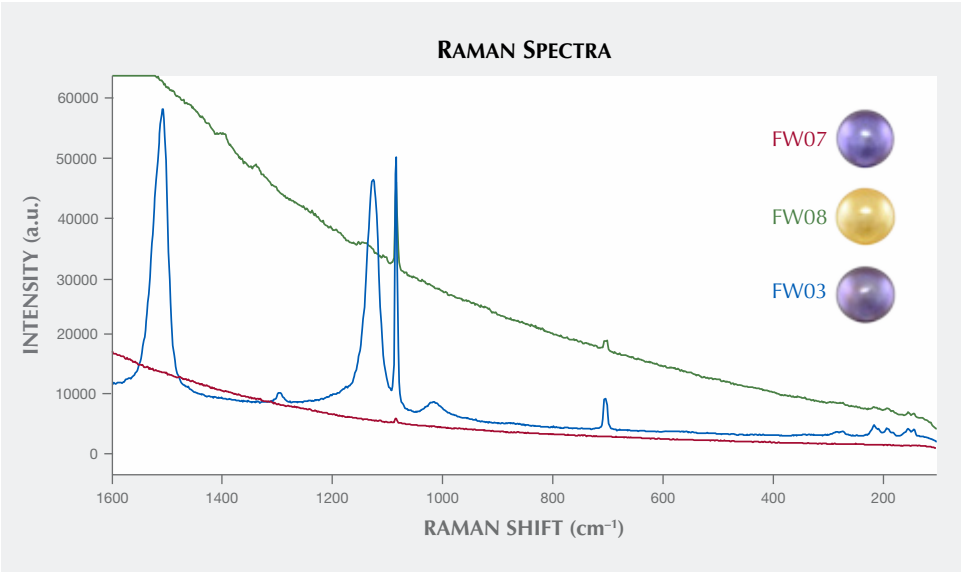

Figure 5. Representative Raman spectra of color-treated freshwater pearls (FW07 in red and FW08 in green) show increasing background fluorescence toward higher wavenumbers, significantly reduced aragonite peaks, and a lack of natural pigment peaks, compared to the naturally colored freshwater pearl (FW03 in blue). Spectra are not baseline corrected.

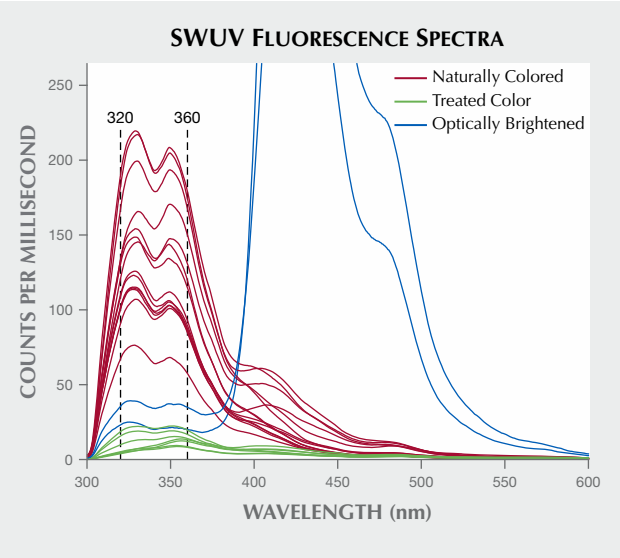

Figure 6. Short-wave UV fluorescence spectra of the pearls showed various fluorescence intensities at around 320–360 nm under SWUV excitation. The naturally colored pearls (in red) produced a higher fluorescence signal compared to the color-treated pearls (in green). In addition, two samples (FW01 and FW19, in blue) also showed strong fluorescence at around 420–430 nm, an indication of optical brightening. Spectra are cut off to better present the area of interest (320–360 nm).

elements such as F, Cl, P, S, N, and C cannot be properly measured by LA-ICP-MS due to their high first ionization energy and interferences. The 16 untreated pearls were also tested with EDXRF and LA-ICP-MS; none of them contained Ag or any other unusual trace element concentrations.

More recently, short-wave UV fluorescence spectroscopy has been applied to pearls in order to check the fluorescence from their organic content. The amino acid tryptophan is a major UV fluorophore found in nacre. It has an absorption band at around 280 nm and can subsequently fluoresce at around 320–360 nm, a key indicator of whether the nacre has been treated or processed, as many of the treatments and processes can reduce this fluorescent feature (Lakowicz, 2006; Hiramatsu and Nagai, 2010; Tsai and Zhou, 2020, 2021). It was found that treated or heavily processed pearls would exhibit reduced nacre fluorescence intensity in this region. A quick check on all of the samples agreed with the Raman results, where all of the seven color-treated pearls emitted very low fluorescence (<25 counts per millisecond under the current instrument setup) compared to the 14 naturally colored pearls (>70 counts per millisecond) (figure 6). The two light-colored pearls (FW01 and FW19) also showed lower nacre fluorescence and an additional strong peak around 420–430 nm due to an optical brightening process (Zhou et al., 2020). However, SWUV fluorescence spectroscopy is not an ideal method for detecting optical brightening, as these chemicals typically produce their maximum fluorescence signal under LWUV excitation. Figure 7 shows the pearls' fluorescence under long-wave UV excitation; five pearls exhibited more prominent fluorescence near 420–430 nm, suggesting that they were processed by optical brighteners. These are the two light-colored pearls (FW01 and FW19), as well as the three natural-color pearls (FW04, FW06, and FW11). The result is also consistent with visual observation under LWUV excitation, as all five pearls displayed strong bluish fluorescence that was readily visible (figure 2). A summary of all the samples, how they were labeled by the vendor, and their final identification results is shown in table 1.

DISCUSSION

Freshwater Edison pearls have emerged as a popular type of cultured pearl in the market during the past decade. Their near-round shape and variety of at-

Figure 7. Long-wave UV fluorescence spectra of the five optically brightened pearls (FW01, FW04, FW06, FW11, and FW19, in blue) exhibited much higher fluorescence at the 420–430 nm region compared to a non-brightened pearl (FW03, in red).

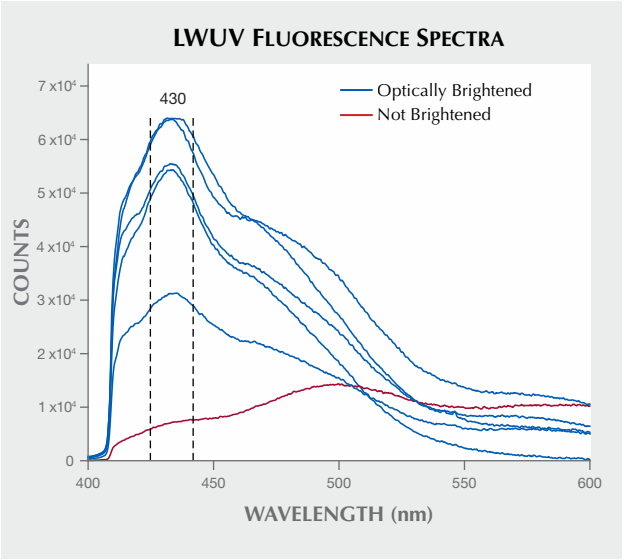

TABLE 1. Summary of general descriptions and characteristics of the pearl samples studied, sample label information, and final identification results.

Sample ID	Image	Weight (ct)	Size	Shape	Color	Identification	Label Information	Detected Treatment or Process
FW01		3.04	7.63 × 7.46 mm	NR	Light pink	BC	No indication of treatment	Optically brightened
FW02		3.86	8.22 mm	NR	Dark bluish gray	NBC	Color treated	Color treated
FW03		4.06	8.31 mm	NR	Strong pinkish purple	NBC	No indication of treatment	No indication of treatment
FW04		4.20	8.40 × 8.25 mm	NR	Pinkish orange	BC	No indication of treatment	Optically brightened
FW05		4.32	8.47 mm	NR	Pinkish purple	NBC	No indication of treatment	No indication of treatment
FW06		4.47	8.61 mm	NR	Brownish pink	BC	No indication of treatment	Optically brightened
FW07		4.59	8.73 × 8.58 mm	NR	Strong pinkish purple	NBC	Color treated	Color treated
FW08		4.62	8.66 mm	R	Strong orangy yellow	BC	Color treated	Color treated
FW09		4.83	8.80 mm	NR	Dark bluish gray	BC	Color treated	Color treated
FW10		4.84	8.86 mm	R	Orange-brown	BC	No indication of treatment	No indication of treatment
FW11		5.03	8.90 mm	R	Pinkish purple	BC	No indication of treatment	Optically brightened
FW12		5.19	9.07 mm	R	Brown	BC	No indication of treatment	No indication of treatment
FW13		10.11	11.35 mm	NR	Pinkish brown	BC	No indication of treatment	No indication of treatment
FW14		11.23	11.74 × 11.64 mm	R	Strong pinkish orange	BC	No indication of treatment	No indication of treatment
FW15		11.61	11.94 × 11.70 mm	NR	Orange-brown	BC	No indication of treatment	No indication of treatment
FW16		12.14	12.07 mm	NR	Purplish brown	BC	Color treated	No indication of treatment
FW17		12.80	12.25 × 12.08 mm	NR	Strong orangy yellow	BC	Color treated	Color treated
FW18		14.70	12.84 mm	NR	Pinkish orange	BC	No indication of treatment	No indication of treatment
FW19		15.04	12.90 mm	R	Very light orangy pink	BC	No indication of treatment	Optically brightened
FW20		15.15	13.12 × 12.74 mm	NR	Dark gray	BC	Color treated	Color treated
FW21		15.26	12.98 × 12.77 mm	NR	Purplish pink	BC	No indication of treatment	No indication of treatment
FW22		15.44	13.12 × 12.65 mm	NR	Strong purplish pink	BC	No indication of treatment	No indication of treatment
FW23		17.47	13.60 × 13.46 mm	NR	Strong pinkish purple	BC	Color treated	Color treated

Abbreviations: NR = near-round, R = round, BC = bead cultured, NBC = non-bead cultured

tractive non-neutral fancy bodycolors represent a significant improvement in Chinese freshwater cultured pearl quality. Many of these Edison pearls exhibit intense bodycolors in the three main hue categories: purple, pink, and orange. These pearl colors are affected predominantly by the donor oyster's nacre color, which has been known to be genetically determined and inherited (McGinty et al., 2010; Karampelas and Lombard, 2013; Ky et al., 2014; Wang et al., 2020). For freshwater pearls, it is also known that polyenic pigments (such as unmethylated and partially methylated polyenes) containing various chain lengths of alternating double and single carbon-carbon bonds are responsible for color appearance (Soldati et al., 2008a; Karampelas et al., 2007, 2009, 2019a). In addition to the effect of genetic inheritance, it is also possible that various carotenoid pigments similar to the natural pigments found in freshwater pearls are used as food additives during the culturing process to enhance the pearls' colors, a common practice that can be found in other aquatic industries (Liao and Miao, 2013; Pereira da Costa and Miranda-Filho, 2020). These dietary supplements will be absorbed and metabolized by mussels growing in the culturing farms, which in turn can be transformed into their own natural pigments. However, this is not considered a form of treatment, and whether the samples obtained for this study underwent this practice is not known to the authors.

Our study suggested that both color treatment and optical brightening have been applied to fancy-color freshwater Edison pearls, and their identification can be achieved by a combination of conventional gemological methods (microscopic observation and long-wave fluorescence observation) and advanced instrumental techniques (Raman spectroscopy, trace element analyses, and long-wave and short-wave UV fluorescence spectroscopy). It is worth noting that conventional UV-Vis reflectance spectroscopy is a very effective method to identify color treatment in golden or dark-colored saltwater pearls (Elen, 2001; Wang et al., 2006; Karampelas et al., 2011; Zhou et al., 2012, 2016). However, the identification of color treatment in freshwater pearls using UV-Vis reflectance spectroscopy is more challenging and less effective in our experience with these samples (results not shown). Freshwater pearls can exhibit many different colors with various tones and saturations, without easily identifiable characteristic absorption peaks such as the 700 nm absorption band found in Tahitian pearls. Among all the techniques, Raman spectroscopy can provide positive identification of natural color origin by the detection of polyenic pigments found on the surface of the pearls. The differences in polyene-related peak positions at 1125–1134 and 1508–1527 cm^{-1} between two groups of samples (purplish and brownish hues vs. orangy and pinkish hues) are most likely due to the different carbon-carbon single- and double-bond chain lengths, with longer chain polyenes producing lower-frequency Raman bands (Hedegaard et al., 2006). On the other hand, trace element analyses such as EDXRF and ICP-MS can effectively identify certain color-treated pearls, especially those treated with silver nitrate. Subsequent short-wave UV fluorescence spectroscopy can further separate natural and treated pearls based on their nacre fluorescence under UV excitation, confirming the results obtained by other techniques. One sample in our study (FW16) was initially labeled as treated when it was received by us. However, both gemological and advanced testing results confirmed that this pearl's color was of natural origin, and there were no indications of optical brightening. While we cannot rule out any other undetectable processes that could be applied to pearls, we believe this is most likely a result of sample mislabeling or misplacement from the source.

White pearls and those with very light hues, especially akoya and freshwater cultured pearls, are routinely processed or treated by various methods after harvest. Bleaching is the most prevalent and is often used in addition to maeshori treatment, an umbrella term for various types of luster enhancement (Otter et al., 2017). Optical brightening agents are also used sometimes in conjunction with bleaching/maeshori to further enhance the appearance of the pearls. This additional process can be detected using long-wave fluorescence spectroscopy, as the brightening agents will fluoresce at a specific wavelength (around 420–430 nm) under long-wave excitation (Zhou et al., 2020). While some aspects regarding the impact of optical brightening on fancy-color freshwater pearls remain inconclusive, this study revealed that some naturally colored freshwater pearls have also been subjected to this process. Although their color is not affected by the optical brightening, their luster could benefit from this process, which can increase the pearls' reflection in the visible spectrum. Finally, we did not observe any optical brightening process applied to color-treated pearls in this group of samples, based on both visual observation of their fluorescence under LWUV and spectroscopic results.

CONCLUSIONS

This study proves that GIA's current testing protocols are effective in detecting color treatments in freshwater cultured pearls. The color origin of fancy-color Edison pearls can be confidently determined with a combination of conventional gemological tests and advanced analytical methods. Raman spectroscopy, trace element analyses, and short-wave UV fluorescence spectroscopy all proved useful in separating natural and treated colors. In addition, some naturally colored Edison pearls in the trade have been subjected to an optical brightening process. This treatment can also be identified using long-wave UV fluorescence observation and spectroscopic methods, through the detection of characteristic fluorescence peaks at around 420–430 nm caused by the brightening agents. While these samples only represented a small pool of this unique type of cultured pearl product, the treatment and optical brightening features are quite characteristic and could be applied to other types of freshwater cultured pearls in the market such as Ming pearls and traditional non-bead cultured pearls.

ABOUT THE AUTHORS

Dr. Zhou is a senior manager of pearl identification, Ms. Ho is a senior staff gemologist, Ms. Shih is a staff gemologist, and Ms. Persaud is a research associate, at GIA in New York. Dr. Tsai is a senior research scientist at GIA in New Jersey. Mr. Sun is a research associate at GIA in Carlsbad. Dr. Qi is a professor at Tongji University in Shanghai.

REFERENCES

Akamatsu S., Zansheng L.T., Moses T.M., Scarratt K. (2001) The current status of Chinese freshwater cultured pearls. *G&G*, Vol. 37, No. 2, pp. 96–113, http://dx.doi.org/10.5741/GEMS.37.2.96

Bersani D., Lottici P.P. (2010) Applications of Raman spectroscopy to gemology. *Analytical and Bioanalytical Chemistry*, Vol. 397, pp. 2631–2646, http://dx.doi.org/10.1007/s00216-010-3700-1

Bui T.N., Leblan S., Delaunay A. (2019) Double grafting in peanut-shaped Ming cultured pearls. *Journal of Gemmology*, Vol. 36, No. 8, pp. 706–708.

Cartier L.E., Ali S.H. (2013) China's pearl industry an indicator of ecological stress. *The Journal of the Gemmological Association of Hong Kong*, Vol. 34, pp. 18–21.

Elen S. (2001) Spectral reflectance and fluorescence characteristics of natural-color and heat-treated "golden" South Sea cultured pearls. *G&G*, Vol. 37, No. 2, pp. 114–123, http://dx.doi.org/10.5741/GEMS.37.2.114

Fiske D., Shepherd J. (2007) Continuity and change in Chinese freshwater pearl culture. *G&G*, Vol. 43, No. 2, pp. 138–145, http://dx.doi.org/10.5741/GEMS.43.2.138

Hänni H.A. (2011) Ming pearls: A new type of cultured pearl from China. *The Journal of the Gemmological Association of Hong Kong*, Vol. 32, pp. 23–25.

Hedegaard C., Bardeau J-F., Chateigner D. (2006) Molluscan shell pigments: An in situ resonance Raman study. *Journal of Molluscan Studies*, Vol. 72, pp. 157–162, http://dx.doi.org/10.1093/mollus/eyi062

Hiramatsu J., Nagai K. (2010) Non-destructive assessment of the effects of heat and sunlight on akoya pearl quality. *Seibutsu Kogaku*, Vol. 88, No. 8, pp. 378–383.

Homkrajae A., Sun Z., Blodgett T., Zhou C. (2019) Provenance discrimination of freshwater pearls by LA-ICP-MS and linear discriminant analysis (LDA). *G&G*, Vol. 55, No. 1, pp. 47–60, http://dx.doi.org/10.5741/GEMS.55.1.47

Karampelas S. (2012) Gem News International: Large natural-color freshwater cultured pearls with drilled beads. *G&G*, Vol. 48, No. 2, pp. 148–149.

Karampelas S., Lombard A. (2013) Gemological characteristics of saltwater cultured pearls produced after xenotransplantation. *G&G*, Vol. 49, No. 1, pp. 36–41, http://dx.doi.org/10.5741/GEMS.49.1.36

Karampelas S., Fritsch E., Mevellec J-Y., Gauthier J-P., Sklavounos S., Soldatos T. (2007) Determination by Raman scattering of the nature of pigments in cultured freshwater pearls from the mollusk *Hyriopsis cumingi*. *Journal of Raman Spectroscopy*, Vol. 38, pp. 217–230, http://dx.doi.org/10.1002/jrs.1626

Karampelas S., Fritsch E., Mevellec J-Y., Sklavounos S., Soldatos T. (2009) Role of polyenes in the coloration of cultured freshwater pearls. *European Journal of Mineralogy*, Vol. 21, No. 1, pp. 85–97, http://dx.doi.org/10.1127/0935-1221/2009/0021-1897

Karampelas S., Fritsch E., Gauthier J-P., Hainschwang T. (2011) UV-Vis-NIR reflectance spectroscopy of natural-color saltwater cultured pearls from *Pinctada margaritifera*. *G&G*, Vol. 47, No. 1, pp. 31–35, http://dx.doi.org/10.5741/GEMS.47.1.31

Karampelas S., Fritsch E., Makhlooq F., Mohamed F., Al-Alawi A. (2019a) Raman spectroscopy of natural and cultured pearls and pearl producing mollusc shells. *Journal of Raman Spectroscopy*, Vol. 51, No. 9, pp. 1813–1821, http://dx.doi.org/10.1002/jrs.5670

Karampelas S., Mohamed F., Abdulla H., Almahmood F., Flamarzi L., Sangsawong S., Alalawi A. (2019b) Chemical characteristics of freshwater and saltwater natural and cultured pearls from different bivalves. *Minerals*, Vol. 9, No. 6, article no. 357, http://dx.doi.org/10.3390/min9060357

Krzemnicki M.S., Friess S.D., Chalus P., Hänni H.A., Karampelas S. (2010) X-ray computed microtomography: Distinguishing natural pearls from bead and non-beaded cultured pearls. *G&G*, Vol. 46, No. 2, pp. 128–134, http://dx.doi.org/10.5741/GEMS.46.2.128

Ky C-L., Blay C., Sham-Koua M., Lo C., Cabral P. (2014) Indirect improvement of pearl grade and shape in farmed *Pinctada margaritifera* by donor "oyster" selection for green pearls. *Aqua-*

culture, Vol. 432, pp. 154–162, http://dx.doi.org/10.1016/j.aquaculture.2014.05.002
Li J., Wu X., Bai Z. (2018) Freshwater pearl culture. In J.-F. Gui et al., Eds., *Aquaculture in China: Success Stories and Modern Trends*, John Wiley & Sons Ltd., New York, http://dx.doi.org/10.1002/9781119120759.ch3_1
Liao J., Miao D.L. (2013) Method for culturing fresh water colored pearls. China Patent No. CN103210860A, China National Intellectual Property Administration.
Lakowicz J.R. (2006) *Principles of Fluorescence Spectroscopy*, 3rd ed. Springer, New York.
McGinty E.L., Evans B.S., Taylor J.U.U., Jerry D.R. (2010) Xenografts and pearl production in two pearl oyster species, *P. maxima* and *P. margaritifera*: Effect on pearl quality and a key to understanding genetic contribution. *Aquaculture*, Vol. 302, No. 3-4, pp. 175–181, http://dx.doi.org/10.1016/j.aquaculture.2010.02.023
Nilpetploy N., Lawanwong K., Kessrapong P. (2018) The gemological characteristics of pipi pearls reportedly from *Pinctada maculata*. *G&G*, Vol. 54, No. 4, pp. 418–427, http://dx.doi.org/10.5741/GEMS.54.4.418
Otter L.M., Agbaje O.B.A., Huong L.T-T., Hager T., Jacob D.E. (2017) Akoya cultured pearl farming in eastern Australia. *G&G*, Vol. 53, No. 4, pp. 423–437, http://dx.doi.org/10.5741/GEMS.53.4.423
Pereira da Costa D., Miranda-Filho K.C. (2020) The use of carotenoid pigments as food additives for aquatic organisms and their functional roles. *Reviews in Aquaculture,* Vol. 12, No. 3, pp. 1567–1578, http://dx.doi.org/10.1111/raq.12398
Scarratt K., Moses T.M., Akamatsu S. (2000) Characteristics of nuclei in Chinese freshwater cultured pearls. *G&G*, Vol. 36, No. 2, pp. 98–109, http://dx.doi.org/10.5741/GEMS.36.2.98
Soldati A.L., Jacob D.E., Wehrmeister U., Hager T., Hofmeister W. (2008a) Micro-Raman spectroscopy of pigments contained in different calcium carbonate polymorphs from freshwater cultured pearls. *Journal of Raman Spectroscopy*, Vol. 39, No. 4, pp. 525–536, http://dx.doi.org/10.1002/jrs.1873
Soldati A.L., Jacob D.E., Wehrmeister U., Hofmeister W. (2008b) Structural characterization and chemical composition of aragonite and vaterite in freshwater cultured pearls. *Mineralogical Magazine*, Vol. 72, No. 2, pp. 579–592, http://dx.doi.org/10.1180/minmag.2008.072.2.579
Sturman N., Otter L.M., Homkrajae A., Manustrong A., Nilpetploy N., Lawanwong K., Kessrapong P., Jochum K.P., Stoll B., Gotz H., Jacob D.E. (2019) A pearl identification challenge. *G&G*, Vol. 55, No. 2, pp. 229–243, http://dx.doi.org/10.5741/GEMS.55.2.229
Tsai T-H., Zhou C. (2020) Rapid detection of color-treated pearls and separation of pearl types using fluorescence analysis. *SPIE Proceedings*, Vol. 11483, Novel Optical Systems, Methods, and Applications XXIII, 1148307, http://dx.doi.org/10.1117/12.2566590
——— (2021) Rapid detection of color-treated pearls and separation of pearl types using fluorescence analysis. *Applied Optics*, Vol. 60, No. 20, pp. 5837–5845, https://doi.org/10.1364/AO.427203
Wang W., Scarratt K., Hyatt A., Shen A.H-T., Hall M. (2006) Identification of "chocolate pearls" treated by Ballerina Pearl Co. *G&G*, Vol. 42, No. 4, pp. 222–235, http://dx.doi.org/10.5741/GEMS.42.4.222
Wang Z., Adzigbli L., Zheng Z., Yang C., Deng Y. (2020) How cultured pearls acquire their colour. *Aquaculture Research*, Vol. 51, No. 10, pp. 3925–3934, http://dx.doi.org/10.1111/are.14765
Wehrmeister U., Jacob D.E., Soldati A.L., Loges N., Hager T., Hofmeister W. (2011) Amorphous, nanocrystalline and crystalline calcium carbonates in biological materials. *Journal of Raman Spectroscopy*, Vol. 42, No. 5, pp. 926–935, http://dx.doi.org/10.1002/jrs.2835
Wong K. (2020) China's pearl suppliers embracing digital opportunities. *JNA*, Sep/Oct, Issue 423, pp. 60-65.
Zhou C., Chen L. (2020) Gem News International: World Pearl Congress. *G&G*, Vol. 56, No. 4, pp. 553–554.
Zhou C., Homkrajae A., Ho J.W.Y., Hyatt A., Sturman N. (2012) Update on the identification of dye treatment in yellow or "golden" cultured pearls. *G&G*, Vol. 48, No. 4, pp. 284–291, http://dx.doi.org/10.5741/GEMS.48.4.284
Zhou C., Ho J.W-Y., Chan S., Zhou J.Y., Wong S.D., Moe K-S. (2016) Identification of "pistachio" colored pearls treated by Ballerina Pearl Co. *G&G*, Vol. 52, No. 1, pp. 50–59, http://dx.doi.org/10.5741/GEMS.52.1.50
Zhou C., Hodgins G., Lange T., Saruwatari K., Sturman N., Kiefert L., Schollenbruch K. (2017) Saltwater pearls from the pre- to early Columbian era: A gemological and radiocarbon dating study. *G&G*, Vol. 53, No. 3, pp. 286–295, http://dx.doi.org/10.5741/GEMS.53.3.286
Zhou C., Tsai T-H., Sturman N., Nilpetploy N., Manustrong A., Lawanwong K. (2020) Optical whitening and brightening of pearls: A fluorescence spectroscopy study. *G&G*, Vol. 56, No. 2, pp. 258–265. http://dx.doi.org/10.5741/GEMS.56.2.258
Zhou Q., Lu R. (2018) Chinese freshwater cultured pearl industry at a crossroads. *Sixth International Gemological Symposium*, *G&G*, Vol. 54, No. 3, pp. 295–296.
Zhou Y., Zhou C. (2015) Lab Notes: Strong pinkish purple freshwater bead-cultured pearls. *G&G*, Vol. 51, No. 2, pp. 179–181.
Zhu C., Southgate P.C., Li T. (2019) Production of pearls. In A. Smaal et al., Eds., *Goods and Services of Marine Bivalves*, 1st ed., Springer, pp. 73–93, http://dx.doi.org/10.1007/978-3-319-96776-9_5

Pearl Classification: The GIA 7 Pearl Value Factors

Joyce Wing Yan Ho and Sally Chan Shih

Prized by many cultures throughout history and frequently referred to as "The Queen of Gems," pearls have long been one of the most sought-after gemstones in both the jewelry industry and the world at large. Their unique appearance and the affordability of cultured pearls in the market have allowed their popularity to grow exponentially over the years.

Pearls form in a wide variety of sizes, shapes, and colors, and there are numerous different types of pearls, both natural and cultured. This diversity created the need for a way to distinguish their various appearances and qualities. Consequently, a number of different grading systems were developed within the pearl industry over the years. The competing, often company-specific methods and coded terminology made the systems difficult to understand and employ consistently. Agreeing on a universal approach to classify pearls has remained one of the main challenges facing the pearl industry.

The idea of devising a pearl classification system similar to GIA's 4Cs system for diamonds first appeared in *Gems & Gemology* in 1942 (Rietz, 1942a,b). The author suggested that pearls could be grouped into several categories such as *gem quality*, *extra-fine quality*, *fine quality*, *good quality*, *fair quality*, *imperfect*, and *poor quality*, based on several factors, namely shape, luster, surface blemishes, color distribution, and iridescence (commonly referred to as *orient*). This approach was further improved by GIA's Richard T. Liddicoat Jr., who in 1967 proposed a new system based on the seven pearl value factors (Liddicoat, 1967). Continued refinement eventually resulted in the development of GIA's current pearl classification system, called the GIA 7 Pearl Value Factors. This comprehensive pearl classification system offers a detailed description of the appearance of loose pearls, strands, and pearls in jewelry. It is a systematic approach to evaluation, through consistent methodology and common terminology that both industry professionals and consumers can understand (Zhou, 2019). This approach and the terminology of GIA's updated system have already been adopted in many parts of the pearl industry for classifying and describing pearls.

The wall chart presented here is based on a poster presentation from the 2018 GIA International Gemological Symposium (Ho and Shih, 2018). It provides the definitions and classification terminology for each of the seven value factors—size, shape, color, luster, surface, nacre, and matching—as well as digital images to illustrate various examples.

Pearls fall into one of two varieties: nacreous (resembling mother-of-pearl with lustrous nacre) and non-nacreous (such as conch or melo pearls, lacking lustrous nacre but often displaying flame structure on the surface). This system applies to nacreous pearls (see figure 1) and exclusively for the three dominant types of saltwater cultured pearls: akoya,

Figure 1. The GIA 7 Pearl Value Factors system classifies pearls according to size, shape, color, luster, surface, nacre, and matching. Composite photo by GIA staff.

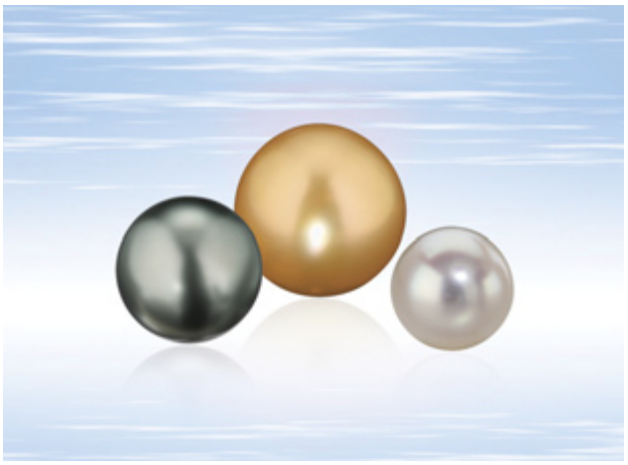

See end of article for About the Authors and Acknowledgments.
Gems & Gemology, Vol. 57, No. 2, pp. 135–137,
http://dx.doi.org/10.5741/GEMS.57.2.135

Figure 2. This akoya strand can be described using the GIA 7 Pearl Value Factors. Size: 5.51 to 8.82 mm. Shape: Near-round. Color (Overtone): Variously colored (Variously colored). Luster: Excellent. Surface: Lightly spotted. Matching: Very good. Nacre: Acceptable. Photo by Sood Oil (Judy) Chia.

South Sea, and Tahitian. A color scale for all types of nacreous cultured pearls and physical master sets of the three types of pearls were created to ensure a very high degree of consistency. Every GIA laboratory location that provides pearl services uses the same classification system and meticulously matched master sets to produce repeatable results. Adopting GIA's pearl classification terminology throughout the gem and jewelry industry would foster improved communication within the trade and, by default, bridge the communication and confidence gap between buyers and sellers using easily understandable language.

This wall chart is intended as a comprehensive but simplified overview of how GIA gemologists classify pearls using the GIA 7 Pearl Value Factors system (see figure 2, for example). While GIA employs an extensive set of master pearls to achieve maximum consistency in pearl classification, we hope the chart serves as a useful reference for all of our readers.

ABOUT THE AUTHORS

Ms. Ho and Ms. Shih are senior staff gemologists (pearls) at GIA in New York.

ACKNOWLEDGMENTS

The authors would like to thank GIA's New York lab staff, especially Akira Hyatt for her valuable suggestions. We greatly appreciate the help from Daniel Dell and Sood Oil (Judy) Chia with the aesthetics of the wall chart and the quality of the images.

REFERENCES

Ho J.W.Y., Shih S.C. (2018) Pearl classification: GIA's approach. *Proceedings of the Sixth International Gemological Symposium*, *G&G*, Vol. 54, No. 3, pp. 300–301.

Liddicoat R.T. Jr. (1967) Cultured-pearl farming and marketing. *G&G*, Vol. 12, No. 6, pp. 162–172.

Rietz P.C. (1942a) The classification and sales possibilities of genuine pearls. *G&G*, Vol. 4, No. 1, pp. 9–12.

Rietz P.C. (1942b) The classification and sales possibilities of genuine pearls. *G&G*, Vol. 4, No. 2, pp. 25–28.

Zhou C. (2019) A brief history of pearl testing through *Gems & Gemology*. In *Sixteenth Annual Sinkankas Symposium—Pearl*, Gemological Society of San Diego and Gemological Institute of America, pp. 74–83.

Namak Mandi: A Pioneering Gemstone Market in Pakistan

Habib Ur Rehman, Bilal, Syed Owais, Obaid Ur Rahman, and Andy H. Shen

Figure 1. In this regional map, red lines trace the routes from the mines of various gemstones to the Namak Mandi market. Abbreviations: KPK = Khyber Pakhtunkhwa; AJK = Azad Jammu and Kashmir.

Descending into Peshawar for the first time, a foreign tourist might be surprised to learn that amid the clutter of buildings in this historical city lies an important gem trading center. This market serves a wide range of buyers and sellers from Afghanistan, Uzbekistan, Tajikistan, and Iran who deal with locally mined gemstones from Azad Jammu and Kashmir, Gilgit-Baltistan, and parts of Khyber Pakhtunkhwa in Pakistan (figure 1). They might also be surprised that this trading hub does not have a modern name. Namak Mandi, meaning "salt market" in Urdu, was originally established decades ago as a trading center and storage facility for salt (Hussain, 2015). Fifty years ago, no one could have imagined it becoming a primary trading center for rough and faceted gemstones in Pakistan. The au-

See end of article for About the Authors and Acknowledgments.
Gems & Gemology, Vol. 57, No. 2, pp. 138–149,
http://dx.doi.org/10.5741/GEMS.57.2.138

Figure 2. An overhead view of the Namak Mandi gem market. The immediately visible buildings on the right and left of the street below are collectively referred to as Namak Mandi; this street has gained popularity as "Pareshan Chowk," which literally means "intersection of anxiety." Every day, in the late afternoon, retailers and dealers anxiously stand by to sell their goods to the buyers and window shoppers. Photo by Shakeel Anwar Khan.

thors led an excursion to Namak Mandi to document its transformation into a gem trading hub and to understand the variety of gemstones and commerce taking place in the market.

FROM SALT TO GEMSTONES: NAMAK MANDI'S TRANSFORMATION

Namak Mandi is the largest market in Pakistan for trading rough gemstones (figures 2 and 3). There is no record of exactly when it made the quantum leap from salt market to becoming Pakistan's pioneering trading hub for gemstones. According to anecdotal evidence, Namak Mandi's gemstone market began in the 1970s. Since there were only a handful of traders, the market did not operate systematically and there were no trade standards. With the Soviet invasion of Afghanistan, the influx of millions of Afghan refugees into Pakistan turned out to be a blessing in disguise. First, the number of traders multiplied as Afghan entrepreneurs penetrated the gem market. Afghan and local dealers from mining areas began to migrate with their stones and established themselves in Peshawar (figure 1). In fact, Afghan traders soon became the driving force for the market, accounting for 60–70% of sales up until 2007. Those from Kunar Province of Afghanistan exported tourmaline (figure

*Figure 3. Goods being sold at Pareshan Chowk (intersection of anxiety). Left: A retailer selling prayer beads (*tasbeeh*) made of medium- to low-quality gems. Right: Before buying gemstones, locals usually prefer to check them in natural light. Photos by Shakeel Anwar Khan.*

4A) to Namak Mandi, along with spodumene from Nuristan (figure 4B; Rehman et al., 2020) and emerald from the Panjshir region. Within Pakistan, merchants from Swat Valley (Khyber Pakhtunkhwa) traded emerald (figure 4C), while those from the Gilgit-Baltistan region brought aquamarine (figure 4D), and pink topaz came from Katlang, a township in the Mardan District (figure 4E).

Many inhabitants of different regions of Pakistan also moved to Peshawar for the gemstone trade. These included Chitral, Skardu, Swat, Karachi,

Figure 4. A: Tourmaline (5.0 × 4.5 × 2.0 cm) from Nuristan, Afghanistan. B: Spodumene (11.4 × 4.0 × 1.4 cm) from Nuristan. C: Emerald in matrix (5.2 × 3.9 × 2.5 cm) from Swat, Pakistan. D: Aquamarine crystal (7.1 × 4.9 × 4.4 cm) from Gilgit, Pakistan. E: Pink topaz (3.0 × 1.5 × 1.0 cm) from Katlang, Mardan, Pakistan. F: Faden quartz (7.5 × 2.0 × 1.0 cm) from Baluchistan, Pakistan. G: Petroleum quartz (2.5 × 1.6 × 1.3 cm) from Baluchistan. H: Brookite (3.3 × 2.0 × 1.8 cm) from Baluchistan. Photos by Ghulam Mustafa, Khalid Habib, and Bilal Omar.

Rawalpindi, and Islamabad. More recently, traders from Baluchistan Province have also entered the market, introducing stones such as Faden quartz with an internal thread-like pattern (figure 4F), quartz with yellowish to deep yellow petroleum inclusions (figure 4G; as described by Laurs, 2016), and brookite (figure 4H). The 1980s saw the Namak Mandi market gain international attention. Still, it was not without a downside: Police and local officials often believed that the people involved in the gemstone business were money launderers. In interviews with experienced tradesmen, it became clear that because there was no legal framework for extracting, processing, and trading of gemstones, the officials likened it to the narcotics trade.

ESTABLISHMENT OF EXPORTERS' ASSOCIATION

With Afghan merchants leading the expansion of gemstone trading in Namak Mandi, it was not surprising to see them establishing a stronghold, as they possessed knowledge of the market on a local and international level. In a move to somewhat formalize

the trade and, perhaps, to check the Afghan monopoly, local traders led a move to register their businesses with the All Pakistan Commercial Exporters Association (APCEA), established in 1984. In 1988, the Ministry of Commerce granted it official recognition to assist exporters registered with the organization. The APCEA caters to the needs and challenges faced by exporters from all industries. Since Namak Mandi's exporters did not have an official agency that could handle their needs (e.g., quick processing of exports and payment of export duties), they found it expedient to register their businesses with the APCEA. The association plays a positive role for Namak Mandi in many ways. By informing the authorities about the significance of the gemstone trade for the local economy, it saves traders and exporters from police harassment. It also actively supports exporters in processing their documents at customs offices for sale abroad. Owing to the commercial success of Namak Mandi with the support of the APCEA, the gemstone sector has become more prominent, and many local traders are keen to know more about this lucrative trade to capitalize on this market. The APCEA also organizes an international gemstone exhibition each year in the capital city of Islamabad.

Gemstone Business Tree. The gemstone business in Namak Mandi and in Pakistan as a whole can be categorized into three main groups of dealers:

1. *Rough and Faceted Stones:* This category is comprised of those who have some lapidary skills. It is worth mentioning that there is no professional organization in Pakistan delivering lapidary training. Since most of the local lapidaries are not formally educated, each would develop specialist knowledge about a specific type of gemstone. In Namak Mandi, it is common to find dealers who specialize in emerald, kunzite, aquamarine, or tourmaline. These dealers invest their money in a specific gemstone and are considered experts in determining the base price of that particular type of gemstone.
2. *Mineral Specimens:* Specimen dealers can be grouped into two categories: the local traders who showcase mineral specimens in shops at Namak Mandi, and those who understand on-

Figure 5. Lapis lazuli from Afghanistan. Sellers usually wet the surface with water to better reveal color and texture. The lapis sellers usually polish a side of each slab (left) and fashion cabochons (bottom right) so that a buyer can easily check their quality. Photos by Shakeel Anwar Khan.

Figure 6. Nephrite buyers often inspect the rough (both indoors and outdoors) with a strong dual-intensity flashlight (A). The buyers usually examine the color, texture, and transparency of the rough. They also pay attention to how much of the material could be used to make profitable jewelry. This nephrite is from the Hamid mine in the Mohmand area, Khyber Pakhtunkhwa. B and C: Spoons and daggers shaped out of nephrite. Photos by Shakeel Anwar Khan.

line selling and export mineral specimens to Canada, Australia, the United States, and other developed countries. The latter comprise almost 80% of specimen dealers. They often take pictures and videos of local traders' collections of mineral specimens for online marketing. If a customer demands a specific item, an online trader, after negotiating the price with the local (shopkeeper) trader, adds his profit to the price and parcels it off. Most exporters do this type of business because there is almost zero risk of losing one's money. That is, they can make money without having to buy and keep the specimens in rented shops; like the middlemen, they make money without incurring financial risk.

3. *Ornamental Stones:* Namak Mandi's ornamental stone dealers mostly deal in lapis lazuli and nephrite. World-famous lapis lazuli comes from Afghanistan (figure 1). The exquisite color of lapis from Kokcha in Badakhshan Province is especially popular (figure 5). There are many mines in Badakhshan, some of which are simply named mine 1, 2, 3, and so forth. Mine 4 is particularly esteemed among the traders. The mine is referred to as *Ma'dan-e-char*, Persian for "mine 4." Lapis lazuli from this mine has an exceptionally vivid blue color, with very little or no pyrite and calcite. At Namak Mandi, the mere mention of a lapis coming from *Ma'dan-e-char* is considered a guarantee of quality. As this gemstone hails from Afghanistan, most lapis traders tend to be of Afghan origin.

Within Pakistan, nephrite mostly comes from the Mohmand region of Khyber Pakhtunkhwa (figure 1). The area produces some of the world's most brightly colored emerald green nephrite (figures 6 and 7). According to interviewees, nephrite from the Hamid mine and the Siraj mine in the Mohmand region are in especially high demand in China. Chinese consumers desire its emerald green color and absence of black oxide spots. While some of the nephrite from Khyber Pakhtunkhwa is used in jewelry and for different types of carvings and beads for sale in the local market, most of it is exported to China, Hong Kong, and Japan.

Merchandising Tactics and Negative Effects. There is a saying in Namak Mandi: "Demand a lot from God and your customer." This quote is seen as the way to become profitable in business endeavors. Another saying goes, "If you learn the tricks of trading

Figure 7. Bangles and different decorative materials made of nephrite. The nephrite shown in the photos is from the Hamid mine in the Mohmand area of Khyber Pakhtunkhwa. Photos by Shakeel Anwar Khan.

in Namak Mandi, you can deal in any market in the world." Keeping this in mind, below we highlight a few pricing and trading tactics.

Colored gemstones have no internationally recognized pricing mechanism. Seemingly aware of this, Namak Mandi traders tend to take advantage, inflating their stone prices using various tactics, such as declaring a higher cost price than what they actually paid. First, when a dealer (Mr. A) indicates the slightest interest in a gemstone, Mr. B might witness this display of interest and take a gamble and buy a speculative stake with Mr. A without exchanging money. That is, if Mr. A buys a gemstone for US$1,000, Mr. B will swear that its value is at least US$1,500 and that if he could afford it, he would have bought it for at least that price. Similarly, if Mr. A has more business "friends," each of them will make similar claims to drive the price even higher. In this way, a gemstone purchased for just US$1,000 will have its price raised many times. Thus, when Mr. A is about to sell it, he will swear to a customer—often in the presence of his business associates—that he bought it for US$3,000, and thus he will set its price at around US$4,000. This ritual of increasing the price of a gemstone by solemn oaths and buying a speculative stake without exchanging a good has developed out of religious reasons. That is, for religious reasons, a Namak Mandi trader would take solemn declarations from his business peers to set a new cost price of his item while avoiding any allegation of dishonesty when telling people of the new cost price.

Second, some families engaged in mining resort to another tactic. The mine owner inflates the cost price by giving each family member a share in every piece of extracted gemstone. The price cost of a stone, normally determined by adding the costs of labor, machinery, transportation, and so forth, is determined in this case by showing it to experienced tradespeople and the like. If the experts set a "cost price" of US$1,000 and a mine owner has four family members, then he will count a share of US$500 for each of the four family members. It is important to highlight that this only occurs verbally, without ever giving the shares to the family members. This will increase the stone's cost price by US$2,000 (US$500 each × 4), resulting in a new price of US$3,000.

Third, gemstones coming for auction from Afghanistan are dealt with in a different way. Bidders tend to engage in blind bidding for the stones. Hundreds of bidders will buy a share in a specific lot without ever seeing a single gemstone. According to the conventions of the Islamic faith, one cannot buy something that exists only in the abstract. Nonetheless, the practice of buying shares in an unseen lot of gemstones at auction has become a mainstream practice at Namak Mandi.

Finally, traders tend to be inconspicuous about their inventory, not displaying gemstones and closing the curtains once customers enter their stores. They use these tactics so that other traders do not see the stones they are showcasing to their customers; it also allows them to avoid price competition with their competitors.

Customers and traders alike frequently become disheartened, believing they have been cheated or have paid far above market price. Some eventually leave the gemstone industry altogether. These questionable business practices seem to reflect a persistent notion that government bureaucracies in

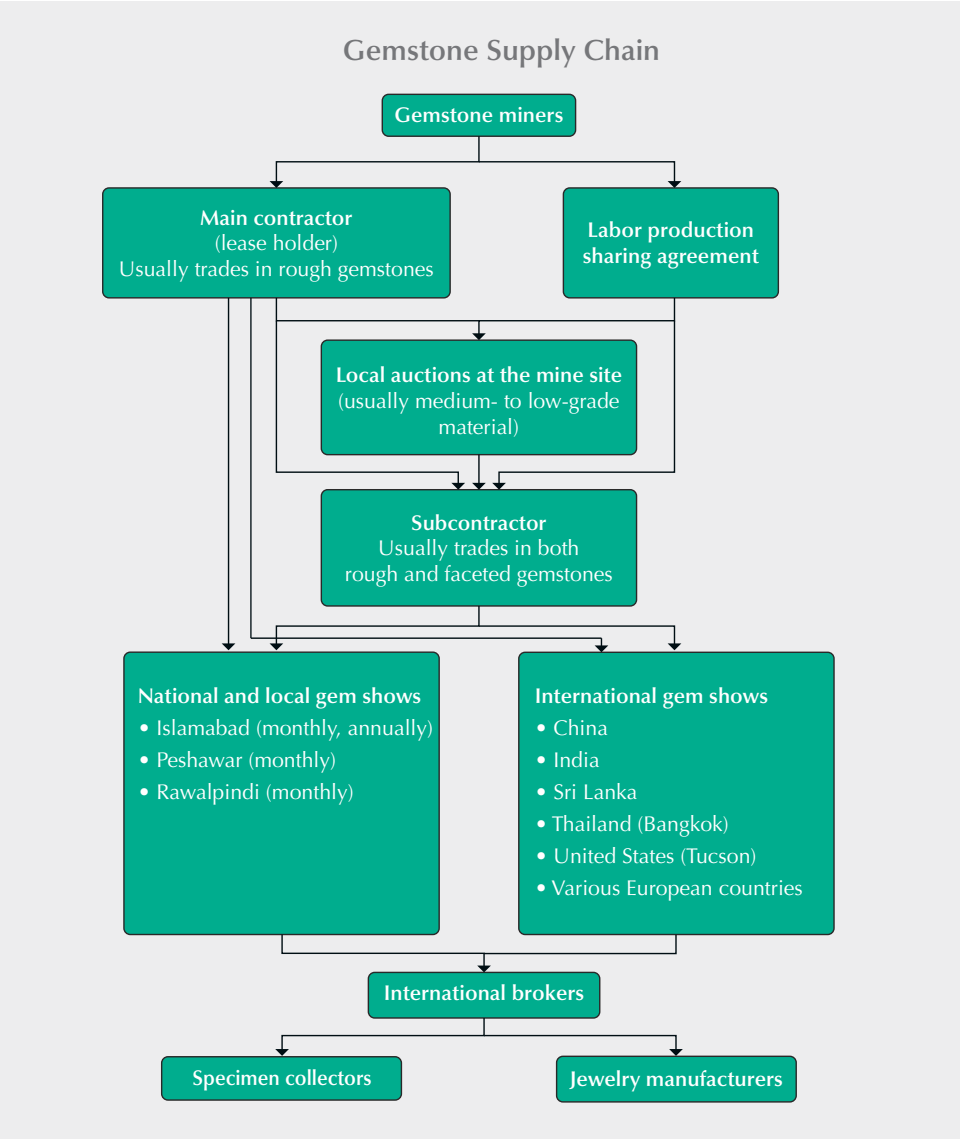

Figure 8. The flow of gemstones in Pakistan from mine to end consumers domestically and internationally.

Pakistan do not function to serve the masses. Citizens often have to request access to information, such as import/export policies, that is constitutionally guaranteed as a "fundamental right." For instance, the drive to register one's business with the APCEA was a purely voluntary effort among gemstone traders. That is, a state agency or department did not direct or advise them how to effectively and smoothly import and export gemstones: It was the business acumen of a few entrepreneurs that led to the custom of registering one's firm with the APCEA. Likewise, some traders are now taking the initiative in addressing ethical issues in pricing and trading tactics, albeit slowly. Most importantly, according to some interviewees, customers' ability to quickly share their concerns regarding trading practices at Namak Mandi on social media platforms, especially Facebook, is incentivizing dealers to become more responsible and ethical.

Regardless of the ethical norms regarding price setting, Pakistan's largest auctions take place in Namak Mandi, and the highest bids are often placed by local merchants. Namak Mandi's merchants frequent trade shows and other exhibitions such as those held in China, the Tucson show in the United States, and Bangkok. They import many stones into Pakistan and export them to other countries.

Gemstone Supply Chain at Namak Mandi. As illustrated in figure 8, there are two ways for a gemstone to go from the mine to the end user through the Namak Mandi gem market. The first route is

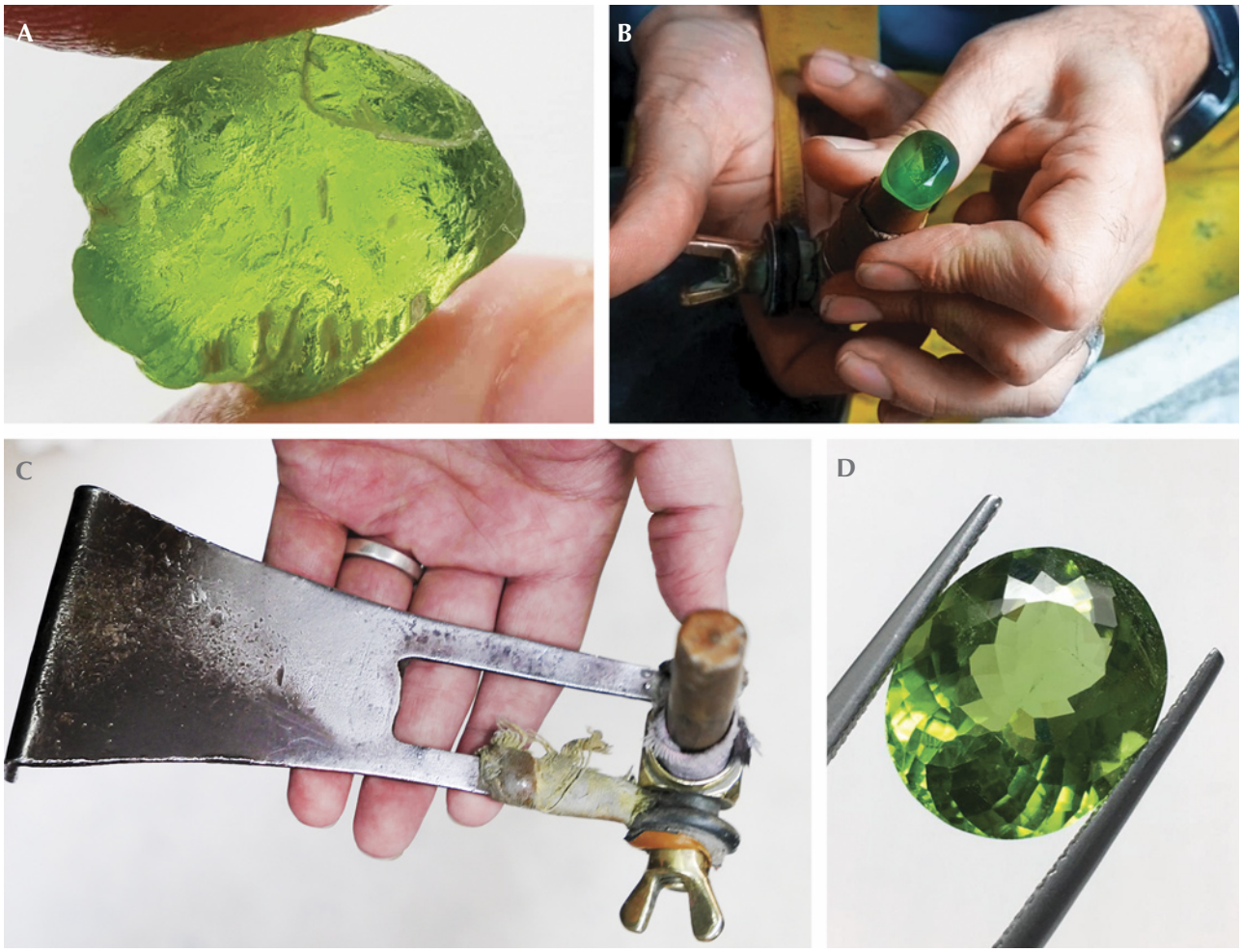

Figure 9. The angoora *faceting process used by cutters at Namak Mandi. A: A rough peridot. B: The pre-formed, dopped peridot. C: Instead of a modern faceting machine, local lapidaries use the* angoora *to save weight and maximize profits. D: The completed faceted peridot. Photos by Shakeel Anwar Khan.*

through the main contractor—the individual who leased the mine. After mining, the gems are sorted according to quality. Whenever stones are bought from him directly, he will narrate a long story recounting how much money was spent on leasing and mining. Known as the toughest negotiator, the main contractor always demands a very high price for his product. Such sellers mostly deal in rough gems: The high-quality samples often go to the international market, while the medium- to low-quality material is sold locally at Namak Mandi or elsewhere in Pakistan.

A second route through which a gemstone travels from mine to market is through the subcontractor. He has two sources for collecting gemstones: the mine owner and the miners themselves. Usually, miners have a labor production sharing agreement with the subcontractor. As depicted in the flowchart (figure 8), miners sell off their share to subcontractors. The subcontractor selling the mined product (rough and faceted) in Namak Mandi and elsewhere is more like a middleman or a commission agent. Because miners do not have the know-how and requisite financial resources for dealing with traders at Namak Mandi and other markets, they have to rely entirely on selling the items to subcontractors. According to our information, miners are at liberty to sell their product at local auctions but prefer subcontractors, who offer fairer deals.

PERSISTENT AND EMERGING TRENDS

A first-time visitor to Namak Mandi who has some knowledge of gemstone trading hubs such as China, Thailand, and Sri Lanka would immediately notice

that it has probably some of the lowest-quality cutting. Namak Mandi's cutters still use a tool called the *angoora*, shown in figure 9C. The *angoora* is a metallic handle, one side of which is bent in such a way that it works as a base for angular positioning of the tool. On its opposite side (toward the thumb side in figure 9C), it has an adjustable hole with a copper screw to hold the wooden dop-stick, called a *khandee* (figure 10) in Pashtu. The tool does not have any angle settings. It is also important to highlight that the entire process using the angoora and khandee is done by hand, using the unaided eye.

Before cutting and polishing with the *angoora*, a lapidary first pre-forms a gemstone, either by hand or using a *khandee*. This is done to shape the stone so that it can be easily and firmly mounted on the top of the *khandee* (figures 9A and 9B). To dop the stone, the lapidary uses a combination of superglue and hot wax that is wrapped around the top of the *khandee* to firmly fix a gemstone onto it for faceting. The combination of glue and wax is referred to locally as *ma'waa*. The stone is manually positioned in the hot wax, a skill that takes years to develop. The next task is to place the crown angles, which is also done entirely by hand. Next, the lapidary inserts the *khandee* into the *angoora*. Since the *angoora* does not have angle settings, it is entirely up to the ability and experience of the lapidary to meticulously shape the stone, checking and rotating it every few seconds to place facets evenly according to the design desired by the customer.

Figure 10. The khandee *(wooden dop-stick) used with the* angoora *for faceting gemstones. Photo by Bilal.*

Once the faceting is complete, the lapidary takes the stone out of the *angoora* to facet the table. Next, a copper lap is used to polish the stone. Here again, the entire process is done by hand. For instance, while observing a local lapidary, Mr. Sajid, we noticed that he regularly used kerosene to wipe the surface of the copper lap clean. He would also apply diamond powder to achieve the required polish. Once the process was done, the gemstone was removed from the *khandee* and flipped upside down to follow the same procedure to facet and polish the pavilion. It took Mr. Sajid about an hour to complete the entire faceting and polishing process (figure 11). Mr. Sajid also informed us that some stones could take longer if the desired shape had a more complex pattern with many more facets than standard cuts. While the process is time-consuming, most traders doing business outside Pakistan recut the stones in Thailand, Sri Lanka, or China to increase their value in the international market.

Nonetheless, the *angoora*'s use is justified on two grounds. First, it saves stone weight, allowing for a higher price per carat. According to the local lapidaries using the *angoora*, modern faceting results in loss of weight. Our understanding is that because they lack formal training and education, Namak Mandi's lapidaries do not have the proper know-how of a modern faceter. Hence, they justify clinging to the *angoora* by saying that it retains weight. Second, in the words of Mr. Sajid, an *angoora* expert: "Just as we prefer an Afghani handmade carpet over a machine-made piece, so do people [in/around Namak Mandi] prefer a stone faceted with *angoora*." This remark, which was echoed by other lapidaries and retailers, can be interpreted in two ways. First, it is worth mentioning that mastering a modern faceting machine might cognitively require a higher level of formal education than using an *angoora*, but to become an expert in using the *angoora*, one must invest years of apprenticeship under an *ustad* (mentor). Modern faceting is counterintuitive to the decades-old tradition of *ustad-shagird* (mentor-mentee). It

Figure 11. A highly experienced cutter, Mr. Sajid, guided the authors through the entire process of faceting with the angoora*. Photo by Shakeel Anwar Khan.*

could also be argued that because experienced *angoora* users took years to master the art, they have a vested interest in continuing the tradition rather than accepting a change that, besides requiring an investment of time and financial resources, would ultimately wipe out their hard-earned skills.

In addition to the *angoora* culture, we documented Namak Mandi's online gemstone market. Somewhere around 2010, a handful of traders in Peshawar started doing business on eBay. At the time, this was a niche marketing strategy for exporting gemstones from Pakistan to the rest of the world, but it enabled them to gain repeat and long-term customers. Many merchants, particularly those originating from Afghanistan, would introduce the younger generations to the gemstone industry. The younger traders began to find innovative ways of selling their products. But Namak Mandi faces two obstacles in achieving the full potential of online sales. First, eBay accounts are usually linked to the most popular payment system, PayPal, which does not operate in Pakistan. Sellers tend to migrate abroad and set up their accounts from countries such as Thailand. Second, rogue traders tend to generate negative perceptions of the Pakistani gemstone market. They create Facebook accounts, attracting buyers with flowery language, and then sell them gemstones for above-market price or defraud their customers by providing the wrong stones altogether. The sellers also use camera effects to completely misrepresent the true features of the stone. In most cases, eBay closes such accounts. Although the fraud rate has fallen dramatically as eBay introduces new measures to combat these transactions, such practices have hindered Namak Mandi's online gemstone market. Thus, scandals and stories regarding online fraud are gradually making inroads for more ethical and responsible trading.

Finally, Pakistani women are starting to buy and sell gemstones online, which could be a game changer. Pakistan's gem trade in general and Namak Mandi, in particular, is a male-dominated marketplace. Women tend to avoid trading in such a "hostile" market. To navigate around this challenge, women entrepreneurs are doing business on eBay. Many are brokers: They arrange deals between traders in Pakistan and buyers who are based locally or globally. Since the few women who have entered the online marketplace are reportedly doing business quite ethically, they could ultimately influence their male counterparts to operate just as ethically, lest they lose their share of the market.

CONCLUSIONS

Over the last 50 years, Namak Mandi has evolved from a salt storage and trading market into a thriving gemstone business hub pulling local and Afghan traders. The exchange of rough and faceted stones, mineral specimens, and ornamental stones has turned it into a pioneer gemstone market in Pakistan. This transformation has come about with the sole support of APCEA and, literally, zero support from the relevant government departments. Nonetheless, the local and online business at Namak Mandi has been marred by complaints about unethical business practices. These primarily include: (1) occasionally duping the customers with low-quality gemstones and (2) charging exorbitant prices for the merchandise. Similarly, the lack and non-acceptance of modern faceting facilities potentially hinder Namak Mandi's traders from firmly finding a niche in or competing with regional gemstones centers in Thailand, China, India, or Sri Lanka. By and large, women traders' recent entry into the market, who reportedly do business ethically and responsibly, could pave the way for improving business culture overall.

ABOUT THE AUTHORS

Mr. Rehman is a PhD student at the Gemmological Institute, China University of Geosciences in Wuhan. He is also a lecturer at the Gems & Jewellery Centre of Excellence (GJCoE), University of Engineering & Technology (UET) in Peshawar, Pakistan. Mr. Bilal is a visiting lecturer at GJCoE, UET in Peshawar. Dr. Owais is assistant professor of sociology at the University of Peshawar. Mr. Ur Rahman is a visiting lecturer at GJCoE, UET in Peshawar. Dr. Shen (corresponding author) is a distinguished professor at the Gemmological Institute, China University of Geosciences in Wuhan.

ACKNOWLEDGMENTS

We are grateful to Ehtisham Ullah Khan, CEO of the Himalaya Gem Testing Laboratory, and also to Amjad Ali Shinwari, Khalid Habib, and Haji Zawir Khan for sharing their experience regarding the gemstone trade in Namak Mandi. We are also thankful to Meher Mohammad (secretary of the APCEA) and Haji Minhaj-Ud-Din (former chairman and now chief organizer of the APCEA exhibition) for sharing the details regarding APCEA, and to Bilal Omar (owner of Mineral Capture) and Ghulam Mustafa (owner of Fine Arts Minerals) for providing some specimens for photography. The authors would like to thank Shakeel Anwar Khan for taking photographs for our report.

REFERENCES

Hussain Y. (2015) The indelible experience of Namak Mandi, Peshawar. *Youlin Magazine—A Cultural Journal*. Available from: https://www.youlinmagazine.com/article/the-indelible-experience-of-namak-mandi-peshawar/NDg1

Laurs B.M. (2016) Gem Notes: Faceted quartz with petroleum inclusions from Baluchistan, Pakistan. *Journal of Gemmology*, Vol. 35, No. 1, p. 15.

Rehman H.U., Martens G., Tsai Y.L., Chankhantha C., Kidkhunthod P., Shen A.H. (2020) An x-ray absorption near-edge structure (Xanes) study on the oxidation state of chromophores in natural kunzite samples from Nuristan, Afghanistan. *Minerals*, Vol. 10, No. 5, p. 463, https://doi.org/10.3390/min10050463

Lab Notes

Editors
Thomas M. Moses | Shane F. McClure

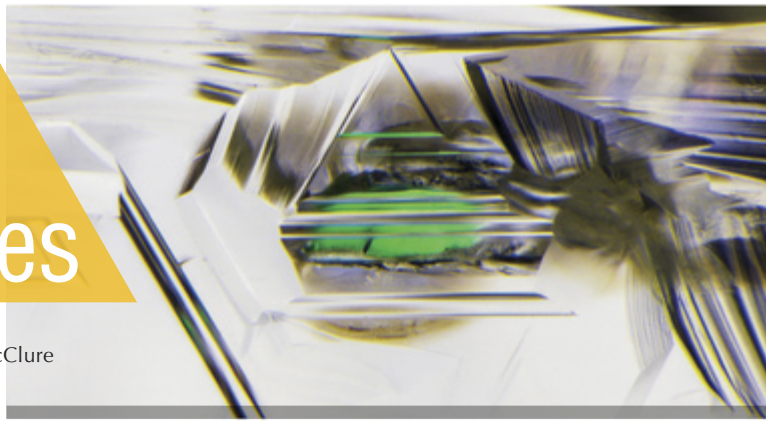

Atypical Dyed BERYL

A green stone mounted in a ring was recently submitted to the New York lab. The ring's prongs prevented a full reading of the stone's refractive index, but a maximum reading of 1.578 indicated the material was potentially beryl. Face-up, the even distribution of color made an identification of emerald appear likely (figure 1). However, careful microscopic examination revealed an even distribution of thin green zoning resembling mica platelets typical of amazonite (figure 2). Oblique fiber-optic lighting exposed a network of incipient basal cleavage perpendicular to the c-axis (figure 3). Using a handheld spectroscope, a characteristic of dyed green beryl was observed: a broad absorption band in the red region in the absence of chromium lines. Denser green color concentrations were also present in larger surface-reaching fissures.

While dyed beryl is occasionally submitted to GIA, it is mostly translucent and immediately identifiable due to its unnatural color. This impressive emerald imitation was the first of its kind submitted to the New York or Carlsbad labs. It serves as an important reminder that careful, methodical gemological testing is necessary to detect these subtler treatments.

Tyler Smith

Figure 1. A mounted green stone with a superficial resemblance to emerald was later revealed to be dyed beryl.

CVD Laboratory-Grown DIAMOND With Counterfeit GIA Inscription

In recent months, GIA has seen a number of laboratory-grown diamonds submitted for update or verification services with counterfeit inscriptions referencing GIA natural diamond reports ("GIA laboratory prevents attempted fraud," GIA press release, May 17, 2021, https://www.gia.edu/gia-news-press/gia-lab-prevents-attempted-fraud). One recent example is a 3.07 ct round brilliant submitted to the Antwerp lab for update service (figure 4). It bore an inscription matching a GIA report for a natural diamond that had been submitted in 2018. Microscopic examination quickly revealed,

Figure 2. Thin, evenly distributed concentrations of green dye in the beryl, as seen through the table. Field of view 1.76 mm.

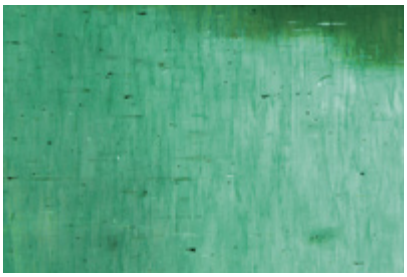

Figure 3. Basal cleavage under oblique illumination. Shallow cavities can be seen toward the top, where the fissures reach the surface of the stone. Field of view 2.90 mm.

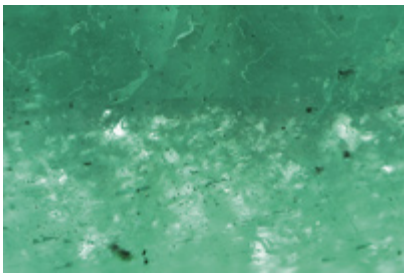

Editors' note: All items were written by staff members of GIA laboratories.

Gems & Gemology, Vol. 57, No. 2, pp. 150–157.

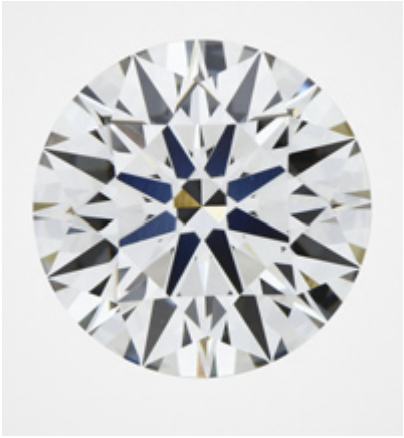

Figure 4. This 3.07 ct CVD lab-grown diamond was submitted with a counterfeit GIA inscription that corresponded to a previously graded natural diamond.

TABLE 1. Comparison of the natural diamond submitted to GIA in 2018 and the laboratory-grown diamond submitted with a counterfeit inscription in 2021.

	Natural	Laboratory-grown
Weight (ct)	3.078	3.075
Shape	Round brilliant	Round brilliant
Measurements (mm)	9.33–9.38 x 5.74	9.39–9.41 x 5.76
Girdle	Slightly thick	Medium
Cut	Excellent	Excellent
Symmetry	Excellent	Excellent
Polish	Excellent	Excellent
Color	G	H
Long-wave UV fluorescence	None	None
Clarity	IF	VVS_2
Inclusions	-	Pinpoints, needles
Diamond type	Ia	IIa

however, that the inscription was in fact fraudulent. Further analysis indicated a laboratory-grown origin.

Comparison showed an attempt to precisely match the laboratory-grown diamond to the information contained in the original report (table 1). Both were round brilliants with excellent cut properties and very close in carat weight and measurements. The natural diamond, however, did have a slightly better color and clarity (G-IF compared to H-VVS_2). The clarity grade of the laboratory-grown diamond (VVS_2) was set by two types of inclusions: pinpoints and needles.

Further analysis of the laboratory-grown diamond was performed using advanced spectroscopic techniques. Whereas the original diamond was type Ia and had a high concentration of nitrogen such that it saturated the detector in the one- phonon region (1335–1085 cm^{-1}), Fourier-transform infrared (FTIR) analysis revealed that the newly submitted diamond was nominally type IIa. The spectrum showed the weak presence of isolated nitrogen at 1344 cm^{-1} and the absence of both the 3107 cm^{-1} and the CVD-specific NVH^0 band at 3123 cm^{-1}. Photoluminescence (PL) spectra taken with various laser excitation wavelengths and at liquid nitrogen temperature showed the strong presence of the SiV^- doublet (736.6/736.9 nm), a defect commonly observed in CVD laboratory-grown diamonds. This strong SiV^- center was also conspicuous in the UV-Visible absorption spectrum taken at liquid nitrogen temperature. Other defects detected with PL spectroscopy were strong $NV^{0/-}$ (575 and 637 nm) centers, a strong H3 (503.2 nm) center, and weak nickel-related defects (883/884 nm doublet).

DiamondView imaging displayed a typical CVD growth structure with a green-blue layered pattern and banded layers, indicating a start-stop growth (figure 5). A weak greenish blue phosphorescence was observed after switching off the UV source.

Based on all the observations, we concluded this was a CVD laboratory-grown diamond that had undergone HPHT treatment after growth. As with all laboratory-grown diamonds submitted to GIA, it was then inscribed with "LABORATORY-GROWN" (figure 6, left). The

Figure 5. DiamondView imaging confirmed CVD growth and subsequent HPHT treatment.

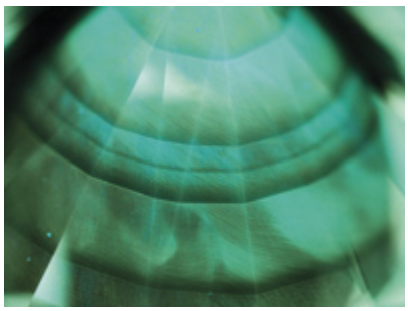

Figure 6. In accordance with GIA procedures, the LABORATORY-GROWN inscription was added to the girdle (left) and the counterfeit report number inscription was rendered illegible (right).

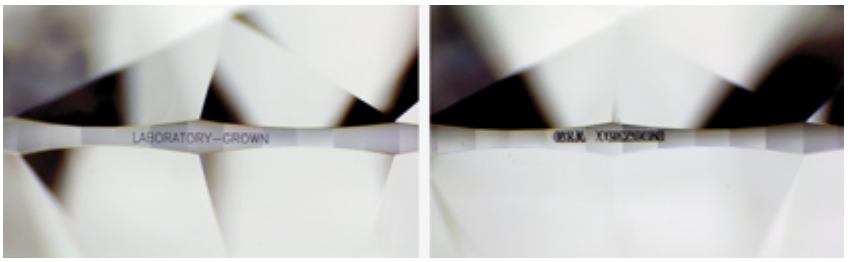

Figure 7. A Melo pearl measuring 20.50 × 19.25 × 18.85 mm and weighing 55.10 ct. A fine crack is visible across the center of the surface.

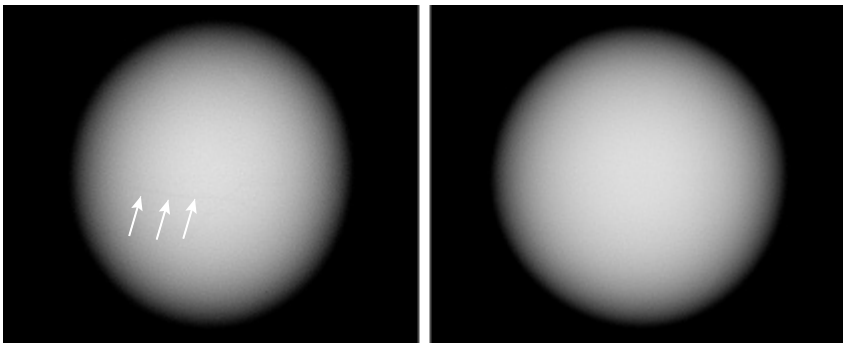

Figure 9. Microradiographs in two directions showed no obvious internal growth structure. Only a fine dark line showed in one orientation, which corresponded to a surface-reaching crack (left, indicated by the white arrows).

counterfeit inscription was overwritten (figure 6, right) and a new GIA report number was placed on the girdle.

This example demonstrates the importance of careful examination to verify a diamond's origin. A close comparison of the CVD diamond with the earlier report on a natural diamond showed a very precise attempt at matching.

Ellen Barrie and Sally Eaton-Magaña

Melo PEARL Found in a Melo Shell

Over the years, there have been a number of reports relating discoveries of natural pearls in edible oysters (e.g., Fall 2019 Gem News International, pp. 439–440; Fall 2020 Lab Notes, pp. 420–422). However, similar discoveries are much rarer in gastropods, such as species of the *Melo* genus. Such finds often make headlines, as was the case recently in Thailand when a few discoveries were reported on social media. One of these remarkable stories, titled "A delicious find," was posted on www.facebook.com/GIAEducation on April 9, 2021. It detailed the discovery of a large oval orange Melo pearl measuring 20.50 × 19.25 × 18.85 mm and weighing 55.10 ct that was submitted to GIA's Bangkok laboratory for testing in September 2020 (figure 7). The owner claimed to have accidentally found this pearl in an inexpensive Melo shell he purchased with another shell from a local market in Rayong Province, eastern Thailand.

This note offers additional detail on the pearl that was the subject of that story. To the eye, the pearl looked exactly as a Melo pearl should. Its size and color were consistent with that type of pearl, and it exhibited various flame structure patterns on its surface: short patchy flames, thin elongated flames, and "triangular" flames reminiscent of Christmas trees (figure 8). These features were consistent with flame structures previously observed on Melo pearls (D.J. Content, Ed., *Pearl and the Dragon: A Study of Vietnamese Pearls and a History of the Oriental Pearl Trade*, Houlton, Maine, 1999, pp. 90–92; H. Htun et al., "Melo 'pearls' from Myanmar," Fall 2006 *G&G*, pp. 135–136; V. Pardieu, "Concise Field Report: Melos and their pearls in Vietnam," *GIA Research News*, https://www.gia.edu/ongoing-research/melo-pearls-from-vietnam, 2009). Some other associated minor surface features were visible, together with a long fine crack traversing one area (figure 8, left). Microradiography revealed no obvious internal growth structure (figure 9). Only the fine crack previously mentioned showed

Figure 8. Various flame structure patterns visible on the pearl's surface: short patchy flames with a fine surface-reaching crack (left), thin elongated flames with some minor natural features (center), and flames reminiscent of Christmas trees (right). Fields of view 19.20, 7.20, and 3.60 mm, respectively.

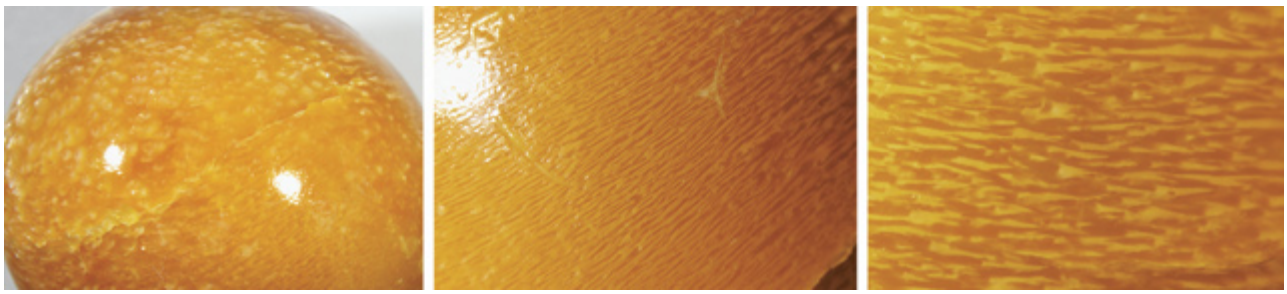

as a dark fine line in the correct orientation (figure 9, left, indicated by the white arrows). The absence of any surface modification and the presence of natural surface features, in addition to the lack of banded structure typically observed in shell samples, proved this was a pearl and not an imitation fashioned from Melo shell (Summer 2006 Lab Notes, pp 166–167; N. Sturman et al., "An imitation Melo pearl," *GIA Research News*, https://www.gia.edu/gia-news-research/imitation-melo-pearl, 2011).

Spectral analyses using Raman, photoluminescence (PL), and UV-Visible (UV-Vis) spectroscopy proved the pearl's color was of natural origin. Raman spectra revealed features at 701, 705, and 1085 cm^{-1} identifying aragonite, together with polyenic peaks at 1130 and 1520 cm^{-1} responsible for the orange coloration. These polyenic peaks are consistent with other naturally colored porcelaneous pearls (S. Karampelas et al., "Polyacetylenic pigments found in pearls and corals," *30th International Gemmological Conference Proceedings*, 2007, pp. 49–51; Summer 2018 Lab Notes, pp. 211–212).

An interesting declaration made by the pearl's owner probably explains the presence of the fine eye-visible surface crack. The Melo shell containing the hidden pearl was boiled, and the Melo pearl was only discovered when the meat was being prepared for consumption. Hence, it is likely that the temperatures and duration applied during the cooking process caused the crack's formation. This point has been mentioned by a number of pearl traders during discussions with lab gemologists over the years, so it seems an important consideration when such cracks are observed. Even so, the notable size, unmodified surface, perfectly formed oval shape, and intense natural color all combined to make this a desirable and special pearl.

Nanthaporn Nilpetploy

Imitation MOLDAVITE

Recently GIA's Carlsbad laboratory received for identification a 46.13 ct yellowish green rough stone. The lack of a polished flat surface prevented a refractive index reading, while the specific gravity was measured as 2.45. Under microscopic examination, very few gas bubbles were found and some straight, approximately evenly spaced surface features were observed (figure 10). Closer examination revealed these features were likely artificially acid-etched flow lines. The presence of gas bubbles coupled with flow lines led the author to infer an artificial glass or a natural glass, possibly moldavite, though moldavite has more natural-looking flow lines (figure 11). The SG reading was also slightly higher than the expected SG of 2.36 for moldavite. Additionally, moldavite typically contains numerous gas bubbles. Suspecting an artificial glass, the author analyzed the stone with a Fourier-transform infrared (FTIR) spectrometer. The FTIR reading showed absorption bands at approximately 2900 and 3480 nm, which confirmed an artificial glass.

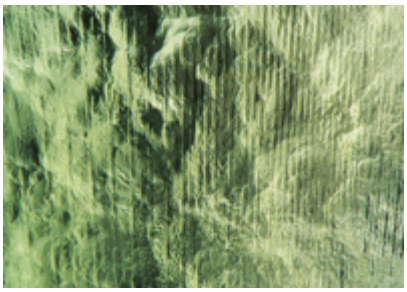

Figure 10. Acid-etched flow lines on artificial glass imitating moldavite. Field of view 2.34 mm.

Moldavites are a form of tektite, an impact glass created by the melting of rock caused when a meteorite strikes the earth's surface. The most famous moldavites, found in southern Bohemia in the Czech Republic, were formed by the impact of the meteor that created the Ries crater 500 km away in southern Germany 14.7 million years ago. With rising prices for moldavite over the past few years, moldavite imitations have become more prevalent (Spring 2015 Gem News International, pp. 103–104).

Figure 11. Natural flow lines on moldavite. Field of view 7.19 mm.

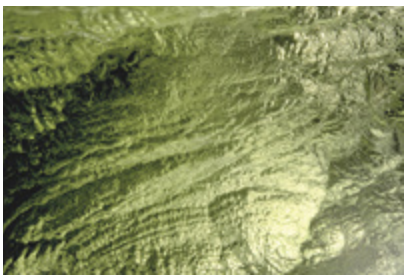

Michaela Stephan

Exquisite OPAL Strand

The Carlsbad laboratory recently received for identification a strand of 28 graduated round gray beads displaying spectacular play-of-color (figure 12). At the time of inspection, the strand weighed 115.5 grams total. Standard gemological properties were consistent with opal. All 28 beads had a spot RI reading of approximately 1.39 and fluoresced very weak yellow under short-wave UV and weak yellow to long-wave UV. No indications of dye, color treatment, clarity enhancement, or coating were present. All of the beads showed a natural play-of-color phenomenon under microscopic examination. A single drop of water was placed on the surface of each bead and observed under direct transmitted light in brightfield mode in the microscope. Each bead absorbed the water, revealing them to be porous. Therefore, it was concluded that all 28 beads were natural hydrophane opal with natural color. Crazing was not observed in any of them.

Hydrophane opals are porous enough to absorb water, which can cause a change in appearance and a temporary increase in weight. It is therefore not advisable to immerse them in water (Fall 2013 Lab Notes, pp. 175–176).

This opal strand was remarkable due to the unusually bright and vibrant spectral play-of-color seen evenly across all 28 beads. Play-of-color in precious opal is caused by light interacting with stacked submicroscopic silica spheres. Light waves bend as they pass

Figure 12. This spectacular opal strand displayed unusually bright, vibrant play-of-color across all 28 beads.

between these spheres, causing the light to diffract into the spectral colors of the rainbow. The resulting color is determined by the size of the spheres. For example, approximately 0.1 micron spheres produce a violet color and approximately 0.2 micron spheres display a red color (https://www.gia.edu/opal-description).

Michaela Stephan

Transparent RHODONITE with Clarity Enhancement

Recently the Carlsbad laboratory received a transparent vivid orangy red rhodonite for identification service (figure 13). Standard gemological testing revealed a double refractive index of 1.727–1.738, and a specific gravity of 3.66 was obtained. The stone was inert to both long-wave and short-wave UV light. These properties were consistent with rhodonite (R. Webster, *Gems*, 5th ed., rev. by P.G. Read, Butterworth-Heinemann, Oxford, 1994, p. 365). Rhodonite, with the formula $CaMn_3Mn[Si_5O_{15}]$ (mindat.org), is a member of the triclinic crystal system and occurs in manganese-bearing rocks.

During microscopic analysis, scattered curved needle-like inclusions (figure 14) were observed as well as fractures with clarity-enhancing residue that also contained high-relief areas where gas bubbles were trapped (figure 15). Although the source of this particular rhodonite is unknown, curved needle inclusions in transparent rhodonite from Brazil were previously reported in 2004 and 2008 (Fall 2004 GNI, pp. 260–261). The appearance of the needle-like inclusions was consistent with those previously identified as cummingtonite (P. Leverett et al., "Ca-Mg-Fe-rich rhodonite from the Morro da Mina mine, Conselheiro Lafaiete, Minas Gerais, Brazil," *The Mineralogical Record*, 2008, Vol. 39, pp. 125–130).

In addition to Brazil, Australia is a well-documented source of gem-quality rhodonite (P. Millsteed et al., "Inclusions in transparent gem rhodonite from Broken Hill, New South Wales, Australia," Fall 2005 *G&G*, pp. 246–254). Despite being clarity enhanced, this saturated gem-quality rhodonite was exceptional for its bright vivid color, transparency, and size.

Amy Cooper

Figure 13. A large 11.32 ct rhodonite showing vivid orangy red color and visible needle-like inclusions.

Figure 14. These scattered randomly oriented curved needle-like inclusions are likely the mineral cummingtonite. Field of view 2.56 mm.

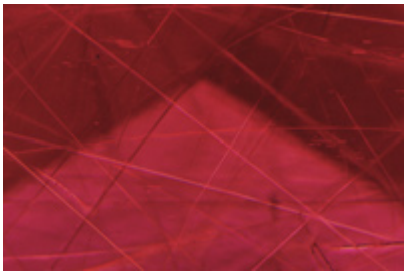

Figure 15. Low-relief fractures with high-relief trapped gas bubbles offer proof of clarity enhancement in the faceted transparent rhodonite. Field of view 3.12 mm.

RUBY

Amphibole Mineral Inclusions in Mozambique Ruby

Amphibole, a mineral supergroup with a diverse chemical composition of the general formula $AB_2C_5T_8O_{22}W_2$,

Figure 16. Densely distributed amphibole inclusions in ruby. Field of view 9.40 mm.

where A = □ (vacancy), Na^{+}, K^{+}, Ca^{2+}, Pb^{2+}, Li^{+}; B = Na^{+}, Ca^{2+}, Mn^{2+}, Fe^{2+}, Mg^{2+}, Li^{+}; C = Mg^{2+}, Fe^{2+}, Mn^{2+}, Al^{3+}, Fe^{3+}, Mn^{3+}, Cr^{3+}, Ti^{4+}, Li^{+}; T = Si^{4+}, Al^{3+}, Ti^{4+}, Be^{2+}; and W = OH^{-}, O^{2-}, F^{-}, Cl^{-}, is a collectors' item as a loose stone; its members are known as constituent minerals of nephrite (X. Feng et al., "Characterization of Mg and Fe contents in nephrite using Raman spectroscopy," Summer 2017 *G&G*, pp. 204–212). In addition, amphibole appears as crystal inclusions in both ruby and sapphire reported from Mozambique and Kashmir (e.g., Winter 2018 Lab Notes, pp. 435–436). Recently, the GIA lab in Tokyo received a Mozambique ruby densely included with rounded anhedral crystals (figures 16 and 17). The Raman pattern of the surface-reaching crystals most closely matched the RRUFF reference

Figure 17. Photomicrograph of rounded anhedral amphibole crystals. Field of view 3.25 mm.

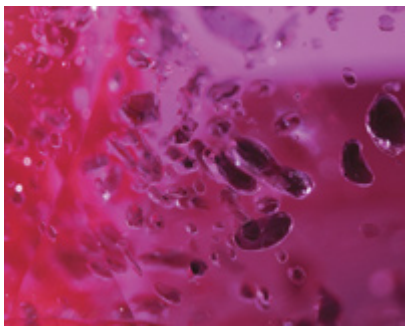

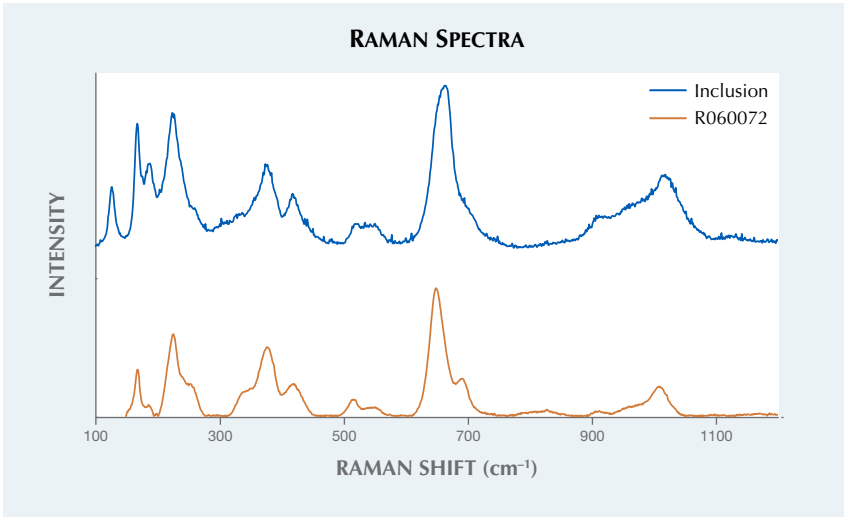

Figure 18. The Raman spectrum of the amphibole mineral inclusions (blue) and the reference spectrum of pargasite from the RRUFF database (R060072).

spectrum (no. 060072) of the calcic amphibole pargasite (figure 18). The Raman peak at 669 cm^{-1} corresponded to the symmetric stretching vibration of T elements, which are tetrahedral ring structures composed mainly of the Si-O_b-Si linkage (O_b = bridging oxygen) and often used to fingerprint various amphibole species (N. Waeselmann et al., "Nondestructive determination of the amphibole crystal-chemical formulae by Raman spectroscopy: One step closer," *Journal of Raman Spectroscopy*, Vol. 51, No. 9, 2020, pp. 1530–1548). The FTIR pattern showed some peaks between 3600 and 3800 cm^{-1} in the principal OH-stretching region of octahedral metal components, which are C cations in the general formula of amphibole (figure 19). The FTIR pattern showed a peak at 3643 cm^{-1} in addition to peaks at 3671 and 3704 cm^{-1}, suggesting the possibility that

Figure 19. The FTIR spectrum of the Mozambique ruby, indicating the amphibole-related peaks between 3600 and 3800 cm^{-1}. The 3309 cm^{-1} peak is associated with corundum.

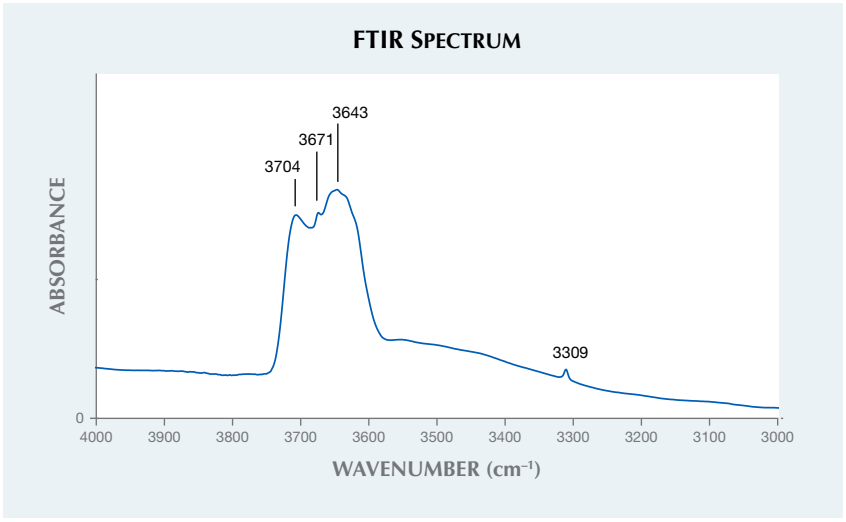

other elements such as Fe occupied those sites typical of pargasite in some portions (e.g., M.C. Day et al., "Gem amphiboles from Mogok, Myanmar: Crystal-structure refinement, infrared spectroscopy and short-range order–disorder in gem pargasite and fluoropargasite," *Mineralogical Magazine*, Vol. 83, No. 3, 2019, pp. 361–371). The FTIR spectra of corundum between 2000 and 5000 cm^{-1} were very useful for the identification of mineral inclusions in corundum. This is the first known report of an FTIR pattern identifying amphibole mineral inclusions in corundum.

Kazuko Saruwatari and Masumi Saito

Chrysoberyl Inclusions in Flux-Grown Ruby

The Tokyo laboratory recently received a 3.02 ct red pear-shaped mixed cut measuring 10.93 × 7.04 × 5.03 mm (figure 20). Standard gemological testing yielded a refractive index of 1.765–1.773; a hydrostatic specific gravity of 4.00; absorption lines at 693, 476, and 468 nm; and a broad absorption band between 500 nm and 610 nm seen using a handheld spectroscope. All of these properties were consistent with ruby. The stone displayed strong red fluorescence under both long-wave and short-wave UV.

Figure 20. This ruby proved to be a flux-grown synthetic ruby with chrysoberyl inclusions.

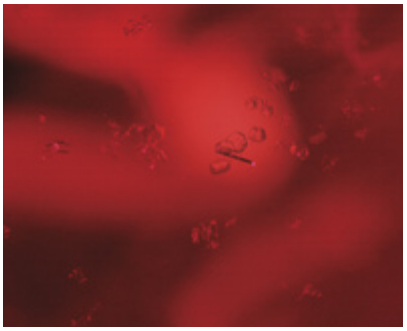

Figure 21. These natural-looking hexagonal colorless crystals and the small nest of inclusions in the flux-grown ruby (top of image and around the hexagonal crystals) could be mistaken for natural corundum inclusions. Field of view 1.41 mm.

Microscopic examination revealed numerous hexagonal colorless inclusions as well as small colorless inclusions that resembled zircon nests often found in natural corundum (figure 21). Also observed were features suggesting the possibility of flux-grown corundum: hexagonal dark reflective long prisms and platelets (figure 22) and healed fissures filled with flux residues (figure 23).

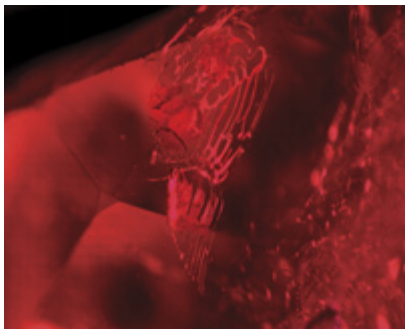

Figure 23. Fingerprints in the flux-grown ruby could also be mistaken for natural residue-filled fingerprints. Field of view 1.23 mm.

Laser ablation–inductively coupled plasma–mass spectrometry (LA-ICP-MS) detected high amounts of Be (35.3–37.1 ppma), Cr (1733.5–2047.2 ppma), Rh (0.6–1.0 ppma), and Pt (0.5–1.1 ppma). Elements normally present in natural corundum such as Mg, Ga, and V were not detected. The chemistry indicated a flux growth process.

Earlier work has shown numerous transparent, colorless hexagonal tabular "ghost-like" inclusions in Chatham flux-grown sapphire (R.E. Kane, "The gemological properties of Chatham flux-grown synthetic orange sapphire and synthetic blue sapphire," Fall 1982 *G&G*, pp. 140–153). In that study, X-ray diffraction analysis (XRD) revealed that the pattern of the ghost-like inclusions was identi-

Figure 22. The hexagonal dark reflective long prisms (left) and platelets (right) observed in the sample are common inclusions in flux-grown synthetic corundum. Field of view 1.28 mm.

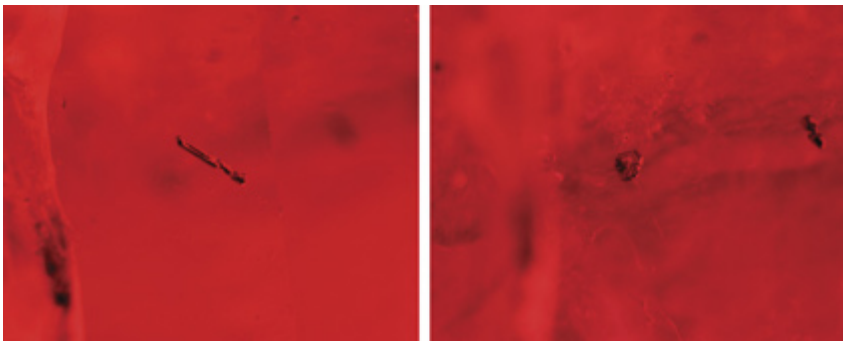

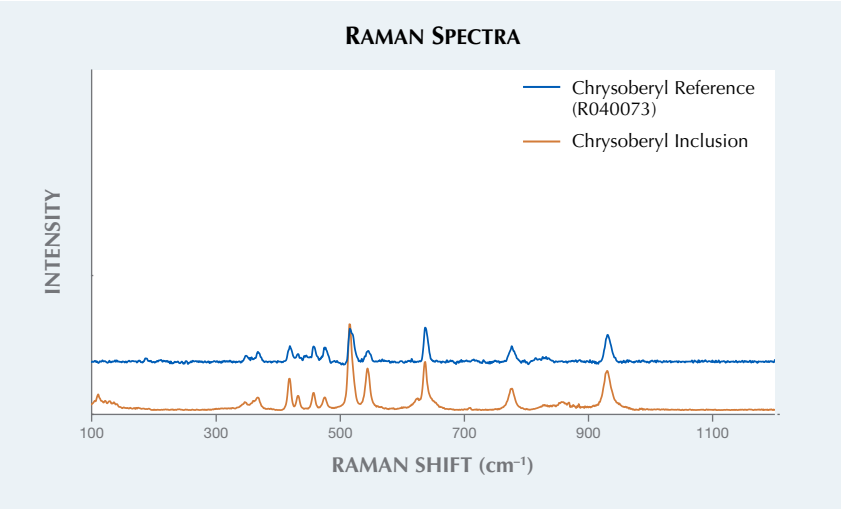

Figure 24. The Raman spectrum of the chrysoberyl inclusion compared to that of the known reference.

cal to that of chrysoberyl. That study also stated that Chatham, who was successful in synthesizing sapphire by the flux method, added heavy concentrations of beryllium, which explained the presence of chrysoberyl and the high beryllium trace element content. More recently, natural-looking transparent hexagonal crystals in a flux-grown pink sapphire have also been reported (Fall 2017 Lab Notes, pp. 367–368). There was no surface-reaching transparent crystal in that pink synthetic sapphire, but the small amounts of beryllium suggested the possibility of chrysoberyl. In the present laboratory-grown ruby, fortunately, one of the transparent crystals reached the surface. With Raman spectroscopy, we were able to identify it as chrysoberyl (figure 24).

The beryllium concentration of this laboratory-grown ruby (up to 37 ppma) indicated possible beryllium diffusion treatment. High chromium (up to 2047 ppma) resulted in a vivid red color. With such a highly saturated bodycolor, we cannot deny the possibility of beryllium diffusion, though the signature orange rim was not found using immersion techniques. The numerous chrysoberyl crystals offer important evidence that the beryllium was already excised during the flux growth process. Beryllium diffusion of corundum requires exposure to extreme heat (above 1780°C; J.L. Emmett et. al., "Beryllium diffusion of ruby and sapphire," Summer 2003 *G&G*, pp. 84–135). These chrysoberyl inclusions do not show the typical indications following heat treatment, meaning this stone was not beryllium diffused after its growth.

With LA-ICP-MS and Raman spectroscopy, we were able to confirm that flux-grown laboratory-grown ruby with high beryllium content could indicate the presence of natural-looking chrysoberyl crystals.

Yuxiao Li

PHOTO CREDITS
Sean-Andrew Z. Pyle—1; Tyler Smith—2, 3; Ellen Barrie—4, 5, 6; Nuttapol Kitdee—7; Kwanreun Lawanwong—8; Michaela Stephan—10, 11; Angelica Sanchez—12; Diego Sanchez—13; Nathan Renfro—14, 15; Kazuko Saruwatari—16; Masumi Saito—17; Shunsuke Nagai—20; Yuxiao Li—21, 22, 23

Iridescent Abalone Shell

The glowing rainbow-colored image resembling a topographic map in figure 1 was captured over the polished surface of an abalone shell. Abalone is a common marine gastropod (univalve mollusk) belonging to the family Haliotidae and the genus *Haliotis*. Abalone mollusks are distributed along coastal waters worldwide and associated with rocky habitats. They are well known as nutrition-rich seafood, and their ear-shaped shells are also popular in jewelry owing to their uniquely vibrant iridescent nacre known as mother-of-pearl.

Figure 1. The surface of this colorfully iridescent abalone shell resembles a topographic map. Photomicrograph by Michaela Stephan; field of view 23.14 mm.

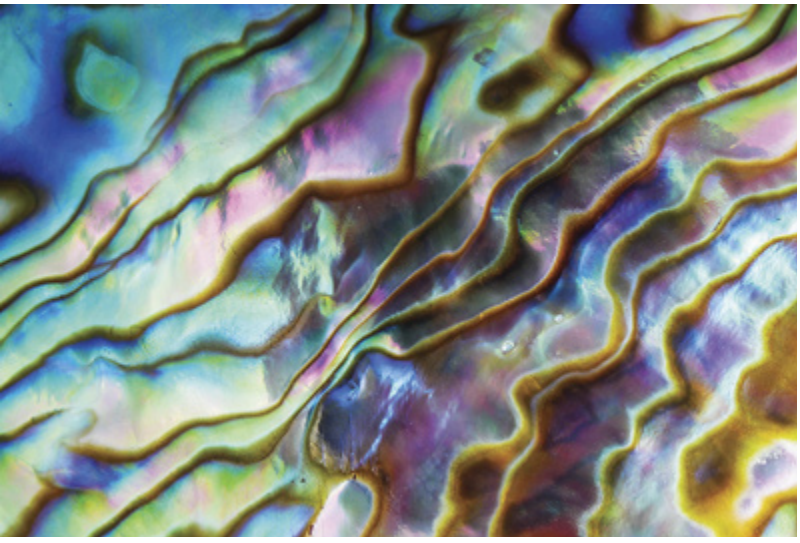

Iridescence is an optical phenomenon frequently observed in gem materials, as well as in nacreous shells and pearls. *Orient* is the specific term for the iridescent effects attributed to interference and diffraction of light in the multilayered aragonite platelet structure. Shells and pearls produced by the *Haliotis* species generate the highest degree of iridescence, with a full range of distinct rainbow colors. These colors are caused by the fine grating structure created by the thin and closely packed nacre layers, similar to that of a diffraction grating (T.L. Tan et al., "Iridescent colours of the abalone shell (*Haliotis glabra*)," *Journal of Gemmology*, Vol. 29, No. 7/8, 2005, pp. 395–399). This extraordinary property lends a charming appearance to shell, pearl, and assembled cultured blister "pearls" (mabe) produced by abalone mollusks and makes them widely popular in the gem and jewelry industry.

Artitaya Homkrajae and Michaela Stephan
GIA, Carlsbad

Colorful Inclusions in Diamond

Inclusions can be found in a variety of different gemstones; they create a window that allows the viewer to picture a stone's formation history. Diamond possesses the ideal characteristics for preserving these features. Chemically inert and durable, it is the perfect host for inclusions.

About the banner: This topaz crystal from Minas Gerais, Brazil, shows interesting circular etch patterns on a prism face, while subsurface fractures display vivid interference colors. This image was taken using episcopic differential interference contrast microscopy. Photomicrograph by Nathan Renfro; field of view 1.44 mm.

Gems & Gemology, Vol. 57, No. 2, pp. 158–165.

Figure 2. The 2.56 ct diamond oval (left) contains green crystals of diopside and enstatite, while the 1.48 ct round brilliant (right) contains a purplish pink pyrope garnet. Photos by Towfiq Ahmed.

In general, inclusions in gem diamonds are considered undesirable. While extremely common in a number of forms, they almost always lower the clarity grade of a diamond to varying degrees depending on their type, size, quantity, and location. This happens because they are "imperfections" within the crystal that can ultimately affect the way light interacts with the stone, detracting from the overall brilliance of a properly faceted gem. In some cases, however, inclusions can make a diamond uniquely special.

Recently the New York lab examined two gem-quality diamonds (figure 2) possessing vivid green and purplish pink inclusions. With Raman spectroscopy, the green inclusions were identified as enstatite and diopside while the purplish pink inclusion was identified as pyrope garnet (figure 3). Both are common in ultramafic rocks, typically from a peridotite host. Chromium, an element characteristic of the earth's very deep rocks, is the chromophore responsible for both the green and the pink within these different minerals. The different lattice environments within these minerals results in distinct octahedral Cr-O bond lengths, and therefore they differ in light absorption and color produced. The vivid green color and shape of the diopside and enstatite are similar to those of the inclusions captured in *The Microworld of Diamonds: A Visual Reference Guide*, by John I. Koivula (Gemworld International, Northbrook, Illinois, 2000). As these diamonds formed, they enveloped the inclusions.

It is rare to see such high-quality diamonds with these types of inclusions. These timeless diamonds possess valuable relics of Earth's beginnings, making their clarity features noteworthy.

Stephanie Persaud, Anthony Galati, and Paul Johnson
GIA, New York

Figure 3. Microscopic observation revealed a green chromium-colored diopside in the 2.56 ct diamond (left) and a purplish pink pyrope garnet inclusion in the 1.48 ct diamond (right). Photomicrographs by Stephanie Persaud; field of view 1.00 mm (left) and 2.50 mm (right).

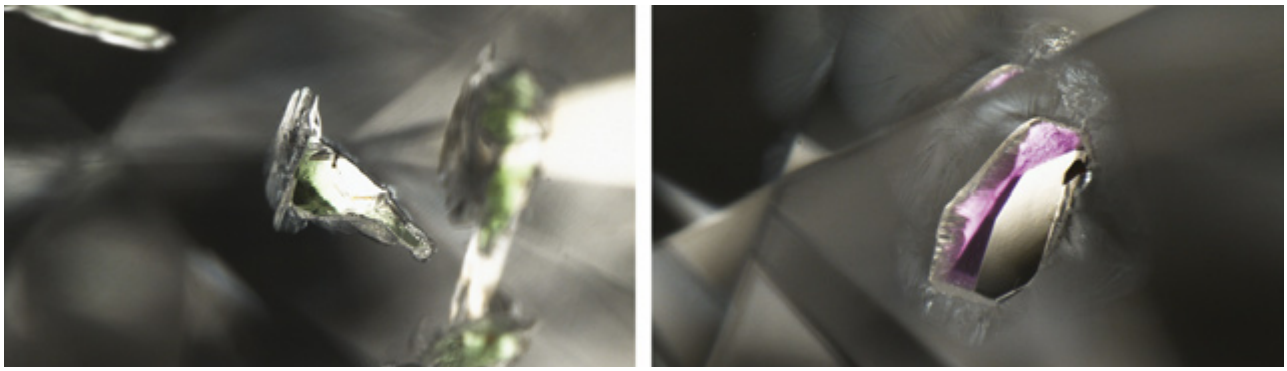

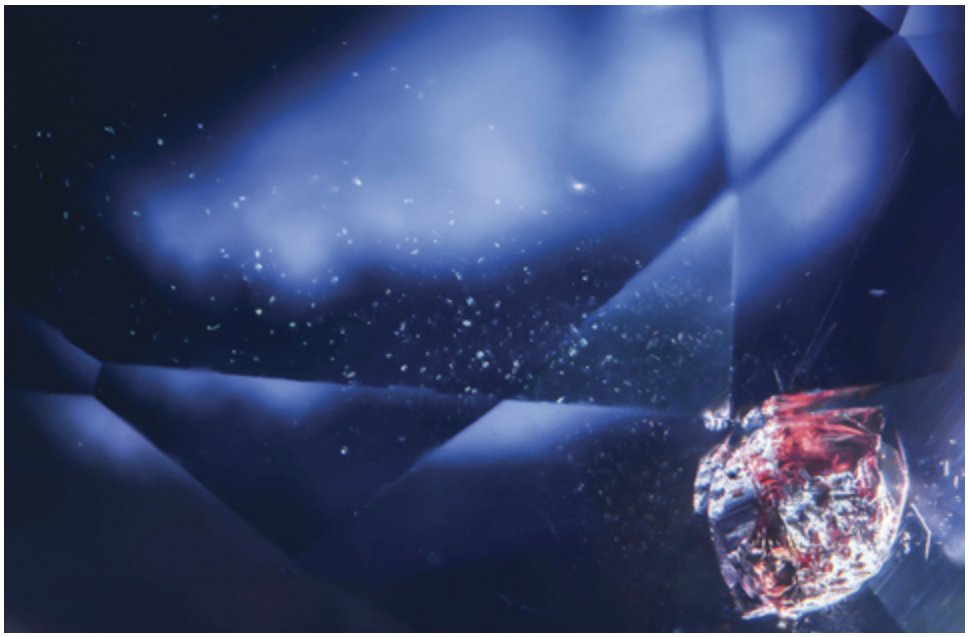

Figure 4. This sapphire contains a beautiful garnet inclusion and a trail of dust-like rutile particles. Photomicrograph by Michaela Stephan; field of view 4.79 mm.

Garnet in Sapphire

The author recently examined a 3.26 ct sapphire that changed from green-blue in fluorescent light to reddish purple in incandescent light. The color-change sapphire contained a large eye-visible crystal inclusion (figure 4). Microscopic examination of the singly refractive inclusion revealed garnet's characteristic dodecahedral crystal shape with rounded edges.

Of all the possible inclusions contained within sapphire, garnet is a rare and beautiful occurrence. When garnet crystal inclusions do occur, they often indicate an origin of Tanzania or the U.S. state of Montana (E.J. Gübelin and J.I. Koivula, *Photoatlas of Inclusions in Gemstones*, Vol. 3, Opinio-Verlag Publishers, Basel, Switzerland, 2008, pp. 228–242). In this sapphire, a large vibrant orange garnet is followed by a trail of dust-like rutile particles, much like an asteroid streaking across the night sky.

Michaela Stephan

Neptunite Inclusion in Benitoite

The authors recently examined a round, slightly zoned blue and near-colorless faceted benitoite that contained an interesting inclusion. Microscopic observation revealed a well-formed euhedral semitransparent reddish brown crystal surrounded by fine short needles and fluid fingerprints (figure 5). Because of the color and structure of the inclusion, both neptunite and joaquinite were considered as the possible identity. In benitoite, these minerals are often found in association and may have a similar color to the inclusion observed in this particular example. One method of separating neptunite from joaquinite is pleochroism. A yellow-orange, orange, and deep red pleochroism is consistent with neptunite, while light yellow and colorless pleochroism is consistent with joaquinite (webmineral.com). This inclusion showed a reddish orange to red pleochroism that was more consistent with neptunite. Raman analysis confirmed the host crystal was benitoite and the orangy red inclusion was neptunite, which has been previously documented (E.J. Gübelin and J.I. Koivula, *Photoatlas of Inclusions in Gemstones*, Vol. 1, 5th ed., 2008, Opinio-Verlag Publishers, Basel, Switzerland, p. 416).

Benitoite is a barium titanium silicate ($BaTiSi_3O_9$). This rare gem is found primarily in San Benito County, California, though it also occurs in other locations worldwide. Neptunite's chemical formula is $KNa_2Li(Fe^{2+},Mn)_2Ti_2Si_8O_{24}$, and it also occurs in San Benito County. Neptunite is found in association with other minerals in New Mexico, Greenland, and Canada, to name just a few (W.L. Roberts et al., *Encyclopedia of Minerals*, 2nd ed., 1990, Van Nostrand Reinhold, New York, pp. 603–604). The gem-quality benitoite material comes from the Benitoite Gem mine and the Junnila Claim (B. Laurs et al., "Benitoite from the New Idria District, San Benito County, California," Fall 1997 *G&G*, pp. 166–187). This faceted benitoite contains one of the best examples of neptunite in benitoite seen by the authors.

Amy Cooper and Nathan Renfro
GIA, Carlsbad

Xenomorphic Olivine Inclusion in Diamond

The author recently examined a faceted diamond that contained an oddly shaped near-colorless crystal with a low-relief tension crack surrounding it. The inclusion was identified by Raman spectroscopy as olivine, a rather common inclusion in diamond. The remarkable thing about this particular example was its shape, which consisted of three spokes intersecting at approximately

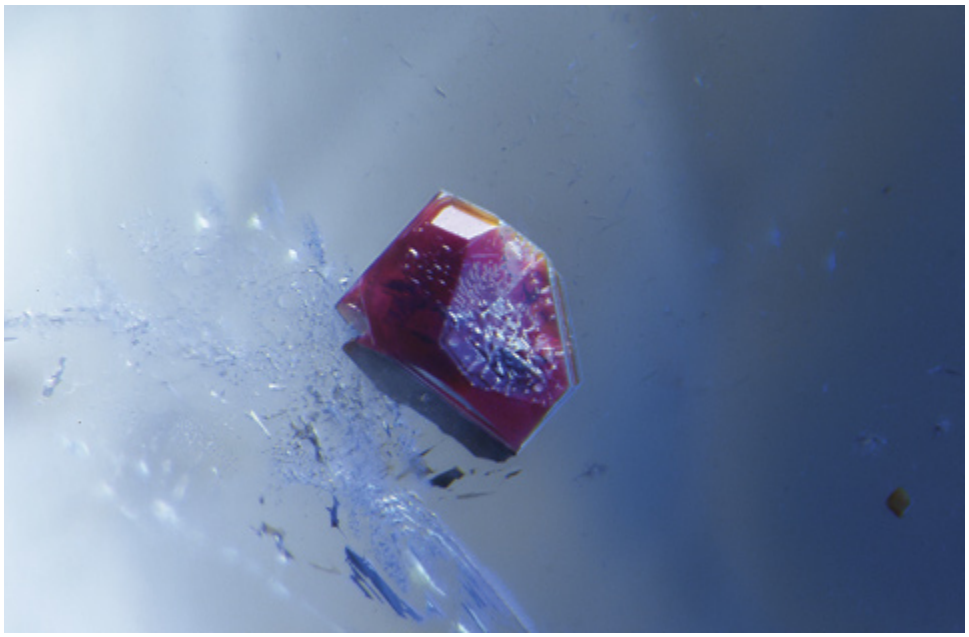

Figure 5. This faceted benitoite contains a small reddish brown inclusion of neptunite that was identified by Raman spectroscopy. Photomicrograph by Nathan Renfro; field of view 1.20 mm. Courtesy of Michael Jakubowski.

120° (figure 6). This is not the shape one would typically associate with the orthorhombic mineral olivine, but there is an explanation for the unusual morphology of this inclusion.

As diamonds form at extreme temperature and pressure conditions, they can impose their morphology on syngenetic minerals that become included in them. When a guest mineral adopts the host diamond's morphology, this is known as *xenomorphism*. The triangular morphology seen here suggests that the olivine inclusion is oriented parallel to an octahedral crystal face of the host diamond crystal. This is one of the most unusually shaped inclusions observed in diamond examined by the author.

Nathan Renfro

Bent Rutile in Rock Crystal Quartz

The authors recently examined a polished quartz disk with an unusual rutile (TiO_2) inclusion (figure 7). Although rutile in quartz is reasonably common and has been well documented, this "bent" rutile was a fun oddity as it also

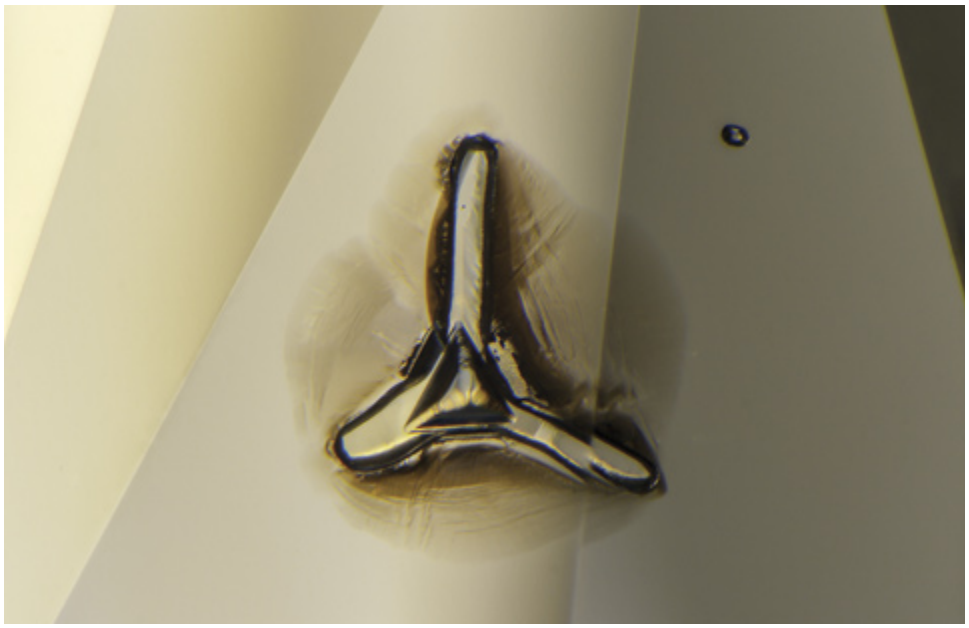

Figure 6. This three-spoke radial inclusion of olivine owes its unique morphology to the extreme temperature and pressure applied to it. This mineral inclusion forced to adopt the shape of its host is an example of xenomorphism. Photomicrograph by Nathan Renfro; field of view 2.25 mm.

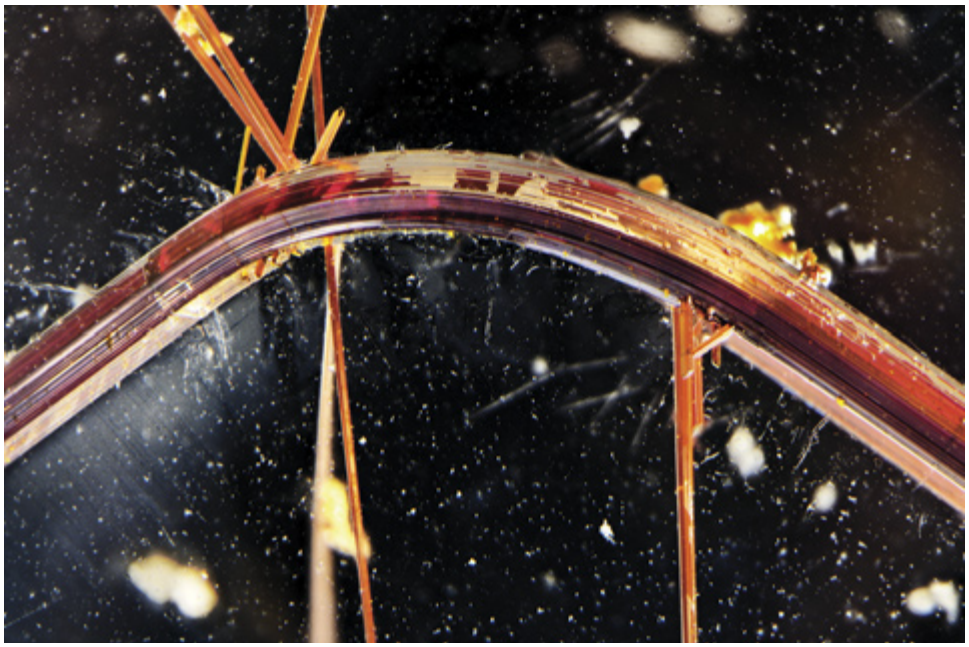

Figure 7. Brownish red "bent" rutile with additional orangy needles displaying sagenitic twinning. Photomicrograph by Nathan Renfro; field of view 11.28 mm. Courtesy of Mike Bowers.

contained small orangy sagenitic twinned rutile needles extending from the primary bend in the rutile needle. Rutile is most often seen as fine, straight needles (E.J. Gübelin and J.I. Koivula, *Photoatlas of Inclusions in Gemstones*, Vol. 2, 2005, Opinio-Verlag Publishers, Basel, Switzerland, pp. 627 and 630). Rutile can play many roles as an inclusion and may contribute to phenomenal effects as well as to the bodycolor of an overall transparent colorless quartz (figure 8). While the exact cause of the bent nature of this rutile inclusion is unknown, the stone is a fascinating example of the unusual formation of inclusions in gems.

Amy Cooper and Nathan Renfro

Yellow Fluid Inclusions in Transparent Sodalite

The authors recently examined a 7.17 ct transparent, near-colorless sodalite submitted for identification service (figure 9). Sodalite is typically encountered as a semitransparent to opaque, violetish blue stone with white calcite veining resembling lapis lazuli.

Hackmanite is the sulfur-bearing variety of sodalite exhibiting tenebrescence (D. Kondo and D. Beaton, "Hackmanite/sodalite from Myanmar and Afghanistan," Spring 2009 *G&G*, pp. 38–43). Tenebrescent minerals reversibly change color when exposed to UV light—from light purple to saturated purple, in the case of hackmanite. While this stone showed the strong orange fluorescence reportedly found in hackmanite, no change in color was observed. This was perhaps due to the short exposure time during testing.

Microscopic observation revealed greenish yellow two-phase fluid inclusions reminiscent of petroleum in quartz (figure 10). Unlike petroleum in quartz, the fluid inclusions were inert to long-wave UV light. Raman spectra of the gas bubble and surrounding liquid were matched to gaseous hydrogen sulfide and hydrogen sulfide in solution, respectively. Methane-related peaks were also present in the liquid phase. These sulfur-rich fluid inclusions provided

Figure 9. This 7.17 ct colorless sodalite was remarkably transparent and contained interesting fluid inclusions. Photo by Sean-Andrew Z. Pyle.

Figure 8. The polished transparent rock crystal quartz containing the bent rutile inclusion. Photo by Robert Weldon.

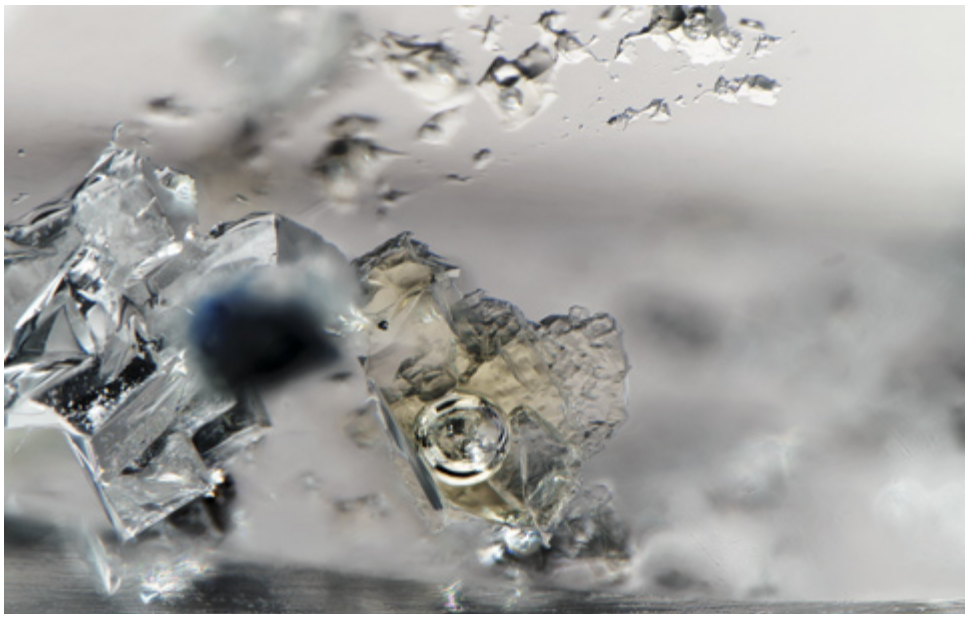

Figure 10. These greenish yellow fluid inclusions were identified as hydrogen sulfide in solution. The gas bubble was matched to hydrogen sulfide gas. Photomicrograph by Tyler E. Smith: field of view 1.99 mm.

interesting geological evidence of the stone's formation, making this rare sodalite even more exceptional.

Ezgi Kiyak and Tyler Smith
GIA, New York

Quarterly Crystal: Heavily Etched Blue Beryl Crystals Reportedly from Pakistan

In previous Micro-World columns, the Quarterly Crystal entry has showcased exceptional crystalline specimens masterfully crafted by geological forces. In some cases, however, it is the darker destructive forces of nature that produce a fine mineral specimen. In 2018, Raza Shah (Gems Parlor, Fremont, California) began unearthing heavily etched dark blue beryl crystals from Khyber Pakhtunkhwa in northern Pakistan. Bryan Lichtenstein (3090 Gems, San Francisco, California) submitted three of these crystals to GIA's Carlsbad lab for identification services (figure 11; see also B.M. Laurs and G.R. Rossman, "Dark blue beryl from Pakistan," *Journal of Gemmology*, Vol. 36, No. 7, 2019, pp. 583–584).

Figure 11. Three blue beryl crystals showing the heavily etched and corroded appearance typical of this material. The largest crystal is 236.8 g, while the other two weigh 16.1 g (left) and 13.8 g (right). Photo by Diego Sanchez.

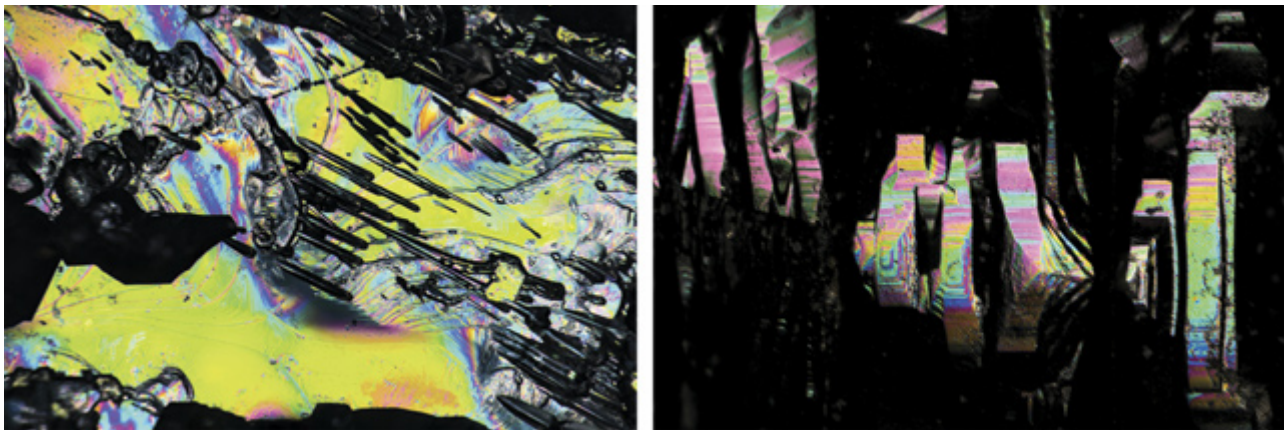

Figure 12. The use of differential interference contrast imaging illustrates the complex growth and subsequent etching processes that lent the beryl crystals their unique appearance. These views are essentially parallel to the c-axis (left) and perpendicular to the c-axis (right). The left image shows terraced, stepped patterns created during crystal growth that are crosscut by oriented, elongate etch pits. Photomicrographs by Aaron Palke; field of view 2.88 mm.

The hexagonal barrel shape that must have characterized the crystals in their initial state is still apparent despite the heavy etching. The geological conditions responsible for beryl growth apparently persisted long enough for many of these crystals to grow to extreme sizes; the largest recovered so far weighs 236.8 g. At some point, these crystals appear to have fallen out of equilibrium with their natural environment and the beryl started dissolving back into the earth. Microscopic observation of the corroded surfaces shows how the dissolution process is controlled by the beryl crystal structure, with dissolution pits and the skeletal remnants of the beryl constrained by the underlying crystal lattice. Differential interference contrast (DIC) microscopy can be used to highlight both growth and dissolution features in the same image (figure 12). While Pakistan is an important source of aquamarine crystals and gems, this heavily etched dark blue aquamarine is truly a unique find.

Aaron C. Palke
GIA, Carlsbad

Gem News International

Contributing Editors
Emmanuel Fritsch, *University of Nantes, CNRS, Team 6502, Institut des Matériaux Jean Rouxel (IMN), Nantes, France* (fritsch@cnrs-imn.fr)
Gagan Choudhary, *Gem Testing Laboratory, Jaipur, India* (gagan@gjepcindia.com)
Christopher M. Breeding, *GIA, Carlsbad* (christopher.breeding@gia.edu)

COLORED STONES AND ORGANIC MATERIALS

Unique metal sulfide inclusion in "Bing Piao" red agate from Liangshan, China. Over the past decade, with the discovery of "Nanhong" agate ore deposits in Sichuan Province, a significant amount of this material has been mined in Meigu County, located in the northeast of Liangshan Yi Autonomous Prefecture. Commercial gem mines in Meigu County are located in three main areas, including Jiu Kou, Wa Xi, and Lian He. Field observations show that the ore body is found either in the interlayer fissures and cavities of Permian Emeishan basalt crystallized from siliceous hydrothermal fluid or as conglomerates of the Permian Leping Formation.

Previous reports found that "Nanhong" agate is colored by natural hematite inclusions. Moreover, these agates are divided into five major categories, including "Bing Piao" (a Chinese term that refers to their inclusions "floating on ice"). This type of agate (see figure 1, left) is colorless and contains red hematite particles distributed in attractive patterns.

Recently, a special type of "Bing Piao" red agate called "black grass" agate by merchants appeared in the market at Liangshan. A bead of this material (figure 1, right) was obtained for examination at the National Gold-Silver Gem & Jewelry Quality Supervision & Inspection Center (Sichuan).

Gemological properties of the semitransparent bead, including its RI of 1.54 and hydrostatic SG of 2.65, suggested agate; this was confirmed by FTIR spectroscopy. Magnification revealed tiny red inclusions that were identified as hematite by Raman spectra (peaks at 225, 244, 291, 410, 610, and 1320 cm^{-1}) using a 785 nm laser. In addition to these attractive red forms made of hematite, the bead hosted many unusual black mineral particles displaying various shapes such as blades, planar clusters, and the like (figure 2). When viewed with reflected light, microscopic observations of their opaque, anhedral form and metallic luster suggested the particles were likely an iron sulfide. A Raman spectrum obtained from a surface-reaching black particle showed two major peaks at 342 and 377 cm^{-1}, matching well with pyrite, according to the RRUFF database (reference spectrum R100166), as shown in figure 3.

To obtain confirmation, the bead was polished down to a plate to perform chemical analysis and phase identification of the black particles using a scanning electron microscope in combination with an energy-dispersive

Figure 1. The cabochon on the left is a normal "Bing Piao" red agate measuring 12.50 × 19.60 × 10.11 mm. The bead on the right, approximately 11.80 mm in diameter, is a special type of "Bing Piao" red agate. Photo by Su Xu.

Editors' note: Interested contributors should send information and illustrations to Stuart Overlin at soverlin@gia.edu or GIA, The Robert Mouawad Campus, 5345 Armada Drive, Carlsbad, CA 92008.

Gems & Gemology, Vol. 57, No. 2, pp. 166–184.

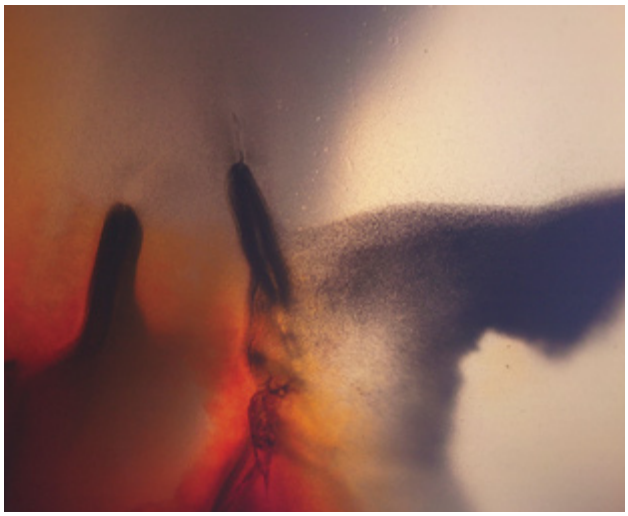

Figure 2. These antennae-like inclusions consist of dot-like black minerals, coupled with red inclusions. Photomicrograph by Xiaoping Shi; field of view 9.00 mm.

spectrometer (SEM-EDS) equipped with an electron backscatter diffraction (EBSD) detector. Qualitative analysis revealed the expected major elements of Fe, As, and S, along with minor Si, likely from the agate host. This was consistent with pyrite composition. The EBSD analyses indicated a cubic structure, and a search of the NIST Structural Database using Aztec software revealed a match for pyrite (FeS_2).

Figure 3. The black particle was identified as pyrite based on comparison with Raman reference spectra from the RRUFF database. Spectra are offset vertically for clarity.

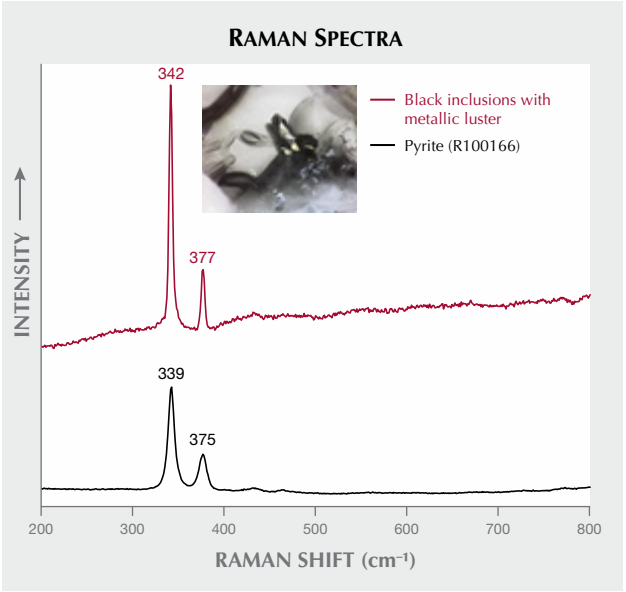

Except for Liangshan, such distinctive black minerals of various forms have not been found in other "Bing Piao" red agate deposits. The pyrite particles, as inclusions that are unique to "Bing Piao" red agate from Liangshan, may therefore be considered reliable indicators of origin. Further gemological studies on these inclusions are required to construct the database for origin determination.

Su Xu and Dapeng Chen
National Gold-Silver Gem & Jewelry Quality Supervision & Inspection Center (Sichuan)
Xiaoping Shi
Sichuan Provincial Coal Design & Research Institute

Natural freshwater pearls from Europe: Russia, Scotland, and Germany. The Carlsbad laboratory received eight European freshwater (FW) pearls from coauthor ES for gemological and chemical characterization (figure 4). Although the exact locations and times of discovery were not recorded, all the samples were obtained directly by ES from reputable sources in each country. The first three samples are of Russian origin and were obtained by Russian fisheries biologist Valery Ziuganov during his studies of the Varzuga River, Kola Peninsula, in the 1990s (E. Strack, "European freshwater pearls: Part 1–Russia," *Journal of Gemmology*, Vol. 34, No. 7, 2015, pp. 580–593; E. Strack, "Freshwater pearls from Russia," *Margaritologia*

Figure 4. The eight European natural freshwater pearls reportedly produced by Margaritifera margaritifera *mussel species, collected from freshwater sources in Russia, Scotland, and Germany. Photo by Diego Sanchez.*

TABLE 1. Internal structures of eight European freshwater pearls revealed by RTX and μ-CT analyses.

Sample number, origin, and weight	Macro image	RTX image	μ-CT image
No. 1, Russia 1.27 ct		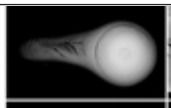	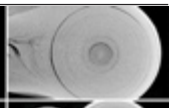
No. 2, Russia 1.83 ct		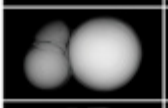	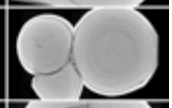
No. 3, Russia 2.68 ct		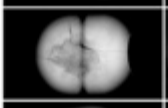	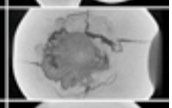
No. 4, Scotland 0.70 ct		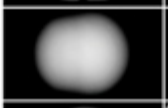	
No. 5, Scotland 1.52 ct		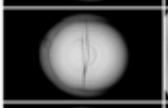	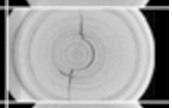
No. 6, Germany 0.94 ct		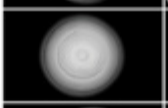	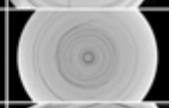
No. 7, Germany 1.61 ct		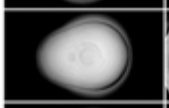	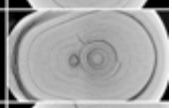
No. 8, Germany 2.11 ct		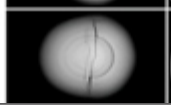	

newsletter, No. 11, 2018). Two samples from Scottish rivers were provided in 2004 by Cairncross Jewellers, the only company allowed to buy pearls from the fishers in Perth, Scotland. The last three are from Lüneburg Heath in northern Germany and were supplied around 1997 by a local family that had collected and fished for pearls over the decades. European FW natural pearls have reportedly been produced for centuries from mussels belonging to the *Margaritifera margaritifera* species, which has been referred to as the "freshwater pearl mussel" (E. Strack, *Pearls*, Rühle-Diebener-Verlag, Stuttgart, Germany, 2006). Today, most natural FW pearls produced in North America and cultured FW pearls from Asia form in various mussel species within the *Unionidae* family. Both families are member of the Unionoidea superfamily.

The samples exhibited two different surface structures: nacreous and non-nacreous. Upon examination with a loupe and microscope, samples 1–4 (see table 1) exhibited nacreous surfaces, with fine overlapping platelets visible under high magnification. Surface wrinkling was also seen in single areas on samples 1 and 3, along with fine surface fractures; the wrinkled feature in each was previously noted as a characteristic of a FW environment (Strack, 2015, 2018). The nacreous samples ranged from 0.70 to 2.68 ct and measured from 4.77 × 4.33 mm to 7.08 × 6.72 mm. According to GIA classification procedures, their shapes were semi-baroque, baroque, and circled oval, while their bodycolors varied from light pinkish brown to light purplish pink and very light pinkish brown. Sample 3 showed a dull surface lacking luster and overtone, while the other three displayed orient and pink overtones.

Conversely, samples 5–8 exhibited a non-nacreous surface appearance and lacked overlapping platelets characteristic of most FW pearls. They ranged from 0.94 to 2.11 ct and measured from 5.12 mm to 7.32 × 6.98 mm. The shapes were uniformly round, oval, and drop, and all the samples were brown-yellow. At higher magnification, using strong illumination such as fiber-optic lighting, all the pearls displayed mosaic or cellular surface patterns of differing sizes and shapes. The small cells, which looked like pinpoint features in lower lighting conditions, resulted in a dimpled surface texture (figure 5). A cellular pattern was also observed in a small area on the base of sample 1. The non-nacreous appearance and cellular surface structures resembled those commonly observed on pen pearls from the *Pinnidae* family (N. Sturman et al., "Observations on pearls reportedly from the *Pinnidae* family (pen pearls)," Fall 2014 *G&G*, pp. 202–215), as well as some non-nacreous non-bead cultured pearls from the *Pinctada maxima* mollusk (A. Manustrong et al., "Known non-nacreous non-bead cultured pearls and similar unknown pearls of likely cultured origin from *Pinctada maxima*," *GIA Research News*, 2019, https://www.gia.edu/gia-news-research/known-non-nacreous-non-bead-cultured-pearls). Non-nacreous natural pearls from *Pteria* species mollusks have also reportedly displayed hexagonal-like cellular patterns (S. Karampelas and H. Abdulla, "Black non-nacreous natural pearls from *Pteria* sp.," *Journal of Gemmology*, Vol. 35, No. 7, 2017, pp. 590–592).

Figure 5. At higher magnification, the four non-nacreous pearls displayed mosaic or cellular surface patterns of different sizes and shapes. This image shows the cellular structure on the surface of sample 7 when illuminated with a fiber-optic light. Photomicrograph by Nathan Renfro; field of view 1.00 mm.

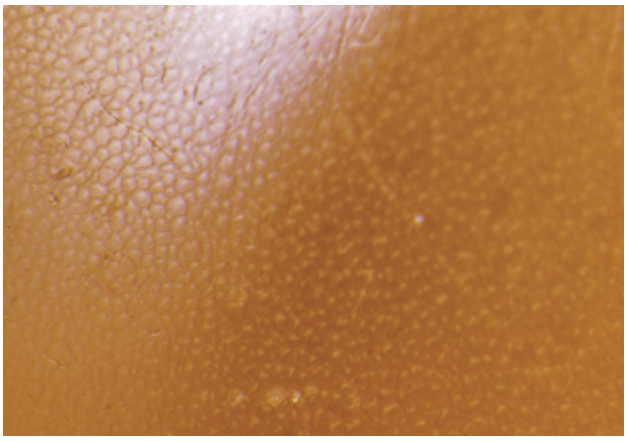

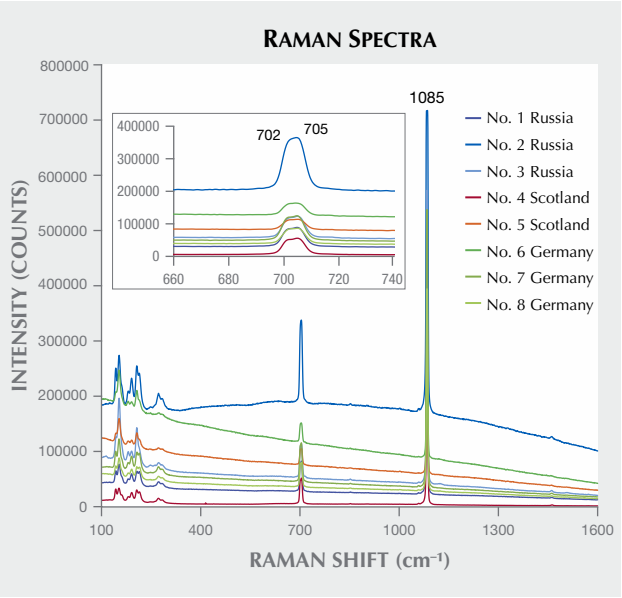

Figure 6. Raman spectra of all eight samples obtained using an 830 nm diode laser revealed clear aragonite peaks, a doublet at 702 and 705 cm^{-1} (magnified in the inset), and a single intense band at 1085 cm^{-1}. These results allowed the four non-nacreous pearls to be separated from pen pearls, which are normally composed of calcite (Sturman et al., 2014). Spectra are offset vertically for clarity.

Under long-wave ultraviolet radiation (365 nm), the nacreous samples exhibited weak bluish yellow fluorescence over most of the surface, while a yellow reaction was observed on the limited yellowish brown areas. The non-nacreous samples exhibited uniform weak to moderate chalky yellow fluorescence similar to that reported for pen pearls (Sturman et al., 2014), but different from the strong orangy red fluorescence observed in non-nacreous *Pteria* pearls (S. Karampelas and H. Abdulla, 2017).

A Raman spectrometer was used to examine the surface composition of all the pearls, initially using a 514 nm argon-ion laser. Owing to the high background fluorescence observed in most of the samples, an 830 nm laser provided better peak resolution. Clear aragonite peaks at 702, 705, and 1085 cm^{-1} were recorded in all the samples (figure 6), and the results allowed the four non-nacreous pearls to be separated from pen pearls, which are normally composed of calcite (Sturman et al., 2014). Raman spectra collected using the 514 nm laser revealed weak polyene peaks at approximately 1125 cm^{-1} and 1512 cm^{-1} in samples 1, 3, and 4, indicating their colors were natural. Polyene peaks were not observed in samples 2 and 5–8, possibly due to the samples' high fluorescence. The 830 nm laser is not helpful in resolving polyenic peaks. Surface observations did not reveal color modification in any of the samples.

UV-Vis reflectance spectra were collected from the smoothest and most homogeneously colored area of each sample in the 250–800 nm range. An absorption feature at about 280 nm that is usually observed in nacreous pearls was clearly seen in samples 1–4 but absent in samples 5–8. Samples 1, 2, and 4 showed reflection minima in the blue to yellow range, which corresponds with their predominantly pink hue. These results correlate with those in a previous study on naturally pink FW pearls of natural origin from the Mississippi River System in the United States (Summer 2019 GNI, pp. 282–285) and with reports on natural-color FW cultured pearls from *Hyriopsis* species mollusks (S. Karampelas et al., "Role of polyenes in the coloration of cultured freshwater pearls," *European Journal of Mineralogy*, Vol. 21, No. 1, 2009, pp. 85–97; A. Abduriyim, "Cultured pearls from Lake Kasumigaura: Production and gemological characteristics," Summer 2018 *G&G*, pp. 166–183). Owing to the very light color of sample 3, the spectrum obtained was nearly flat, as would be expected for white pearls, and hence no features of any significance were observed. The spectra obtained from samples 5–8 showed a lower reflectance than the four previously reported samples due to their more saturated colors. All the spectra showed similar patterns, with an incline from 400 to 750 nm in the visible region, comparable to the reported spectra of dark-colored pen pearls (Sturman et al., 2014) and non-nacreous non-bead cultured pearls from *Pinctada maxima* (Manustrong et al., 2019).

Table 1 shows the internal structures of the eight samples using real-time microradiography (RTX) and X-ray computed microtomography (μ-CT). Sample 1 and all the non-nacreous samples showed clear organic-rich concentric ring structures with faint radial features radiating outward from the center across the concentric rings. The radial structures are associated with cellular surface patterns. All three sections of sample 2 showed weak growth arcs corresponding to their shapes. Sample 3 exhibited a wavy concentric growth pattern together with a dark organic-rich patch, while μ-CT analysis revealed a small dark core in the structure. Sample 4 displayed the least amount of visible structure—only a few very faint growth arcs, even when examined using μ-CT. Cracks of varying lengths and degrees of visibility were present in the samples. The structures observed confirmed their stated natural origin. However, a smaller nucleus with a lighter gray core next to the main nucleus in sample 7 did raise some concerns. If the pearl was submitted to a gemological laboratory without any known provenance, the smaller structure could be mistaken for the lighter gray carbonate "seed" features sometimes found in saltwater non-bead cultured pearls (M.S. Krzemnicki et. al., "Tokki pearls: Additional cultured pearls formed during pearl cultivation: External and internal structures," *32nd International Gemmological Conference*, 2011, https://www.ssef.ch/wp-content/uploads/2018/01/SSEF_Tokki_pearls.pdf). However, the authors are not aware that this type of feature has ever been reported in non-bead cultured pearls from a FW environment.

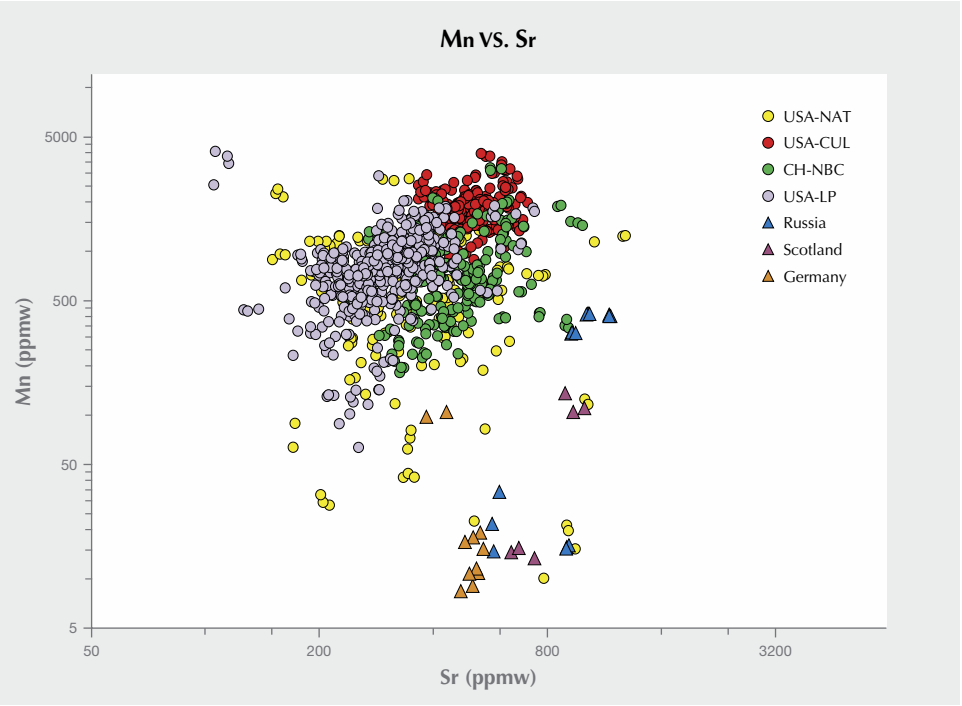

Figure 7. All the European pearl samples contained Mn levels below 500 ppm, which helped separate them from the majority of freshwater pearls previously studied. Mn and Sr levels obtained by LA-ICP-MS analysis were consistent with the EDXRF results. Yellow spots represent results from American natural pearls (USA-NAT), red spots from American cultured pearls (USA-CUL), green spots from Chinese NBC pearls (CH-NBC), and purple spots from American natural pearls from the Mississippi River System (USA-LP).

Chemical compositions were initially analyzed by energy-dispersive X-ray fluorescence (EDXRF) spectrometry, and some of the samples were tested twice in different positions. Most samples contained relatively low manganese (Mn) levels (0 to 240 ppm) compared to the majority of natural and cultured FW pearls in GIA's database. The usual Mn range observed is between 150 and 2000 ppm. Samples 1, 3, and 6–8 showed Mn concentrations below 50 ppm. It was interesting to note that in sample 5, Mn was absent at one end but present (170 ppm) at the opposite end. Additionally, the samples with low Mn levels (<50 ppm) did not show visible reaction under X-ray excitation (H. Hänni et al., "X-ray luminescence, a valuable test in pearl identification," *Journal of Gemmology*, Vol. 29, No. 5/6, 2005, pp. 325–329), as would be expected for such low traces of the element. Strontium (Sr) contents were relatively low (< 1000 ppm) in all the samples, which is characteristic of FW origins. However, the very low concentration of Mn and lack of X-ray fluorescence reactions could create some doubts and lead to some misidentifying them as saltwater (SW) pearls.

Detailed trace element concentrations were analyzed using laser ablation–inductively coupled plasma–mass spectrometry (LA-ICP-MS) with the same parameters used in previous FW pearl studies (A. Homkrajae et al., "Provenance discrimination of freshwater pearls by LA-ICP-MS and linear discriminant analysis (LDA)," Spring 2019 *G&G*, pp. 47–60; Summer 2019 GNI, pp. 282–285). At least three ablation spots were tested on each sample, and the results for the 22 elements selected are shown in table 2. The five elements (sodium, magnesium, Mn, Sr, and barium) found to be useful discriminators in the differentiation of FW from SW pearls and in classifying FW pearls from different sources are bolded in the table. Mn and Sr contents obtained were consistent with the EDXRF results. All the samples contained low Mn levels (<500 ppm), separating them from the majority of FW pearls previously studied (figure 7; see Homkrajae et al., 2019; Summer 2019 GNI, pp. 282–285). The ternary diagram of relative percentages between Ba, Mg, and Mn that was used to verify the growth environment conditions of the questionable FW pearls in previous studies (Homkrajae et al., 2019; Summer 2019 GNI, pp. 282–285) was used once again to confirm the formation environment of the six samples containing low levels of Mn (below 100 ppm). All six samples plotted alongside those of the FW pearls previously studied, confirming their FW origin. These results also help to distinguish non-nacreous samples from saltwater non-nacreous non-bead cultured pearls produced by *Pinctada maxima* (Manustrong et al., 2019). The values of these five discriminant elements, as well as those for lead (Pb), correspond with the chemical results reported on natural FW pearls produced by *Margaritifera margaritifera* mollusks found in the Spey River, Scotland (S. Karampelas et al., "Chemical characteristics of freshwater and saltwater natural and cultured pearls from different bivalves," *Minerals*, Vol. 9, No. 6, 2019, p. 357). The Sr-Ba concentration plot is also shown in figure 8. This result supports the observation made by Karampelas et al. (2019). Furthermore, the pearls from each European locality could be separated from each other in this plot, though it should be noted that this was based on a very limited number of known samples.

For centuries, the freshwater mussel species *Margaritifera margaritifera* was abundant in the rivers and streams

TABLE 2. LA-ICP-MS chemical composition values (in ppmw) of the European pearls studied.

Element	Maximum	Minimum[a]	Average[b]	Detection Limits
Li	1.64	bdl	0.15	0.013
B	98.0	bdl	16.7	0.12
Na	**2300**	**1150**	**1760**	**1.55**
Mg	**1890**	**31.8**	**163**	**0.016**
P	292	8.23	134	0.76
K	475	3.83	78.5	0.11
Ca	404000	389000	395000	24.9
Ti	0.27	bdl	0.27	0.045
Cr	1.82	bdl	0.83	0.13
Mn	**426**	**8.42**	**135**	**0.014**
Fe	209	167	173	0.36
Co	0	bdl	bdl	0.12
Ni	0.78	0.51	0.56	0.022
Cu	24.2	0.87	6.79	0.029
Zn	1.66	bdl	0.37	0.030
Ga	10.1	0.59	3.72	0.039
Sr	**1170**	**382**	**751**	**0.034**
Y	0.037	0	0.004	0
Mo	0.61	bdl	0.061	0.002
Ba	**381**	**22.5**	**147**	**0.009**
La	0.016	0	0.003	0
Pb	0.19	bdl	0.062	0.006

[a]*bdl = below detection limits*
[b]*Data below detection limits is treated as zero when calculating average values*

of Europe, and the pearls produced were part of European culture and history. The American native mussel species followed a similar path. However, environmental changes, and the impact of pollution from industry and agriculture have damaged ecosystems and directly affected the mussels' habitat and lifespan (Strack, 2006). Freshwater pearl fishing in Europe is currently prohibited or under regulation due to the decline of mussel populations. Studying these rare European FW natural pearls provided valuable data that has enlarged GIA's identification database, offering a useful reference for the gemological community.

Artitaya Homkrajae and Ziyin Sun
GIA, Carlsbad
Elisabeth Strack
Hamburg, Germany
Sally Chan Shih
GIA, New York

Unique non-bead cultured freshwater pearls from Lake Biwa, cultured for 14 years. Lake Biwa in Shiga Prefecture has been producing pearls since 1928, when commercial freshwater pearl culturing first started in Japan. Although production decreased in the late twentieth century due to environmental issues and the declining mussel population (S. Akamatsu et al., "The current status of Chinese freshwater cultured pearls," Summer 2001 *G&G*, pp. 97–113), Biwa pearls harvested in the twenty-first century, as well as vintage ones, are popular in the Japanese market. *Hyriopsis schlegelii*, an indigenous freshwater mollusk found in the lake prior to the 1980s, was originally used as the host for pearl culturing before it was replaced by the hybrid *Hyriopsis schlegelii* × *Hyriopsis cumingii* freshwater mollusk.

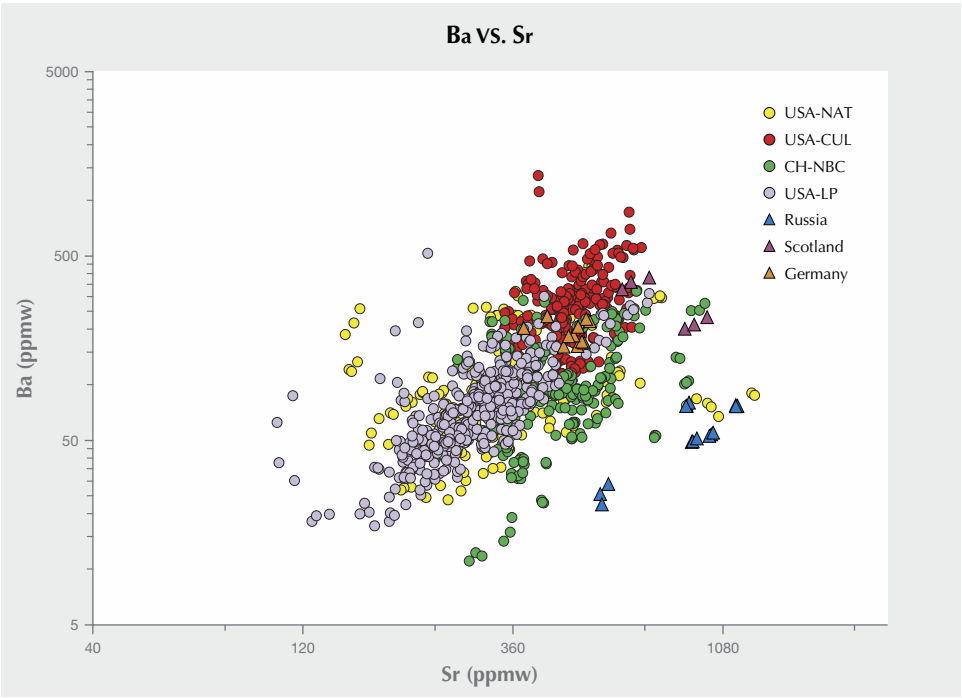

Figure 8. American and Chinese freshwater pearl samples studied previously, together with the samples from this study, were plotted in the Sr-Ba concentration plot. This result supports the observation made by Karampelas et al. (2019). Although the study was based on a limited sample pool, the pearls from each European locality could also be separated using this plot.

Figure 9. The two Biwa pearl samples that were cultured for 14 years and acquired from Jinbo Pearls, measuring 19.75 × 10.38 × 9.84 mm (pearl A, left) and 23.48 × 12.36 × 11.08 mm (pearl B, right). Photo by Shunsuke Nagai.

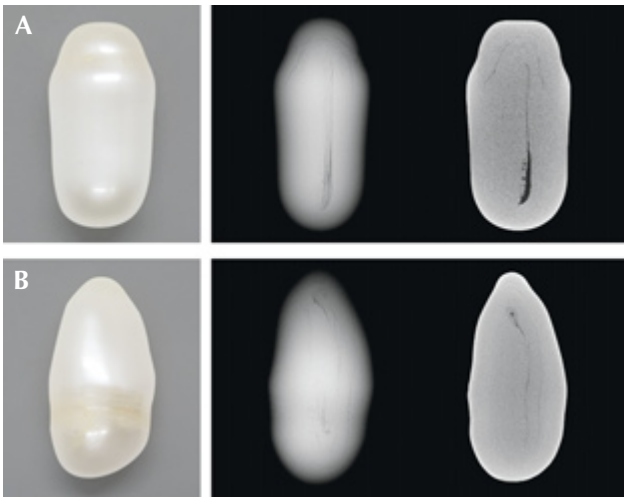

Figure 10. Left: Macro images of pearls A and B. Photos by Nanthaporn Nilpetploy. Center and right: The internal structures as revealed by RTX and µ-CT analysis, respectively.

GIA's Tokyo laboratory received for study 28 pearl samples with a stated Biwa provenance from Jinbo Pearls, a Shiga-based company that deals exclusively with freshwater pearls from Lake Biwa. Two of the largest samples (figure 9), weighing and measuring 16.08 ct, 19.75 × 10.38 × 9.84 mm (pearl A) and 22.85 ct, 23.48 × 12.36 × 11.08 mm (pearl B), respectively (figure 10, left), were selected for further detailed study. The intriguing fact was that they were reportedly grown over a period of 14 years—from 2002 to 2016. This is an unusually long growth period, since freshwater non-bead cultured (NBC) pearls normally take three years to form in Japanese farms. However, the farm where these samples originated was abandoned by the owner due to personal issues. Remarkably, several mussels were found alive when the farm was rechecked before being officially closed by the owner's relatives in 2016. These two pearls were collected from two of the surviving mussels.

Real-time microradiography (RTX) examination revealed a faint linear feature along the length of each pearl (figure 10, center). X-ray computed microtomography (µ-CT) analysis showed these features more clearly and revealed an additional small dark void at the end of pearl A's linear structure (figure 10, right). Their internal structures corresponded well to other non-bead cultured freshwater pearls described in previous studies (M.S. Krzemnicki et al., "X-ray computed microtomography: Distinguishing natural pearls from beaded and non-beaded cultured pearls," Summer 2010 *G&G*, pp. 128–134). Additionally, optical X-ray fluorescence analysis showed a strong yellowish green reaction with weak yellowish orange areas within some imperfections around the circumference of the pearls (indicated by white arrows, figure 11, A-2 and B-2).

Each pearl was cut in half (cut surfaces were cleaned with isopropyl alcohol) and the examination results were compared with those obtained prior to sawing. Surprisingly, both showed stronger reddish orange optical X-ray fluorescence reactions within small areas along the central structure lines (RTX and µ-CT analysis) visible on each sawn face (figure 11, A-4 and B-4) than on any external surface areas when the pearls were intact. Such reactions are sometimes seen in natural and freshwater cultured pearls (Summer 2013 Lab Notes, pp. 113–114; Spring 2019 Lab Notes, pp. 94–96; S. Karampelas et al., "Chemical characteristics of freshwater and saltwater natural and cultured pearls from different bivalves," *Minerals*, Vol. 9, No. 6, 2019, article no. 357, pp. 16–17). It was especially interesting that the reactions seemed to correlate with the dull frosty white surface areas along the central structure lines on the sawn-faces when observed under the microscope at higher magnifications (indicated by black arrows in figure 12, A-3 and B-3). This observation was consistent with previous studies on freshwater cultured pearls (Spring 2019 Lab Notes, pp. 94–96).

Raman analysis of these areas showed they consisted of two $CaCO_3$ polymorphs: aragonite and vaterite. Aragonite features were visible at 701, 704, and 1085 cm^{-1}, while vaterite features were noted at 740, 750, 1075, and 1090 cm^{-1}. Aragonite and vaterite in cultured FW pearls have previously been recorded (U. Wehrmeister et al., "Vaterite in freshwater cultured pearls from China and Japan," *Journal of Gemmology*, Vol. 30, No. 7/8, 2007, pp. 399–412; A.L. Soldati et al., "Structural characterization and chemical composition of aragonite and vaterite in freshwater cultured pearls," *Mineralogical Magazine*, Vol. 72, No. 2, 2008, pp. 579–592; H. Ma et al., "Vaterite or aragonite observed in the prismatic layer of freshwater-cultured pearls from South China," *Progress in Natural Science*, Vol. 19, No. 7, 2009, pp. 817–820). Furthermore, calcite was also detected in pearl A, where peaks at 280, 714, and 1085 cm^{-1} were observed. The first two peaks were isolated and did not appear in association with any other peaks (groupings

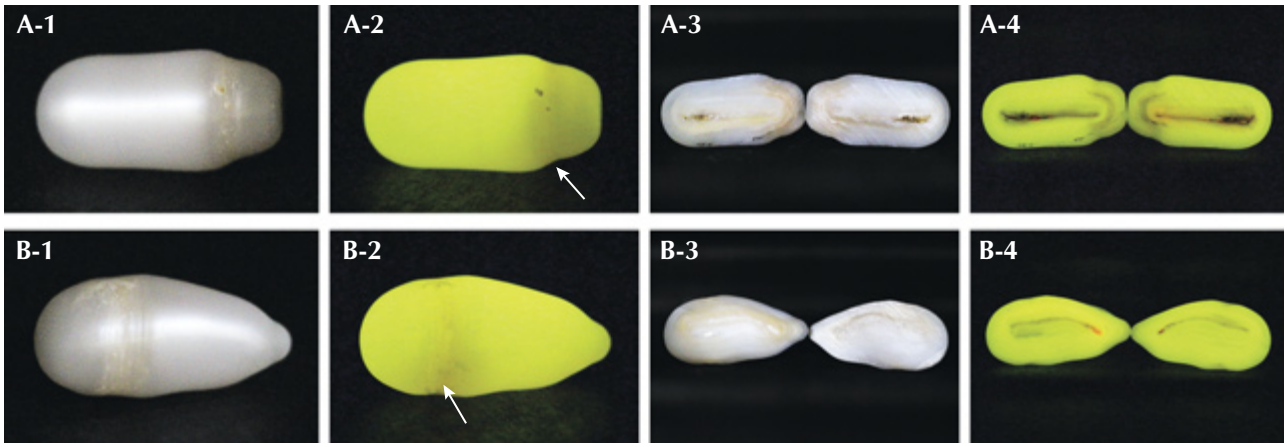

Figure 11. The fluorescence reactions of both pearl samples under optical X-ray fluorescence. The pearls prior to sawing (A-1, B-1) showed strong yellowish green reactions, with some weak yellowish orange areas within some imperfections around their circumference (white arrows, A-2, B-2). The sawn pearls (A-3, B-3) showed strong yellowish green reactions, with stronger reddish orange areas in some positions (A-4, B-4). Images by Kwanreun Lawanwong.

or doublets), proving they were another $CaCO_3$ polymorph. Up until recently, calcite had not been reported in freshwater cultured pearls, though it was found in a small area of pearl A in this study and was also noted in a pearl discussed in a recent study (S. Eaton-Magaña et al., "Raman and photoluminescence mapping of gem materials," *Minerals*, Vol. 11, No. 2, 2021, article no. 177, pp. 24–27).

Further advanced analysis of the cross sections' trace element concentrations was conducted using laser ablation–inductively coupled plasma–mass spectrometry (LA-ICP-MS). The reddish orange fluorescent areas were shown to contain much higher Mg (1250 ppmw for pearl A and 2260 ppmw for pearl B) and lower Na (1210 ppmw for pearl A and 1310 ppmw for pearl B) concentrations than other areas of the samples not exhibiting the reaction (Mg lower than 77 ppmw and Na higher than 1930 ppmw). This result is consistent with those detailed in the literature (Soldati et al., 2008; Eaton-Magaña et al., 2021). The results seemed to correspond with the Raman data, and the different Mg and Na ratios helped to separate aragonite and vaterite, though it is difficult to differentiate calcite from either without performing Raman analysis.

Figure 12. Photomicrographs of the cross sections showing some dull white frosty surfaces (black arrows, A-3, B-3) that correspond to the areas showing reddish orange fluorescent reactions under optical X-ray fluorescence. Field of view 19.20 mm (A-1, B-1), 14.40 mm (A-2, B-2), and 2.88 mm (A-3, B-3). Photos by Kwanreun Lawanwong.

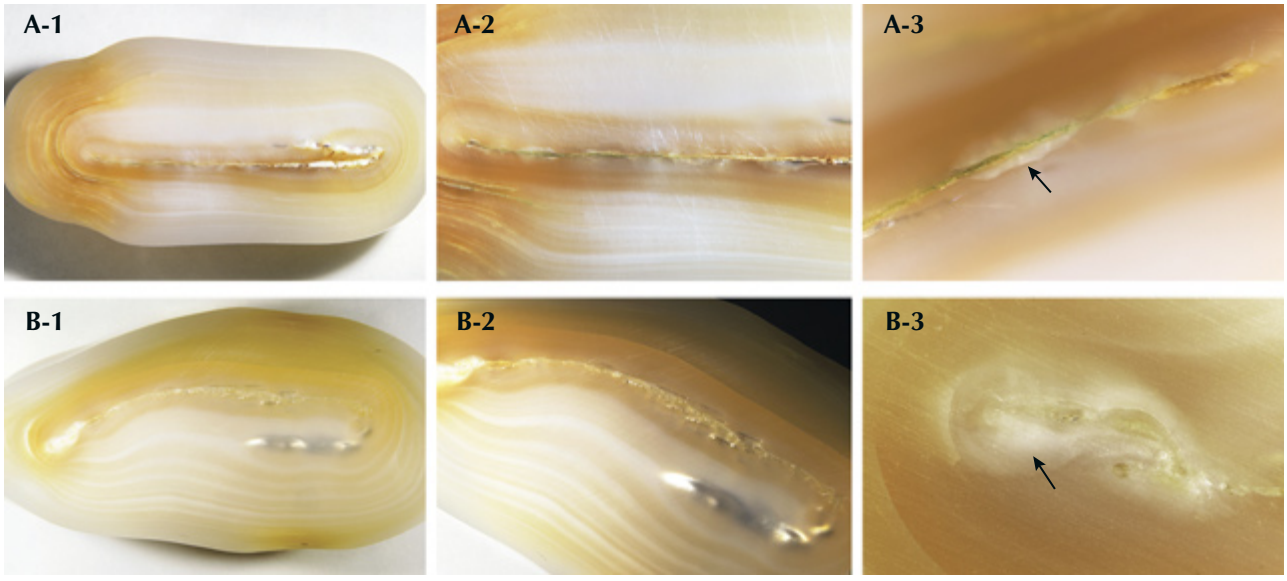

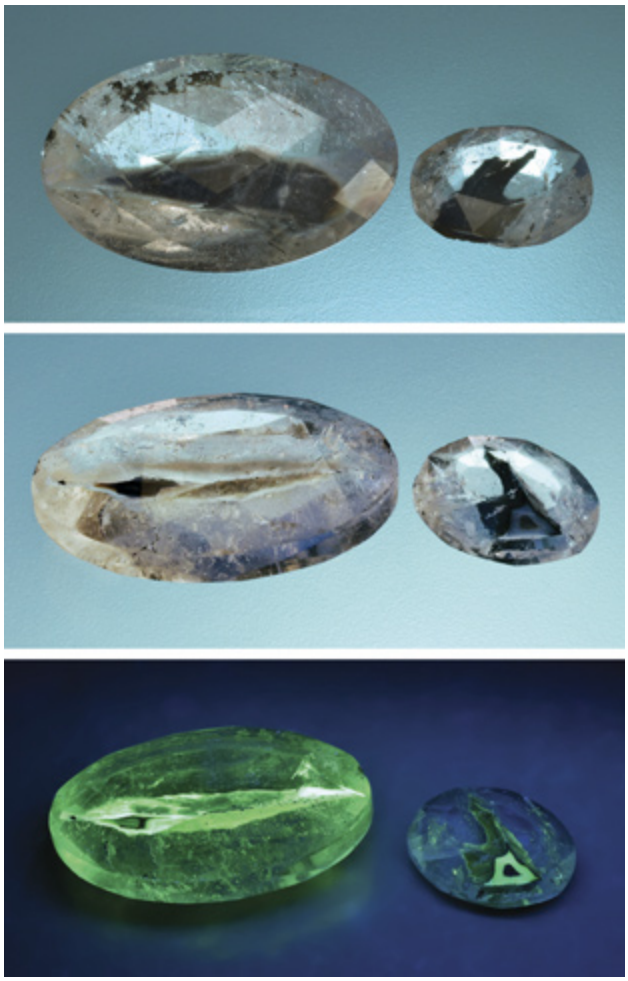

Figure 13. Two faceted quartz with agate inclusions from Brazil, weighing 66.61 ct and 12.28 ct (shown in two positions and in short-wave UV). Photos by Jaroslav Hyršl.

Vaterite within the structure of NBC FW pearls is thought to be related to the biomineralization process that results following the tissue/mantle insertion (Wehrmeister et al., 2007), and its presence is a strong indicator of a cultured origin. These two unique pearls are a part of 28 Biwa pearl samples collected over various time frames. Since they are worthy of being singled out for discussion, this brief report is a precursor to a more detailed review of both pearls and the other Biwa pearl samples referenced.

Nanthaporn Nilpetploy
GIA, Bangkok

Yusuke Katsurada
GIA, Tokyo

Agate inclusion in quartz from Brazil. Agates are undoubtedly one of the most common precious stones from Brazil. They come from basalts in the state of Rio Grande do Sul, on the border with Uruguay. This region is probably also the source of several unusual faceted quartz samples, purchased by the author in Brazil in 2019. These stones are up to 35 mm long and, except for abundant two-phase inclusions, contain flat, irregularly shaped inclusions. On two stones (figure 13), these inclusions reach the surface and show a typical agate structure, with several black, gray, and light brown layers. Their identity was proved by very weak quartz peaks in the Raman spectrum. Unexpected was their strong fluorescence in UV light, which is much stronger in short-wave UV. This fluorescence is concentrated in gray layers and is very likely caused by a trace presence of uranium, quite common in many agates and opals.

Jaroslav Hyršl (hyrsl@hotmail.com)
Prague

Mobile inclusions in a decorative quartz object. A client recently submitted an interesting transparent, highly polished, barrel-shaped object for identification. It weighed approximately 109.2 g, measured approximately 90 × 37 × 22 mm, and clearly exhibited a long brown internal feature (figure 14) containing multi-phase inclusions along the length of the predominantly colorless body. Standard gemological testing resulted in an RI reading of 1.55 (spot) and SG value of 2.61. Microscopic examination revealed fluid, fingerprint, and crystal inclusions typical of a natural growth environment. As a result, the object was identified as natural quartz, which was confirmed by FTIR and Raman analysis.

However, the most notable feature of this specimen was its unique and impressive mobile inclusion scene. On first impression, the long brown inclusion appeared to be a crystal, but it turned out to be a negative crystal filled with countless tiny mobile brownish particles (figure 15) and a large colorless mobile gas bubble. The mobility of these in-

Figure 14. A partial view of the long irregularly shaped brown negative crystal running along the length of its quartz host. Photomicrograph by Lai Tai-An Gem Lab; field of view 6.42 mm.

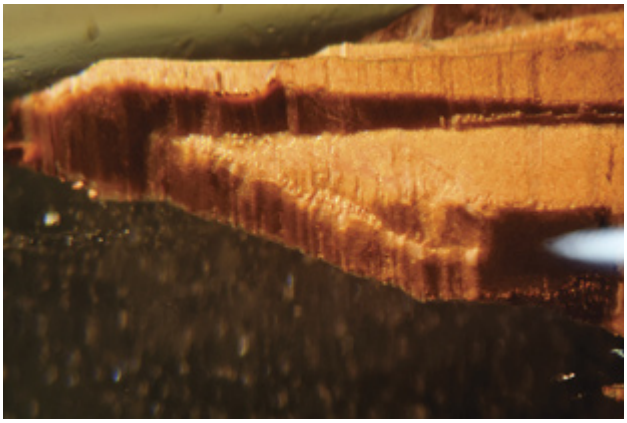

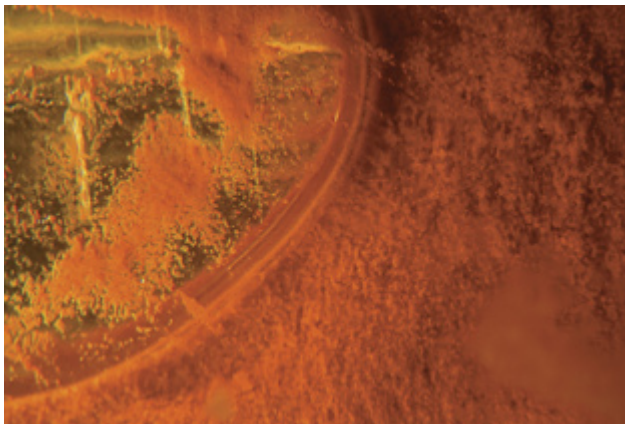

Figure 15. The countless tiny brown particles together with part of the large colorless bubble within the negative crystal. Photomicrograph by Lai Tai-An Gem Lab; field of view 4.57 mm.

clusions within the brown negative crystal was cleverly incorporated into the final design, as the lapidary fashioned the object into a barrel form with flat faces at either end. This allowed the object to be flipped over like an hourglass, so that all the mobile inclusions would be set in motion (figure 16; see video at https://www.gia.edu/gems-gemology/summer-2021-gemnews-mobile-inclusions-quartz). It was also noted that the gas bubble moved at a faster rate than the tiny particles, which made the object even more captivating. The ambient temperature also appeared to affect the speed at which the inclusions moved—the higher the temperature, the faster the rate.

Although the identification of this quartz specimen was straightforward, it was a pleasure to see the artistry employed in its fashioning that permitted its inclusions to be easily seen to maximum effect.

Larry Tai-An Lai (laitaiangemlab@gmail.com)
Lai Tai-An Gem Laboratory, Taipei

Multi-color sapphires reportedly from the Garba Tula district, Isiolo County, Kenya. The Garba Tula sapphire deposit, located in Isiolo County in central Kenya, is a unique igneous gem-corundum producing area. It is a productive source of blue, green, and yellow sapphires (C. Simonet et al., "The Dusi (Garba Tula) sapphire deposit, Central Kenya–A unique Pan-African corundum-bearing monzonite," *Journal of African Earth Sciences*, Vol. 38, 2004, pp. 401–410). Figure 17 shows the overall color appearance of 28 Garba Tula sapphires recently examined in this study. They were purchased from a reliable dealer at the Tucson gem shows in 2019. It was noticed that their color varied from dark blue to yellow through various shades of blue and green. Some showed strong yellow and blue zoning, while samples with bluish and greenish color banding were also observed. Interestingly, one of the sapphires exhibited a color-change appearance (indicated by the black arrow in figure 17). Windows were polished into the samples in order to study their internal features and collect chemical data. For some samples, windows were polished parallel to the c-axis for spectroscopic measurements.

The studied materials revealed a slightly higher refractive index (1.761–1.773) than typical metamorphic sapphires. The other standard gemological properties were typical of natural corundum. The vast majority of these Garba Tula sapphires (75%) displayed no fluorescence under long-wave UV radiation, while 18% fluoresced red and the remainder showed zoned orange fluorescence (with very weak red fluorescence or none). The fluorescence intensity to long-wave UV of Garba Tula sapphires is generally very weak to weak. However, they were totally inert to short-wave UV light.

The characteristic inclusions observed from these 28 Garba Tula sapphire samples are presented in figure 18. More than 90% were included with irregular brownish needles and platelets identified by Raman as hematite/ilmenite (Y. Katsurada et al., "Golden sheen sapphire and syenite/monzonite–hosted sapphire from Kenya," Fall

Figure 16. A series of images showing the movement of the tiny brown particles and the large bubble in the barrel-shaped object. The denser particles drop toward the bottom and the bubble rises to the top. When flipped over, the process starts again, reminiscent of an hourglass. Photo by Lai Tai-An Gem Lab.

Figure 17. Color-calibrated photos of sapphires (0.602–7.133 ct) reportedly from the Garba Tula area in the Isiolo region of Kenya. The black arrow indicates the color-change sapphire. Photo by Sasithorn Engniwat.

2018 *G&G*, pp. 322–323), formed either as planes along the color banding or as a group or cloud. These multiple twinning planes, commonly associated with parallel and/or intersecting growth tubes, were found in more than 80% of the stones. A few samples contained numerous single and scattered clusters identified by Raman spectroscopy as zircon crystals (figure 18, right), sometimes with fine rutile needles and reflective particle clouds, but with fewer irregular brownish platelets. Fingerprint inclusions as well as the other crystal inclusions identified using Raman spectroscopy and the RRUFF reference database, such as apatite and mica, were occasionally observed in the Garba Tula sapphires studied. Moreover, crystals of carbonate minerals were also previously reported in Garba Tula sapphire (Y. Katsurada et al., 2018). However, they typically lack sharp growth structure and milky clouds, as frequently seen in Madagascar and Sri Lanka.

FTIR spectra obtained from the sapphires often showed one or more diagnostic features: a single 3309 cm^{-1} peak as well as OH-related mineral features such as boehmite,

Figure 18. Typical inclusions presented in the sapphires from Garba Tula, Kenya. Left and center: A plane of irregular reflective needles that showed brownish color using fiber-optic lighting and diffused lighting, respectively; field of view 2.88 mm. Right: Numerous single and clusters of zircon crystals, some with tension fractures; field of view 4.8 mm. Photomicrographs by C. Khowpong and S. Wongchacree.

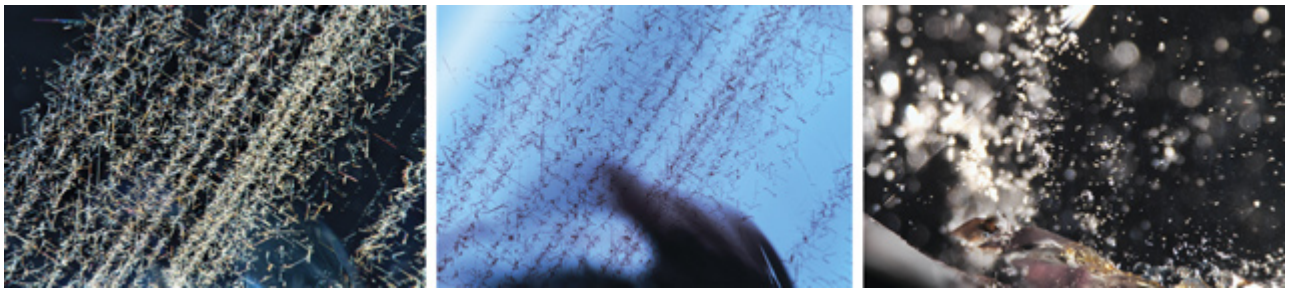

kaolinite, and gibbsite. It was noticed that every sample exhibited a single 3309 cm^{-1} peak without any subordinate peaks, while the boehmite and kaolinite were observed often (>70%) with a small percentage (18%) showing the gibbsite mineral feature.

Interestingly, the UV-Vis-NIR spectrum of greenish blue to blue sapphires from Garba Tula exhibited a metamorphic-type sapphire spectrum, with strong Fe^{3+}-related absorption features at 377, 388, and 450 nm and also an Fe^{2+}-Ti^{4+} intervalence charge transfer (A.C. Palke et al., "Geographic origin determination of blue sapphire," Winter 2019 *G&G*, pp. 536–579). A broad band centered at 880 nm, which is typically used to indicate basalt-hosted sapphire, was not observed.

LA-ICP-MS showed comparable trace element chemistry profiles between the different color areas of the stones, as presented in table 1. The Garba Tula corundum contains significant amounts of Fe and small amounts of Ti. High Fe content ranging from 1555–3177 ppma and 2121–2943 ppma were detected in greenish blue to blue and yellowish to greenish zones, respectively, while the Ti concentration ranged from 3–41 ppma. The high amounts of Fe were also higher than those of Mogok (Myanmar) and Tunduru (Tanzania) sapphires, which have been previously reported as high-Fe metamorphic sources (W. Soonthorntantikul et al., "An in-depth gemological study of blue sapphires from the Baw Mar mine (Mogok, Myanmar)," *GIA Research News*, 2017, https://www.gia.edu/gia-news-research/blue-sapphires-baw-mar-mine-mogok-myanmar). Therefore, the chemical composition of the Garba Tula sapphires, particularly their high Fe, is not common for metamorphic sapphire deposits.

The discovery of this source for yellow, green, and blue sapphires could be interesting for the gem trade. The material represents a true challenge for gemologists working on origin determination, as their formation is quite complicated. Although some properties and chemistry of the Garba Tula sapphires are comparable to the corundum xenocrysts originating from alkali basalt fields, their UV-Vis-NIR and FTIR spectra and their internal features are not consistent with typical basalt-related sapphires. The inclusion scene might, in some aspects, overlap between high-Fe metamorphic and basalt-related sapphires. The reflective/iridescent brownish platelets can be seen in metamorphic sapphires from Mogok, Myanmar, as well as in basalt-hosted sapphires from Thailand and Ethiopia. But none of the glassy melt inclusions usually observed in basalt-related sapphires were noticed in the Garba Tula sapphires. One hypothesis is that they formed in the same way as the basalt-related stones but just were not brought to the surface by the basalt. Therefore, a combination of multiple techniques can be useful in the origin determination of sapphires from Garba Tula.

Ungkhana Atikarnsakul
GIA, Bangkok

DIAMONDS

Rare mixed type IaB-IIb diamond with a long-lasting phosphorescence. Phosphorescence is an optical effect in which electromagnetic radiation absorbed by a substance is released relatively slowly in the form of light. Long-lasting UV phosphorescence of more than 10 seconds' duration is an extremely rare property in natural diamonds, normally limited to hydrogen-rich type Ia chameleon and type IIb diamonds.

Recently, a natural round brilliant weighing 0.20 ct (E-F color, VS_2-SI_1 clarity) was submitted to Stuller Inc. by a client for a custom design. During our diamond screening process, using a phosphorescence imaging-based screening device, the diamond was automatically identified as having an HPHT-grown origin, conflicting with the client's natural origin disclosure. Secondary testing, using a fluorescence spectroscopy-based screening device, identified the diamond as having a natural origin. Under magnification, only a few pinpoints were spotted.

Due to the ambiguous results, the gem was sent to Stuller's Gem Lab for further analysis. The FTIR spectrum (figure 19) showed a mixed diamond type comprising low

TABLE 1. Trace element chemistry of Garba Tula sapphires with different color areas.

Color area		Concentrations (ppma)					
		Mg	Ti	V	Cr	Fe	Ga
Greenish blue to blue	Range	2–29	3–32	0.2–9.0	0.4–55.0	1555–3177	10–85
	Average	7	11	1.6	6.2	2615	36
Yellowish and greenish	Range	2–34	3–41	0.2–8.0	bql[a]–37	2121–2943	12–45
	Average	9	10	2.1	—	2622	32
Detection limits		0.076	0.163	0.012	0.161	1.665	0.008

[a]*bql = below quantification limits*

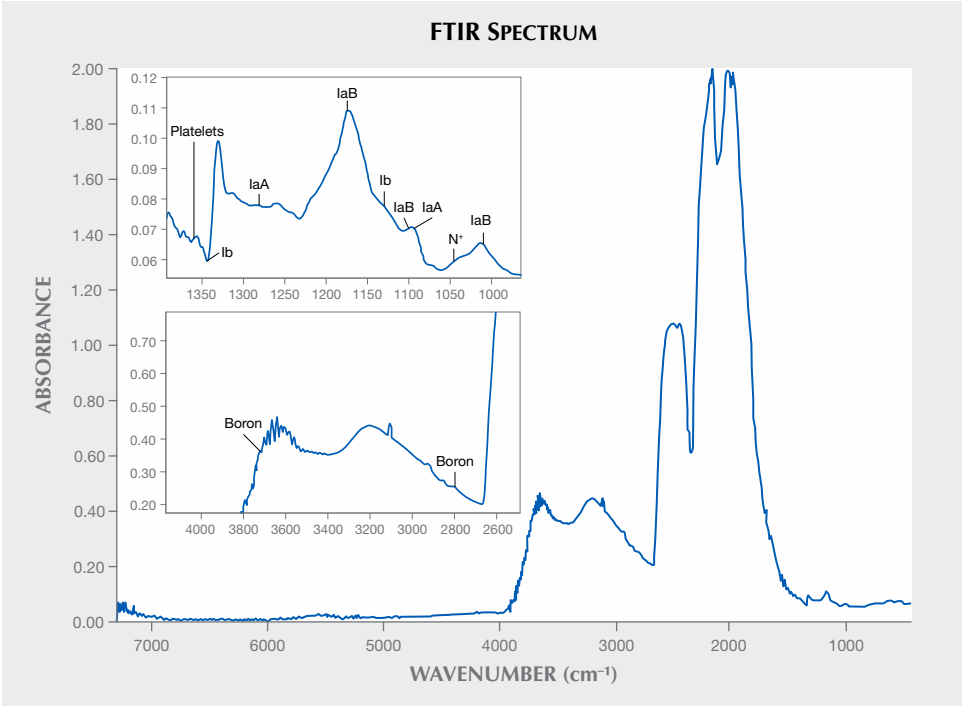

Figure 19. The 0.20 ct diamond's FTIR spectrum. The insets show the type IaB aggregate nitrogen at 1175 and 1010 cm^{-1} (top inset) and IIb boron (bottom inset) at 3725 and 2803 cm^{-1}, confirming a mixed-type stone.

levels of aggregated nitrogen (IaB) and boron (IIb), indicating a natural origin. Similar results were given using fluorescence spectroscopy, which identified N3 peaks, associated with natural origin. Photoluminescence spectroscopy, using a 532 nm laser under liquid nitrogen temperature (77 K), provided results supporting the other instruments and confirming the absence of synthetic origin-related peaks.

In order to identify the cause of the false positive results from the first screening device, the diamond was placed in a SWUV cabinet to analyze its phosphorescence effect. Once excited, the stone emitted a strong bluish green phosphorescence for about 120 seconds (figure 20).

The emitted color and the unusually long duration of the effect are typically associated with HPHT-grown diamonds. Consequently, these properties triggered the false positive results in the phosphorescence imaging-based screening device. In this case, the rare combination of natural diamond types, which includes a boron component, was probably the reason for the unusual phosphorescence.

This case demonstrates the complexity of diamond origin identification and the need for multiple diamond screening devices, each with a different screening technology, to cover all possibilities and ensure a 100% correct identification.

Guy Borenstein and Sean Oneal
Stuller Inc.

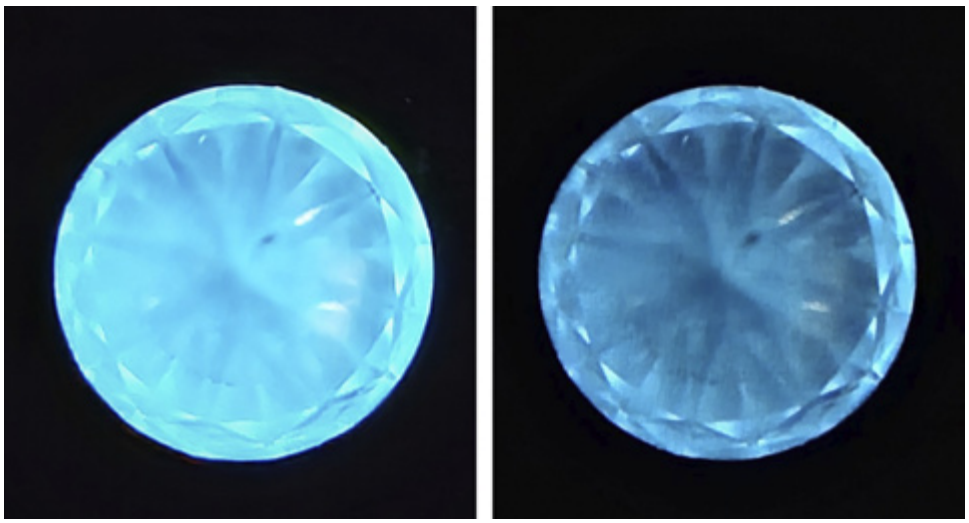

Figure 20. The 0.20 ct diamond's phosphorescence, as seen immediately after exposure to UV radiation (left) and after 60 seconds of elapsed time (right). Images by Guy Borenstein.

SYNTHETICS AND SIMULANTS

Calcareous coral and epoxy composite. Red calcareous coral is very popular in the Taiwanese market and has become far more expensive over the decades due to limited production and increasing demand. Red calcareous coral is usually cut into polished branches, beads, carvings, or cabochons. Recently, a bangle was submitted as calcareous coral to Taiwan Union Lab of Gem Research (TULAB) for identification service. It had a typical coral-red color (figure 21), though it was unusual to see a carved bangle due to the sizes of natural coral specimens that are found.

Standard gemological testing revealed that the refractive indices of this bangle were consistent with calcareous coral, at 1.48–1.65. However, its specific gravity of 2.27 was less than that of calcareous coral (2.6–2.7). Moreover, the short-wave ultraviolet fluorescence of this bangle presented a unique pattern of patches with chalky white to orange fluorescence next to each other (figure 22). Microscopic observations indicated that the patch-like fluorescence seemed to correspond to fragments of red calcareous coral, while the fragments were bonded with red material in which few bubble inclusions were found (figure 23).

To further confirm the identity of this bangle, the patches and the bonding material in between them were analyzed by Raman spectroscopy, and the resulting spectra were then compared with those of epoxy and red calcareous coral reported in the literature (figure 24; see K.E. Chike et al., "Raman and near-infrared studies of an epoxy resin," *Applied Spectroscopy*, Vol. 47, No. 10, 1993, pp. 1631–1635; S. Karampelas et al., "Identification of the endangered pink-to-red *Stylaster* corals by Raman spectroscopy," Spring 2009 *G&G*, pp. 48–52). The results showed that the fluorescing patches were natural calcare-

Figure 21. The carved bangle submitted as "red calcareous coral." Photo by Shu-Hong Lin.

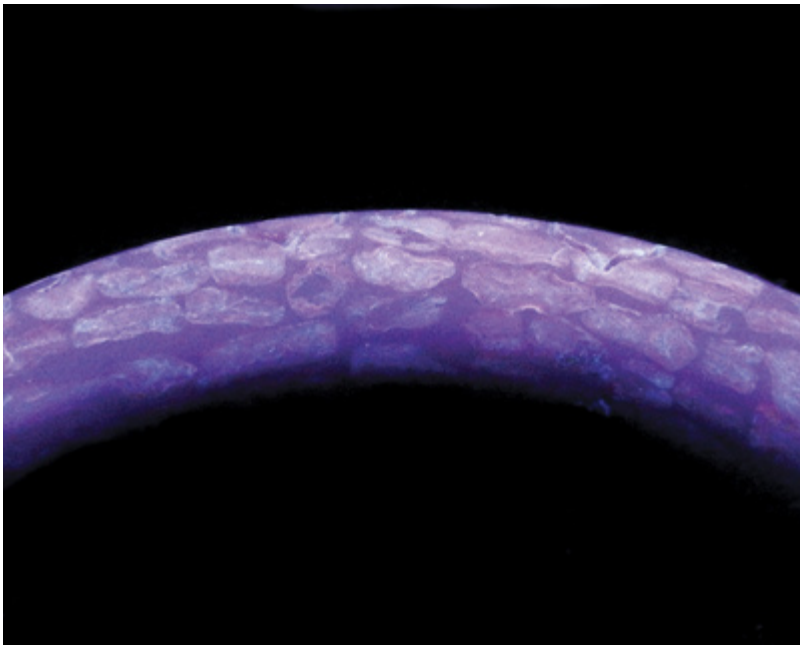

Figure 22. Short-wave ultraviolet fluorescence of the bangle presented a pattern of separate patches fluorescing white to orange. Photo by Kai-Yun Huang.

Figure 23. The microscopic image of the carved bangle indicated that the fluorescing patches seemed to be fragments of red calcareous coral, while the gaps between the fragments were filled with red foreign material with few bubble inclusions. Photomicrograph by Yu-Shan Chou; field of view 5.46 mm.

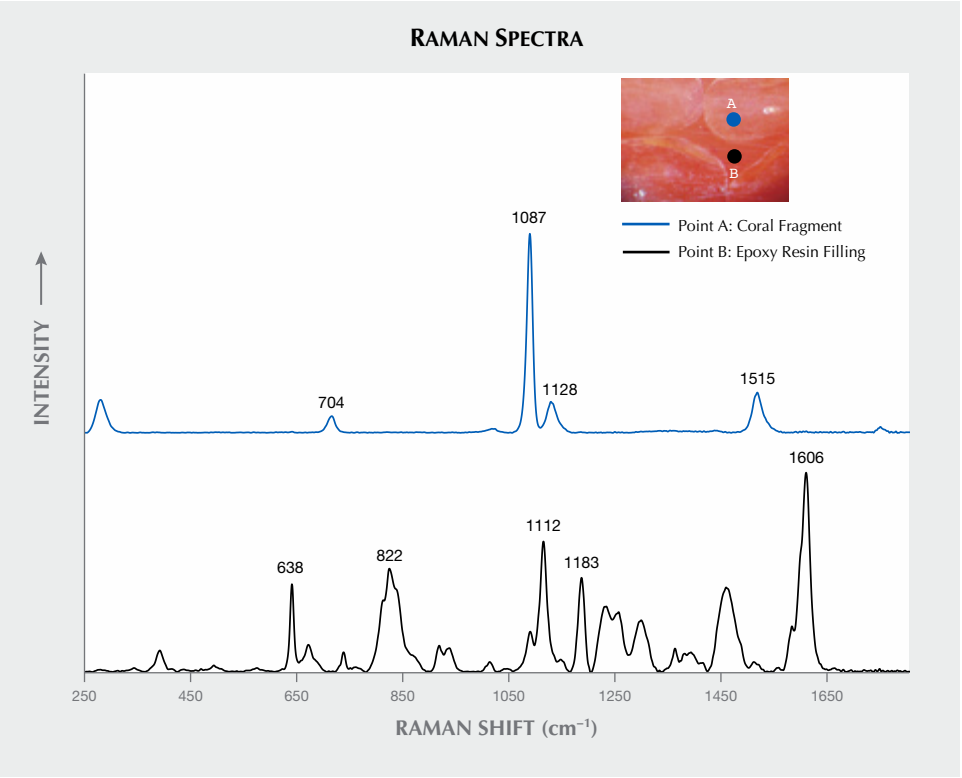

Figure 24. The Raman spectra of the bangle matched those reported in the literature for red calcareous coral and epoxy resin, which meant the bangle was composed of fragments of red calcareous coral (A: Raman peaks at 704, 1087, 1128, and 1515 cm^{-1}) and epoxy filling (B: Raman peaks at 638, 822, 1112, 1183, and 1606 cm^{-1}). The stacked spectra are baseline-corrected and normalized.

ous coral, while the bonding material in between was epoxy resin.

This kind of composite product was likely made by bonding the stacked coral fragments with red epoxy resin to form a bulk material, which was then processed into carvings, cabochons, or even bangles. Although the coral-epoxy composite product looked similar to natural calcareous coral, it could be accurately distinguished through specific gravity, ultraviolet fluorescence reaction, microscopic observation, and Raman spectroscopy.

Shu-Hong Lin
Institute of Earth Sciences, National Taiwan Ocean University
Taiwan Union Lab of Gem Research, Taipei

Kai-Yun Huang
Taiwan Union Lab of Gem Research, Taipei

Yu-Shan Chou
Taiwan Union Lab of Gem Research, Taipei

ANNOUNCEMENTS

Mignone Halls of Gems and Minerals. The American Museum of Natural History in New York City has reopened one of the most beloved spaces for gem enthusiasts with the unveiling of the Allison and Roberto Mignone Halls of Gems and Minerals on June 12, 2021. After a four-year closure, the 11,000-square-foot halls, which house more than 5,000 specimens sourced from 98 countries, have been completely redesigned and reinstalled to tell the intriguing story of how mineral diversity arose on our planet. This exciting public event reflects the reopening of New York City.

The American Museum of Natural History has a long-standing history with minerals and gems that dates back to its founding in 1869. In the 45 years since the previous iteration of the gem and mineral halls opened, the scientific fields of mineralogy and geology have advanced significantly, and the new design reflects these advancements. The halls were organized by Dr. George E. Harlow, curator of the Department of Earth and Planetary Sciences, to showcase to the public the current scientific understanding of gems and minerals, the geological conditions and processes by which they form, and introduce the relatively novel concept of mineral evolution.

Mineral evolution, one of the central themes, seeks to explain how more than 5,500 mineral species came into existence when there were no minerals for hundreds of millions of years after the Big Bang. The new halls show how changing conditions on Earth allowed more chemically diverse minerals to arise. They highlight one of the most important changes, which is the evolution of life that filled the atmosphere with free oxygen, enabling colorful, highly oxidized minerals. These are the same colorful minerals we associate with the gemstones humans have used to decorate themselves for thousands of years.

The redesigned space no longer resembles a simulated subterranean mine, with the multi-leveled carpeted inte-

Figure 25. One of the two giant amethyst geodes displayed at the entrance of the Mineral Hall. This geode weighs 11,000 lbs. (5,000 kg). Photo by Augusto Castillo.

rior that the previous iteration was known for. Instead, an open-floor concept allows visitors to wander seamlessly between the different displays and exhibits. It has three main divisions: the Mineral Hall, the Gem Hall, and the Melissa and Keith Meister Gallery for temporary exhibitions.

Entering the Mineral Hall, the visitor is welcomed by a pair of towering amethyst geodes that formed nearly 135 million years ago (figure 25). The scale and rich purple color of the massive geodes command attention and set the tone for the rest of the space. Behind the geodes, the center of

Figure 26. The Singing Stone is a massive 7,200 lb. (3265 kg) block composed of the copper ore minerals azurite and malachite. Its name comes from the high-pitched sounds produced when the stone absorbed and released moisture from the air. The stone no longer sings now that it sits in a controlled environment. Photo by Augusto Castillo.

the Mineral Hall contains mineral specimens organized by formation environment: igneous, pegmatitic, metamorphic, hydrothermal, and weathering. Highlights include the Singing Stone, a massive block composed of blue azurite and green malachite that was collected in 1891 from Bisbee, Arizona (figure 26), and a 14,500 lb. slab from upstate New York that is studded with garnets measuring up to one foot across (figure 27, opposite page).

The west wall of the Mineral Hall has a running display dedicated to the systematic classification of minerals. The display contains 659 specimens arranged by chemical composition, increasing in complexity across the wall. An interactive periodic table that can be used to explore forming minerals stands at the center of the west wall. The four corners of the Mineral Hall explore the overarching scientific concepts of minerals, from their evolution and diversity to their properties and how they have been used by humans from prehistory to the present day. Adjacent to the gallery of minerals and light is the Gem Hall. It features a dazzling

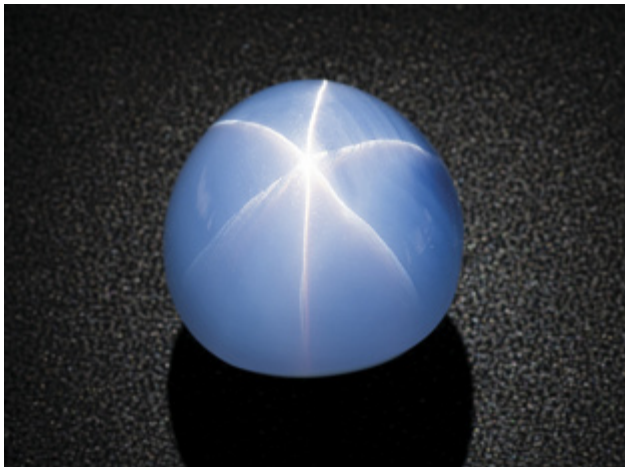

Figure 28. The 563 ct Star of India, the world's largest gem-quality blue star sapphire. Photo by D. Finnin/ ©AMNH.

Figure 27. A towering 14,500 lb. (6,577 kg) slab studded with giant garnets. The garnets formed more than 1 billion years ago, when the original rock transformed at pressure 8,000 times greater than atmospheric pressure and at about 1500°F (815°C). Photo by Augusto Castillo.

Figure 29. The 632 ct Patricia emerald, discovered in 1920 by a local miner, is the largest gem-quality emerald reported from the Chivor mine in Colombia. Photo by D. Finnin/©AMNH.

display of nearly 2,500 objects, including precious stones, carvings, and jewelry from the museum's world-class collection. Highlights include the 563 ct Star of India (figure 28), the largest gem-quality star sapphire known, and the 632 ct Patricia emerald, the largest gem-quality emerald reported from the Chivor mine in Colombia (figure 29).

In addition, the Melissa and Keith Meister Gallery is a rotating exhibit gallery newly added to the Halls of Gems and Minerals. *Beautiful Creatures*, curated by jewelry historian Marion Fasel, features animal-themed jewelry created over the last 150 years. The exhibit included more than 100 jewels from the world's great jewelry houses organized into three categories: land, water, and air. Its time frame coincides with the founding of the American Museum of Natural History in 1869 and explores the extraordinary diversity of the animal kingdom and the inspiration that it has provided for jewelry designers. *Beautiful Creatures* is on display through September 19, 2021.

Augusto Castillo
GIA, New York

Pearl Classification: GIA's Approach

SHAPE

Semi-baroque generally describes asymmetrical but identifiable shapes, while baroque pearls are completely irregular.

SIZE

Pearl weight is measured in carats, and measurements are stated in millimeters to two decimal places.

TYPICAL SIZES

COLOR

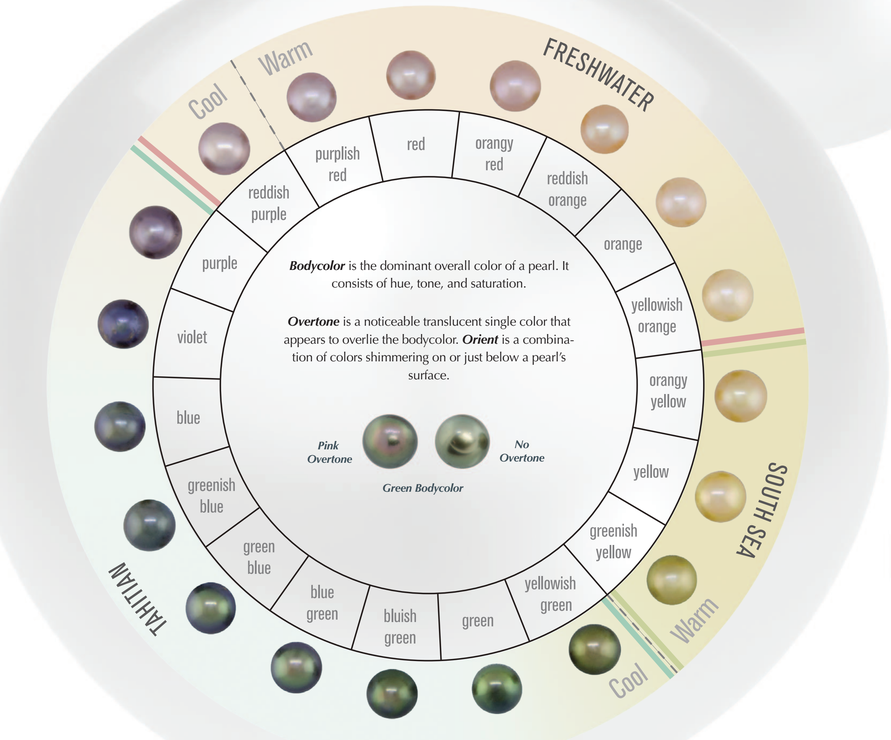

The GIA 7 Pearl Value Factors

Pearls are described in detail by classifying their size, shape, color, luster, surface, matching, and nacre—known together as the ***GIA 7 Pearl Value Factors***.

Each value factor is important in determining a pearl's overall appearance. When consistently applied together, the 7 Pearl Value Factors provide a common language to describe pearls and communicate their quality.

Setting the Standard

GIA developed the 7 Pearl Value Factors for the same reasons it developed the 4Cs of diamond quality: to establish a standard terminology for describing pearl quality, using simple language everyone can intuitively understand.

GIA has developed comprehensive sets of master pearls, dedicated standard viewing environments, and precise protocols for pearl classification, to ensure consistency throughout all GIA laboratories worldwide.

LUSTER

Luster is the light reflected from the surface and underlying nacre layers of a pearl; it is evaluated by the intensity as well as the sharpness of that reflection.

GIA LUSTER SCALE

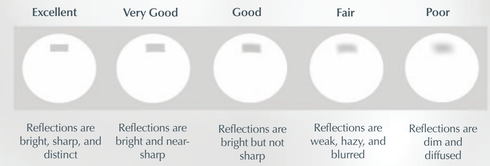

SURFACE

Surface is classified by taking into account the size, number, nature, location, visibility, and type of surface characteristics, blemishes, or irregularities that are confined to a pearl's surface.

GIA SURFACE SCALE

NACRE

Nacre is the substance that makes up a pearl, layer upon layer, giving pearls their unique appearance. Nacre quality is determined by its layering, and for bead cultured pearls its thickness. Adequate nacre thickness is required for bead cultured pearls to be both durable and beautiful.

GIA pearl reports will clearly note if a pearl's nacre is too thin and/or damaged, thereby posing a potential threat to its durability. Additionally, nacre thickness measurements are available as optional descriptions on GIA pearl reports.

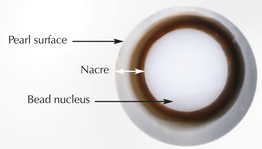

While the majority of the pearls in the market have acceptable nacre, these are examples of unacceptable nacre. Chalky appearance, obvious banding from the bead nucleus, and broken nacre are indications of thin nacre and/or poor layering.

MATCHING

Matching describes the uniformity of pearls in a pair, strand, or jewelry item. It takes into account the consistency of size, shape, color, luster, surface, nacre, and other features throughout the item.

Courtesy of Mastoloni, New York

GIA MATCHING SCALE

Excellent	Pearls are uniform in appearance and drilled on-center
Very Good	Very minor variations in uniformity
Good	Minor variations in uniformity
Fair	Noticeable variations in uniformity
Poor	Significant variations in uniformity
N/A	For single pearls and certain intentionally mismatched items

This chart contains a selection of photos of various cultured pearls. It is by no means comprehensive. The images show the appearance of numerous features a gemologist might observe when viewing cultured pearls.

Published in conjunction with Joyce Wing Yan Ho and Sally Chan Shih (2021), "Pearl Classification: The GIA 7 Pearl Value Factors," *Gems & Gemology*, Vol. 57, No. 2, pp. 135–137. Photos by Sood Oil (Judy) Chia.

GIA®